Geometric three-dimensional modelling of tectonic structures in the Alps and Jura Mountains

Dissertation

zur

Erlangung des Doktorgrades (Dr. rer. nat.)

der

Mathematisch-Naturwissenschaftlichen Fakultät

der

Rheinischen Friedrich-Wilhelms-Universität Bonn

vorgelegt von

Seyed Davood Mohammady Yosef Nejad

aus

Shiraz (Iran)

Bonn, Januar 2020

Angefertigt mit Genehmigung der Mathematisch-Naturwissenschaftlichen Fakultät der Rheinischen Friedrich-Wilhelms-Universität Bonn.

1. Gutachter: Prof. Nikolaus Froitzheim
2. Gutachter: Prof. Dr. Thorsten J. Nagel

Tag der Promotion: 29.05.2020

Erscheinungsjahr: 2021

Acknowledgement

First and foremost, I would like to express my sincere gratitude to my first supervisor Prof. Nikolaus Froitzheim for the continuous support of my Ph.D study and related research, for his patience, motivation, and immense knowledge. His guidance helped me in all the time of research and writing this thesis. I could not have imagined having a better advisor and mentor for my Ph.D study and it was a great honor for me to be his PhD student and work with him.

Secondly, I would like to thank my second supervisor, Prof. Dr Thorsten J. Nagel for his insightful comments and encouragement. He also helped me a lot during my study and I have used his knowledge and experience for my research.

Other past and present group members that I have had the pleasure to work with or alongside are Jacek kossak, Irena Miledanova, Kathrin Fassmer, Matthias Hauke and Ruth Keppler and also so many other nice colleagues in the Steinmann Institute.

I am also hugely appreciative to Dr. Georg Nover in the Petrophysics group for sharing his laboratory with me and allowing me to use his lab so willingly, and for being so dedicated to his role.

I would like to thank my family for all their love and encouragement. For my parents who raised me with a love of science and supported me in all my pursuits.

Finally, but by no means least, many thanks go to my lovely wife and daughter for almost unbelievable support. They are the most important people in my world and I dedicate this thesis to them.

Thank you all for your help and support.

Davood M.Yosefnejad

Bonn, 2020

Table of Contents

This page intentionally left blank.

Abstract

Geometric and kinematic three-dimensional (3D) modelling of complex geological structures experienced an outstanding evolution and has become more and more important nowadays in the field of geoscience as well as oil and gas industry both for research and engineering purposes. Modelling of the geoscience data in 3D format is not only for visualizing the data but also a powerful tool to combine all the surface and subsurface geological data in one environment in order to evaluate complex geological structures and to test different theories for structural geologists, geophysicists and petroleum engineers.

The Jura Mountains and the Eastern part of the Alps are very well studied. However, despite the availability of a large amount of data (geological maps, profiles, seismic data etc.) that have been produced in the last three decades, many issues related to the subsurface structures, subduction of continental crust, structural history as well as collisional and post-collisional processes remain unknown and matter of debate between different scientists.

The long-term goal of this thesis is to integrate all available data together, build a valid geometric and (partly) kinematic three dimensional model, visualize the data in a 3D environment and finally test different hypothesis and ideas by using suitable geoscience software (MOVE from Midland Valley Corporation). For this purpose, I have built two geometric 3D models, first for a small-scale area (Val de Ruz area in the Jura Mountains) and then for a large-scale area (Eastern part of the Alps). After that I have tried to

answer specific and open questions regarding these areas and test whether or not the simulation software could help us for understanding the complex subsurface structures and finding the answers to the unsolved problems. The results of the 3D model for the Val de Ruz area show significant pre-thrusting thickness variations for the Muschelkalk unit. The variation is at least partly due to lateral flow of the Triassic evaporites during the early phase of detachment folding, away from synclines and towards anticlines. Assuming a second decoupling horizon in the Dogger or involvement of the basement in the Jura tectonics is unnecessary for explaining the geology of the study area.

For the Eastern Alps, the added shortening of European and South Alpine basements is at a maximum at the western end of the Tauern Window, probably reflecting pre-Alpine margin geometry (Dolomites indenter). By the shortening calculations I have also estimate the area that is missing due to the collision during the Alpine orogeny which is the area that was destructed by the movement of Adria towards Europe since 30 Ma. The data also shows the average tectonic velocity between 3 to 6 mm per year which is in a good range compared to other available data. In addition to that, the modelling and quantitative calculations show that, about 59% and 25% of the current crust volume from the European and Adriatic continents respectively, have been destructed as a result of collision since 30 Ma. The results extracted from the 3D model and also from the calculations lead to the conclusion that about 812 997 km^3 of the continental crust from the eastern part of the Alps were subducted into the mantle since 30 Ma. From this total destructed volume about 82% belonged to the European continent

and 18% to the Adriatic continent and this amount of subducted crust could represent the minimum amount of material for this part of the Alps.

To conclude, three dimensional models which were tested for the Val de Ruz area and the Eastern part of the Alps, allowed us to integrate a large amount of data, plot them in one environment, gain insight into the complex tectonic structures and finally helped us to tackle some issues for these two areas. These 3D models for both of these areas provide valuable and comprehensive data files that could be used later as an input data for further research and investigation.

This page intentionally left blank.

Chapter 1

Introduction

1.1. Three-dimensional modelling

Understanding the complex subsurface tectonic structures by the 3D reconstruction technique or 3D modelling has experienced an outstanding evolution during the last 20 years. Apart from the visualization of the input and output data in one environment and in 3D format, a major advantage is that the process of modelling implies testing the input data for consistency and testing different tectonic hypothesis for their geometric feasibility. Additionally, the modelling software allows the user to extract additional information from the 3D model such as cross-sections in any desired orientation, orientation statistics and volumes or thicknesses of geological bodies (Yosefnejad et al. 2017).

In the last two decades three-dimensional kinematic and geometric modelling has successfully been used to explore complex tectonic structures both in small and large scales (Tanner et al. 2003; Maxelon and Manckelow 2005; Marquer et al. 2006; Zanchi et al. 2009; Dambrogi et al. 2010; Vouillamoz et al. 2012; Sala et al. 2014). Although they have used different methods and softwares for modelling and projection of their data, all of these researches have proved the usefulness of the 3D modelling for solving the complex geological structures.

In addition to that, it is also proposed by some scientists (e.g. Coward and Dietrich 1989) to restore the Alpine orogenic belt quantitatively in three dimensions for tackling the issues of crustal structure, structural history as well as collisional and post-collisional processes.

In this research, I have used the structural modelling software package MOVE from Midland Valley Corporation and built two 3D models for two specific areas (Val de Ruz area and Eastern part of the Alps). To do so, I have combined all available surface as well as subsurface data to address special problems which are still open for these areas and finally answer some of the questions by 3D numerical modelling. The outline and aim of each chapter will be explained in detail in this chapter and in the following paragraphs.

1.1.1. Selection of study areas and data availability

In this research study I have tested 3D numerical modelling first for a small scale area (Val de Ruz area in Switzerland) and then for a large scale area (Eastern part of the Alps) (Fig. 1.1). Both of these two areas have a highly three dimensional subsurface tectonic structures and are perfectly suitable for building 3D digital models. In addition to that, the subsurface structures and structural history of both of these two areas have been subject of geological research for more than hundred years.

For the Val de Ruz area our input data strongly build on the work of Sommaruga (1995, 1997, 1999) and also Sommaruga and Burkhard (1997) who interpreted industrial seismic profiles from the southern Jura

Mountains and the Molasse Basin and combined them with the surface geology (see Chapter 2 for more details).

The second study area in my research is the whole Eastern part of the Alps (Eastern Alps + Southern Alps). Although this area is very well studied, many issues related to the deep structures still remain unsolved and matter of debate between geoscientists. In contrast to the Val de Ruz area, complete seismic sections are scarce, so I have constructed 30 new cross-sections and inserted them into the model as input data (see Chapters 3 and 4 for more details).

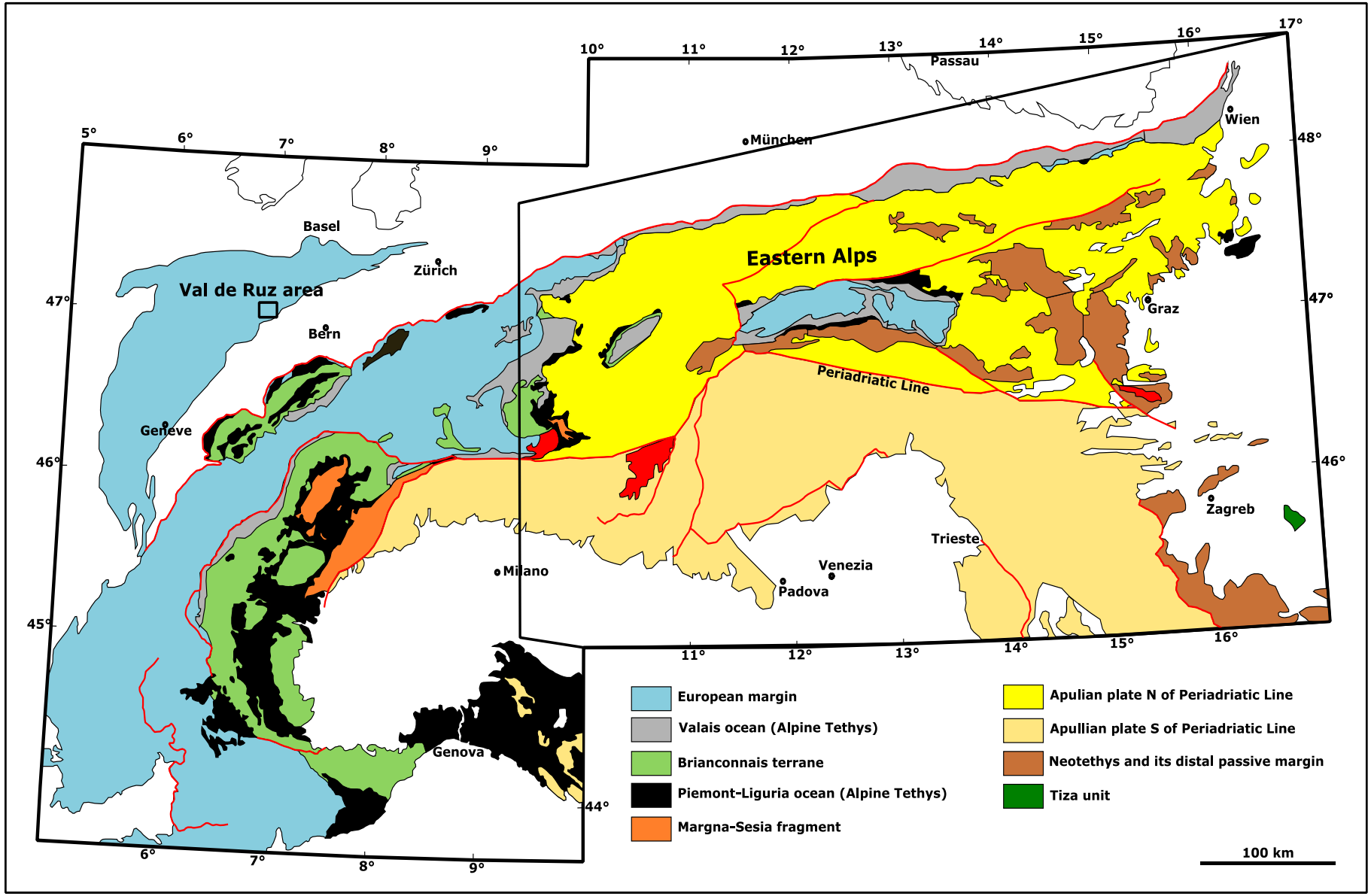

Figure 1.1: Simplified map of the major paleogeographic and tectonic units in the Alps from Schmid et al. 2004. Rectangle in the NW mark the study area of chapter 2 and the big rectangle in the middle to the most Eastern side of the map represent the study area of chapter 3 and 4.

1.2. MOVE

The MOVE application is a core product of Midland Valley Corporation. This application allows fully integrated 2D and 3D model building and analysis. It was designed by geologists for geologists and engineers for numerical modelling purposes and for testing different geological hypotheses and concepts. MOVE provides a platform for users to integrate all available data together (cross-sections, maps, 3D views and Google views) in one environment, construct 2D cross-sections for the desired area and finally build a kinematic and geometric 2D and 3D model which is geometrically valid according to the geological principles.

In other words, this package provides the users to build their model in either two or three dimensions for the desired area and then analyze the input data in various ways, extract more data from the finished model and test different hypotheses and ideas.

Compared to the other software packages in the field of geoscience, such as QGIS and Petrel, MOVE provides better and more user friendly environment (platform). In addition to the above, it is also possible to save the output files in different format and also export the 2D or 3D file to the third party link products such as Petrel.

1.2.1. General procedure in MOVE for building kinematic models

The general procedure for building a complete and valid geometric and kinematic 3D model by MOVE is as follows:

1. Inserting the DEM: In the first step, the Digital Elevation Model (DEM) for the desired area should be inserted into the model.

2. Inserting the geological map: In the next step, the geological map for the area should be inserted as a reference map beneath the DEM. This map will be used later as reference for inserting the profiles and digitizing the fault and thrust lines in the model. Therefore georeferencing the map is necessary and also very important before importing to the model. The geological map must be georeferenced by other third party software packages like QGIS before inserting to the model since it is not possible to georeference the geological map by MOVE. To do so, I have used QGIS for both of these two study areas and all the other reference maps.

3. Digitizing the geological map in 2D: After inserting DEM and georeferencing the geological map, the important characteristics of the area such as fault lines, thrust lines, anticlines and synclines should be digitized in the geological map. It is easier to do this step in map view mode or 2D view mode compared to the 3D view. I have digitized the lines by using the Line tool. This tool provides different options for the users (symbols, colors …) to define the objects in the model and also better visualize different lines in the other views.

4. Inserting the cross-sections in the Model: Before inserting the cross-sections (profiles) in the model, the position of the profiles should be

digitized in the referenced map. This work should also be done in map view. The ideal case is to digitize the profiles parallel to each other in order to reduce the error in the final model. When the positions of the profiles are defined (digitized), the image of each profile can be inserted perpendicular to the DEM and the Geological map in 3D view.

5. Digitizing the fault and thrust lines and defining Horizons in the cross-sections: After inserting the profiles to the model, all the lines of the layers (Horizons or Units) in the profiles should be digitized and defined separately for the model. For this purpose I have used the Horizon tool in section view (2D view) mode. Like the Line tool, the Horizontool also provides the user with different options (symbols, colors …) for defining different objects in the profiles.

6. Building the surfaces: After inserting all the input data (DEM, georeferenced map, profiles) for the model and digitizing the lines and horizons in the referenced map and profiles, the next step is to create the surfaces between the parallel profiles. This work is done by the Surface tool in the Model Building panel. Different options are available in the Surface tool and which option to use basically depends on the horizon and line shapes in the profiles. These different options also affect the error of the final model as well as the shape of the surface in 3D view.

7. Editing the model in 2D and 3D view: Before completing the 3D model, the profiles should be checked for consistency. Move allows the user to examine the input data in either two- or three-dimensional view.

8. Analyzing the profiles: After the model is finished, the software allows the user to analyze the input profiles in more detail. For example, one can

check whether the input profile is balanced or not and then edit and correct the input data as much as possible. For this purpose, I have used the balancing cross-sections tool in Analysis panel.

9. Building the volume blocks: This step allows measuring the volumes between two horizons. The Volume tool is designed for building the volumes or blocks between two surfaces. This tool also has different options but in my research, I have used the Tetra Volume option for this purpose.

These steps were followed and repeated for both of the projects (Val de Ruz area and Eastern Alps) in my research. After the model is finished as mentioned above, one can analyze the model in both 2D and 3D view and extract different types of data as an output like stereo-net plot, profiles in any desired angles and locations in the area, calculating the volumes etc. .

1.3. Outlines and contributions of the thesis

This thesis comprises five chapters. Each chapter is designed to address special issues that will be explained in details in the following paragraphs. Chapter 2 was published in the Swiss Journal of Geosciences in 2017 and chapter 3 and 4 will be submitted as peer-reviewed manuscripts soon. An outline of all these five chapters will be given in the following paragraphs.

In **Chapter 1**, which you just read, a general overview of the kinematic 3D modelling together with its applications in the field of geoscience, introducing the software (MOVE), steps that I have followed for building 3D

models in my study, and finally outlines and contributions of this research study has been given.

Chapter 2 represents the results of the first part of my PhD project. In this part, we have used and tested 3D modelling for a small synclinal basin (Val de Ruz area) in the internal part of the central Jura Mountains. The Val de Ruz area is characterized by different folds and thrusts which are interfering with a system of N-S striking, sinistral strike-slip faults systems. For this area different hypothesis have been proposed and we tried to investigate if 3D modelling could help us to understand the subsurface structures in more detail. For this rhomb shaped basin, I have constructed nine new profiles based on the seismic and surface geology data. The new profiles are better length-balanced than previous profiles and were inserted perpendicular to the overall strike in the model. In our model we assume no faulting in the pre-Mesozoic basement and no hidden flat-ramp tectonics in the subsurface in order to account for structurally high positions. As a consequence, the modelled cumulative, post-deformation thickness of Triassic strata locally exceeds 1500 meters, which we find in accordance with regional observations. From the geological 3D model, new cross-sections in any desired orientation and tectonic thickness variations of the layers can be extracted. The three output cross-sections presented are in excellent agreement with published reflection seismic data. The most important features of our 3D model for this area are (1) large thickness variations due to lateral flow of evaporites, and (2) new and plausible explanation of structural highs in terms of accumulation of Triassic strata by lateral flow.

This chapter was submitted to Swiss Journal of Geoscience in 2016 and accepted in January 2017. The original publication is available at www.Swissgeoscience.com.

Chapter 3 is devoted to the research about the Eastern Alps. For the second part of my PhD research we have decided to build a comprehensive 3D model for the whole eastern part of the Alps (Eastern Alps and Southern Alps) for the first time.

The tectonic evolution of the Eastern Alps involved subduction and collision processes during the Mesozoic and Cenozoic and resulted in a complicated structure at the surface where tectonic nappes are exposed, but also at depth where subducted lithospheric slabs appear to dip in different directions. The structure is highly three-dimensional and not completely understood. Using the modelling software MOVE (Midland Valley Co.), I built a three-dimensional geometric model of the Eastern part of the Alps including the major tectonic thrusts, basement-cover contacts, cross-cutting normal and strike-slip faults, and the Mohorovicic discontinuity (Moho). Modelling involved testing the compatibility of the many cross-sections and contour maps that have been published.

In this chapter I address three fundamental questions regarding the continent-continent collision in the Eastern Alps.

1. How much shortening occurred in the Eastern Alps since 30 Ma until now?

2. How much area from the European and Adriatic continents was destructed due to the collision?

3. What were the tectonic plate velocities and how do they compare with other available data such as GPS data?

The first results of our model allowed to calculate the shortening by two different methods and compare them with other available data. In addition to that I have calculated the average tectonic velocity between 3 and 6 mm per year which is in a good range compared to the other available data despite all the uncertainties due to the scarcity of information about deep crustal structures away from the seismic profiles.

Chapter 4 presents the further results that I obtained from the 3D model of chapter 3 with respect to the subduction of continental crust in the eastern part of the Alps.

In the last three decades, several studies have been carried out to answer some of the questions regarding the subsurface structure, the Alpine kinematics and the amount of subducted continental crust. For this part, I completed the 3D model in chapter 3 to address some of the problems regarding the subduction of continental crust in this part of the Alps. I have also calculated from the shortening data the total amount of material which disappeared. This crust deficit can be explained as a result of different processes like subduction, east-west extension (thinning) and finally erosion. The results imply a deficit of about 1*10^6 km^3 continental crust volume as a result of the collision since 30 Ma for both European and Adriatic continents in the eastern part of the Alps and the crustal deficit for the European continent is almost twice the amount for the Adriatic continent.

The presented data in this chapter contributed to find an answer for the following fundamental questions regarding the geodynamic evolution of the eastern Alpine lithosphere:

1. How much rock volume in the different tectonic units is still present in the Alps?

2. How much rock volume was subducted or destructed due to the Alpine orogeny?

3. What was the the subduction rate in the Alps?

The data in this chapter shows large-scale subduction of continental crust into the mantle both for the European continent and the Adriatic continent which is in line with previous research.

Finally **chapter 5** summarizes the main results and conclusions regarding the 3D modelling of the three previous chapters (chapter 2 to 4) and briefly evaluates the results of each chapter.

This chapter was submitted to Swiss Journal of Geoscience in 2016 and accepted in January 2017. The original publication is available at www.Swissgeoscience.com.

Chapter 2

Three-dimensional modelling of folds, thrusts, and strike-slip faults in the area of Val de Ruz (Jura Mountains, Switzerland)

Abstract

The Val-de-Ruz syncline is a northeast-southwest trending, rhomb-shaped synclinal basin in the internal part of the central Jura Mountains. The Mesozoic sediment succession is decoupled from the basement by a décollement horizon in Middle Triassic evaporite-bearing layers at depth and folding is associated with southeast-dipping thrust splays rooting into this décollement. The folds and thrusts also interfere with a system of N-S striking, sinistral strike-slip faults. A 3D model was constructed from the following input data: A digital elevation model, the 1:25 000 geological map of Switzerland, published contours of the top of basement based on drilling and seismics, and nine newly constructed cross-sections. The latter are based on surface geology and published seismic data. Cross-sections parallel to the northwestward transport direction, i.e. perpendicular to the overall strike, are line balanced. Anticlines are interpreted as faulted detachment folds, which initiated by buckling and associated flow of evaporites from synclinal to anticlinal areas. Anticlines were later broken by northwest-vergent thrusts and subsequently developed into fault-propagation folds during décollement from the basement and northwestward translation. The model assumes no faulting in the pre-Mesozoic basement and no hidden flat-ramp tectonics in the subsurface in order to account for structurally high

positions. As a consequence, the modelled cumulative, post-deformation thickness of Triassic strata locally exceeds 1500 meters, which is in accordance with regional observations. From the geological 3D model, new cross-sections in any desired orientation and tectonic thickness variations of the layers can be extracted. The three output cross-sections presented are in excellent agreement with published reflection seismic data. The most important features of the new model are (1) large thickness variations due to lateral flow of evaporites, and (2) new and plausible explanation of structural highs in terms of accumulation of Triassic strata by lateral flow.

2.1. Introduction

The Jura Mountains in western Switzerland are a foreland fold-and-thrust belt and represent the youngest, most external part on the northwestern side of the Alpine orogen (Fig. 2.1; Laubscher 1961, 1965; Burkhard 1990; Philippe et al. 1996; Sommaruga 1999). They describe the shape of a northwest-facing crescent, which at its southern end merges with the most external chains of the Western Alps. To the northeast of this junction, the Swiss Molasse Basin, representing the Oligocene to Miocene foreland basin of the Alps, lies between the Jura Mountains and the Alps. The mountain range itself consists of Mesozoic to Tertiary sedimentary rocks with upper Jurassic platform carbonates (Malm) forming the backbones of prominent anticlines. To the West, the sediment succession of the Jura Mountains is thrust over the fill of the Rhone-Bresse Graben by several kilometres. In the eastern Jura Mountains, shortening of the sedimentary succession ceases gradually and the last remaining anticlines in the Mesozoic series plunge under the sediments of the

Molasse Basin. The internal, topographically higher part of the Jura Mountains is characterized by faulted detachment folds (“Folded Jura” or “Haute Chaîne”), whereas the external part (“Plateau Jura”) displays lozenge-shaped, undeformed plateaus (“Plateaux”) separated by faulted anticlines (“Faisceaux”). Deformation started in Middle Miocene and lasted at least into Pliocene times (Kälin 1997), with some evidence for still on going folding in the most external part of the Jura (Madritsch et

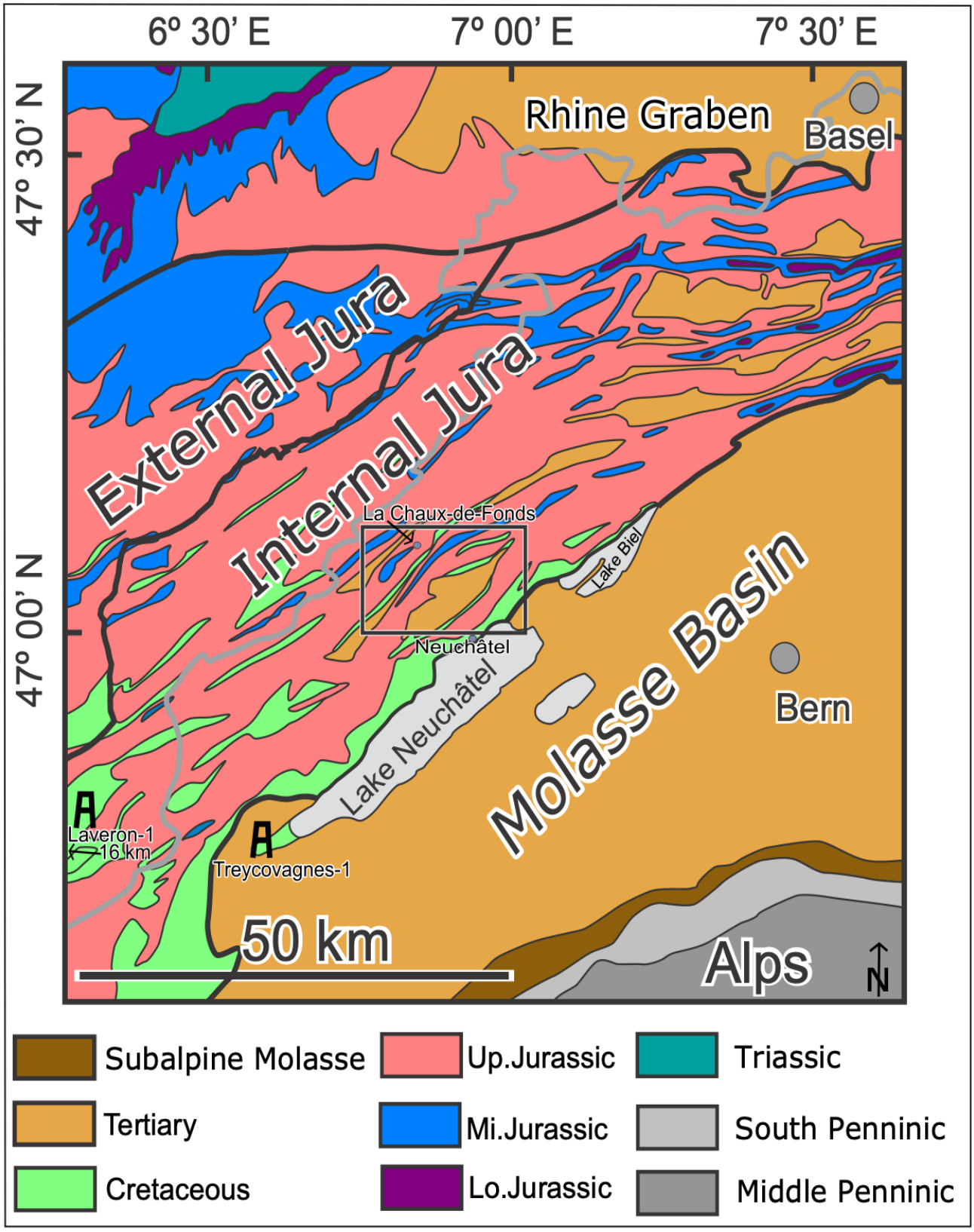

Figure 2.1: Geological overview map of the central Jura Mountains based on the Geological Map of Switzerland (Bundesamt für Wasser und Geologie 2005). Thick black lines are the front of the Jura in the North, the boundary between Internal and External Jura in the middle, and the Jura/Molasse boundary in the South. Grey line is the French/Swiss border. Locations of drill holes Laveron-1 and Treycovagnes-1 are indicated. Rectangle marks the map area of Fig. 2.2.

al. 2010). The folded Jura is classic for studying thin-skinned tectonics and several pioneering studies on décollement tectonics and cross-section

balancing were performed in this mountain chain (Buxdorf 1916; Laubscher 1961, 1965; Mitra 2003; Affolter & Gratier 2004).

The tectonic evolution of the Jura Mountains was governed by decoupling along evaporites in the Middle Triassic (Muschelkalk) and Upper Triassic (Keuper) sedimentary successions. Isopachs of the Muschelkalk and Keuper are similar in shape to the outline of the Jura Mountains, together reaching 1000 m and more in the internal western part while they are only several tens of meters thick in the adjacent Helvetic units in the Alps (Loup 1992; Sommaruga 1997, 1999; Affolter and Gratier 2004). This suggests that the lateral termination of the Jura Mountains to the East and to the South results from the pinching-out of the evaporites. The fact that the Mesozoic strata are spectacularly folded in the Jura Mountains whereas folding is hardly visible in the Molasse Basin has led some researchers to seek the origin of the folding in deformation of the basement under the Jura (e.g. Aubert 1945; Pavoni 1961; Ziegler 1982). Others have assumed that shortening in the Jura Mountains is completely allochthonous and that the corresponding shortening of the basement took place on the other side of the Molasse Basin within the Alps, hence, tens of kilometres to the Southeast (Buxtorf 1907, 1916; Laubscher 1961). This theory, called the “Fernschubhypothese”, is now accepted by most authors although it is acknowledged that pre-existing Paleozoic and Tertiary normal faults played a role in the localization and development of contractional structures, i.e. folds and thrusts (Ustaszewski and Schmid 2006; Malz et al. 2016). The generally southeastward- or hinterland-dipping thrusts in the Jura Mountains are assumed to root into a major floor thrust located within or at the bottom of the Triassic formations (Buxdorf 1907, 1916; Burkhard 1990). The mechanical

basement beneath this floor thrust includes Variscan basement and locally also Permo-Carboniferous troughs (Diebold 1988; Madritsch et al. 2008) as well as Lower Triassic fluvial sediments (Buntsandstein). The floor thrust continues beneath the Molasse Basin and connects shortening of the Mesozoic-Tertiary cover in the Jura mountains with basement shortening in the external zone of the Alps (e.g. Laubscher 1961). Its existence is confirmed by highly deformed Triassic rocks found in wells in the Molasse Basin in the hinterland of the western (Fischer and Luterbacher, 1963) and eastern Jura Mountains (Jordan 1992). The relatively weak deformation in the post-Triassic rocks in the subsurface of the Molasse Basin is explained by the thickness of the Tertiary Molasse sediments, which prevented the Mesozoic layers to lift off and form anticlines or thrust duplexes (e.g. Laubscher 1961). In the ductile Triassic sediments, however, folds with wavelengths around 10 kilometres and a few hundred meters amplitude exist beneath the Molasse Basin as well (Bitterli 1972; Sommaruga 1995). Towards northwest the thickness of the Molasse sedimentary pile progressively decreases while the thickness of the soft Triassic succession increases, allowing the post-Triassic succession to detach from the basement and to become folded and imbricated in the Jura Mountains.

Compared to the Swiss Molasse Basin, which was subject to hydrocarbon prospection, the density of wells and reflection seismic lines is scarce in most of the Jura Mountains and the subsurface architecture remains a matter of debate. In particular, the existence of structurally high domains, i.e. areas where the entire Mesozoic succession is at a relatively high elevation, has been interpreted in controversial ways. These high domains have been explained by (1) local basement highs (Guellec et al. 1990; Pfiffner et al. 1997) or (2)

exceptional thickness of Triassic strata, either of sedimentary or tectonic origin (e.g., Sommaruga 1997; Affolter and Gratier 2004). Recently, Schori et al. (2015) have proposed (3) regional doubling of the lower part of the sedimentary succession above the mechanical basement for the Chasseral area northwest of Lake Biel. This doubling would be the result of a large-offset splay rooting in the floor thrust and forming a map-scale upper flat in Middle Jurassic (Dogger) claystone (Opalinus clay). It would thus account for about 800 meters of structural uplift.

Here I present a three-dimensional digital model of the architecture of the 1:25000 geological map sheet “Val de Ruz” (Bourquin et al. 1968), which is located northwest of the northern end of Lake Neuchatel in the central Jura Mountains (Fig. 2.1, 2.2). The area contains the wide Val-de-Ruz syncline and a series of thrust-related anti- and synclines to the northwest and to the southeast. It is perfectly suitable for building a three-dimensional digital model and testing it since an excellent geological sheet is available, abundant published and interpreted reflection seismic data exist. Moreover, the overall structural architecture including the top of the mechanical basement has been the subject of extensive investigation (Sommaruga, 1997, and references therein). The model was built using the structural modelling software package Move (Version 2014) of Midland Valley Corporation. Three-dimensional geometric modelling has successfully been used to explore complex tectonic structures (Tanner et al. 2003; Maxelon & Mancktelow 2005; Marquer et al. 2006; Zanchi et al. 2009; Sala et al. 2014). Apart from visualization, a major advantage is that the process of modelling implies testing the input data for consistency and testing tectonic hypotheses for their geometric feasibility.

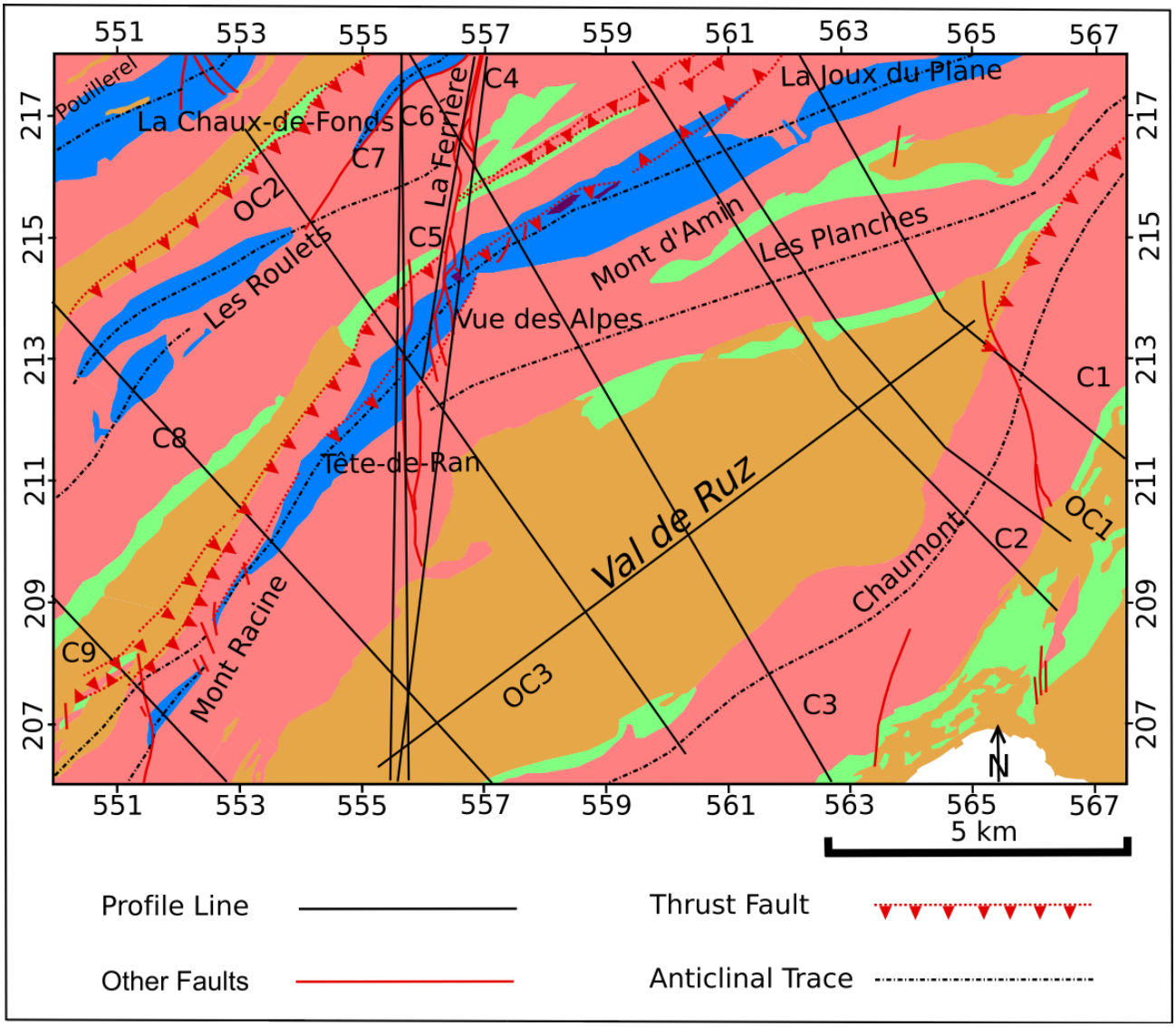

Figure 2.2: Simplified geological map of Val de Ruz without Quaternary cover, based on Atlas géologique de la Suisse 1:25'000, feuille 51 Val de Ruz (Bourquin et al., 1968). Profile lines of input profiles (C1 to C9) and output profiles (OC1 to OC3) are indicated. Coordinates refer to the kilometric grid of Switzerland. For the colours, see Fig. 2.3.

Moreover, modelling software allows the extraction of additional information from the model, e.g. cross-sections in any desired orientation, orientation statistics, and volumes or thicknesses of geological bodies. On the other hand, geological data generally need to be simplified for the modelling process, which may lead to mistakes. Moreover, it has to be kept in mind that a geometrically feasible model is not necessarily correct. In the present study, I constructed a model of the Val de Ruz fold structures (1) in order to investigate if simple geometric assumptions (see below) lead to an acceptable 3D-architecture, and (2) which deformation style would be suggested by the derived architecture.

This contribution strongly builds on the work of Sommaruga (1995, 1997,1999) and Sommaruga and Burkhard (1997), who interpreted industrial seismic profiles from the southern Jura Mountains and the Molasse Basin and combined them with the surface geology into a coherent tectonic picture of the Internal Jura Mountains around the Val de Ruz and the adjacent Molasse Basin. I took the results of these studies as input for my modelling as my newly constructed cross-sections largely agree with their approach regarding structural style. Like these authors, I assume no deformation in the basement and a simple ramp-flat architecture, in which thrusts observed at the surface diverge as splays from the floor thrust at the top of the mechanical basement. I actually imply rather free formation of anti- and synclines in the Triassic rocks and comparably small-offset thrusts in the sedimentary pile above. This simple approach leads to extremely well balanced cross-sections. The model predicts originally thick Triassic sequences, which are considerably over-thickened below antiforms. Accordingly, bulk shortening is limited, i.e. around 7% and at most 17%. I will discuss the proposed architecture, the inherent assumptions and alternative views in the light of regional observations in detail after the presentation of the model.

2.2. Structural edifice in the study area

The study area is characterized by faulted anticlines, which expose Dogger and Malm in their cores, forming topographic highs and synclines, which contain Lower Cretaceous and thin Tertiary sediments (Fig. 2.2). The anticlines trend

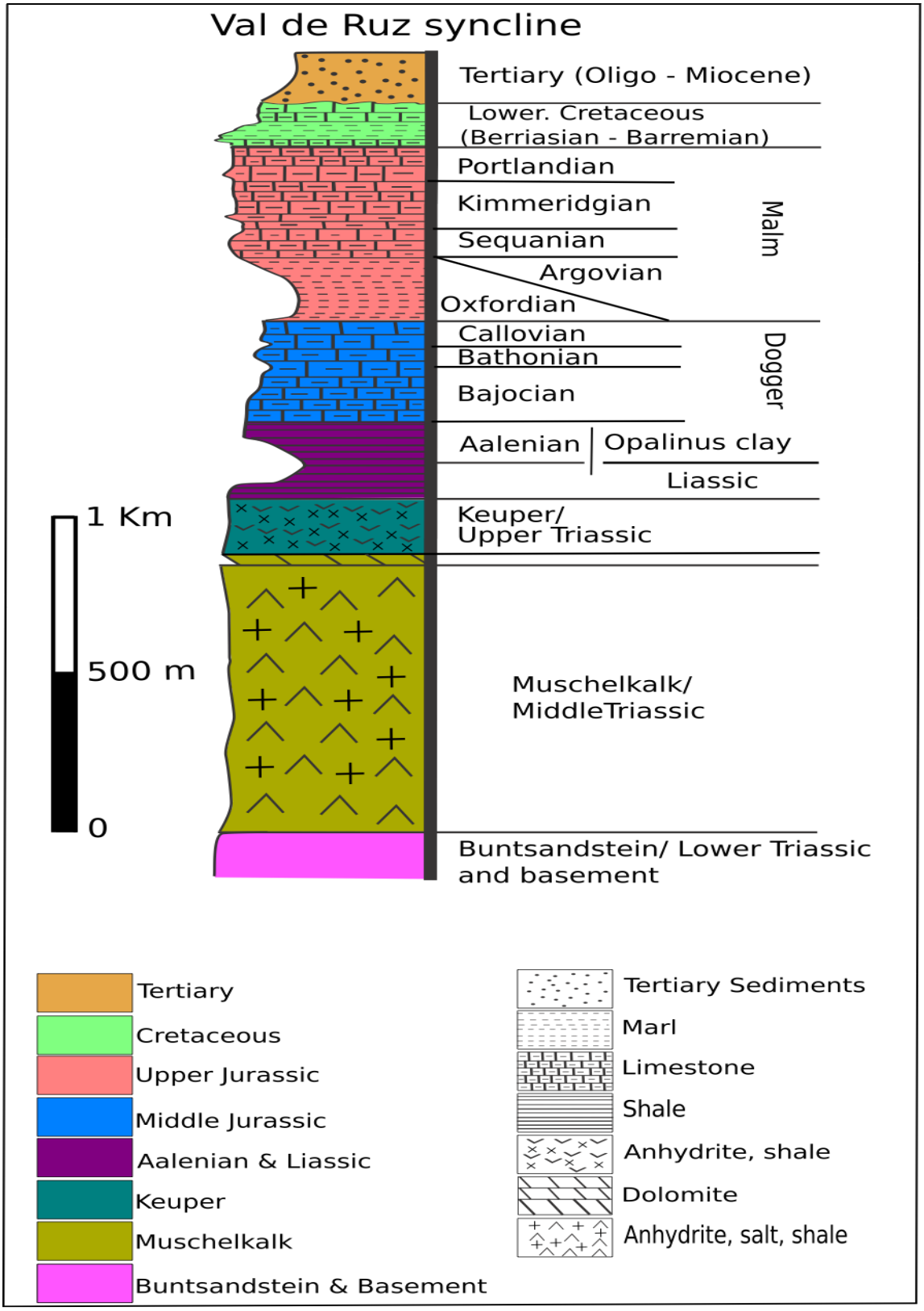

Figure 2.3: Stratigraphic column of Val de Ruz syncline, simplified from Sommaruga (1997). These colours are used in figures 2.2, 2.4, 2. 5, 2.7 and appendix A.

overall southwest-northeast. They are dominantly thrust towards northwest over the synclines but some backthrusting occurs as well. In the southeast of

the study area, the large Chaumont Anticline exposes formations of the Malm. North of Lake Neuchatel, the trend of this anticline changes from north-northeast in the north to northeast further south. An associated thrust cutting across the external limb is only exposed in the Northeast. Towards southwest, this thrust disappears below the Quaternary cover of the Val de Ruz. An additional very minor anticline appears more internally just north of Lake Neuchatel, exposing a narrow stripe of Malm in the core. Northwest of the Chaumont Anticline follows the rhomb-shaped Val-de-Ruz syncline. It contains Oligo-Miocene Molasse sediments but is mostly covered by fluvio-glacial Quaternary sediments. Where not covered by the Quaternary, the dip of the Mesozoic and Tertiary strata is mostly 0-20º towards southeast. Also the smooth, gently northwestward rising topography suggests a rather consistent dip. The dip of sedimentary strata is in good agreement, i.e. in parallelism with the top of the mechanical basement, which was contoured using regional reflection seismic data and is interpreted as the base of the Muschelkalk strata (Sommaruga 1997). The local reflection seismic data across the Val de Ruz is generally of very good quality and shows a simple, undeformed pile of reflectors parallel to the contoured top-basement surface (Sommaruga 1997, 1999). Hence, the Val de Ruz appears to expose an internally almost undeformed, complete sedimentary pile on top of a hangingwall thrust flat. The syncline might thus provide a reference section to estimate the original thickness of the sedimentary pile (Sommaruga 1999). This parameter is essential for

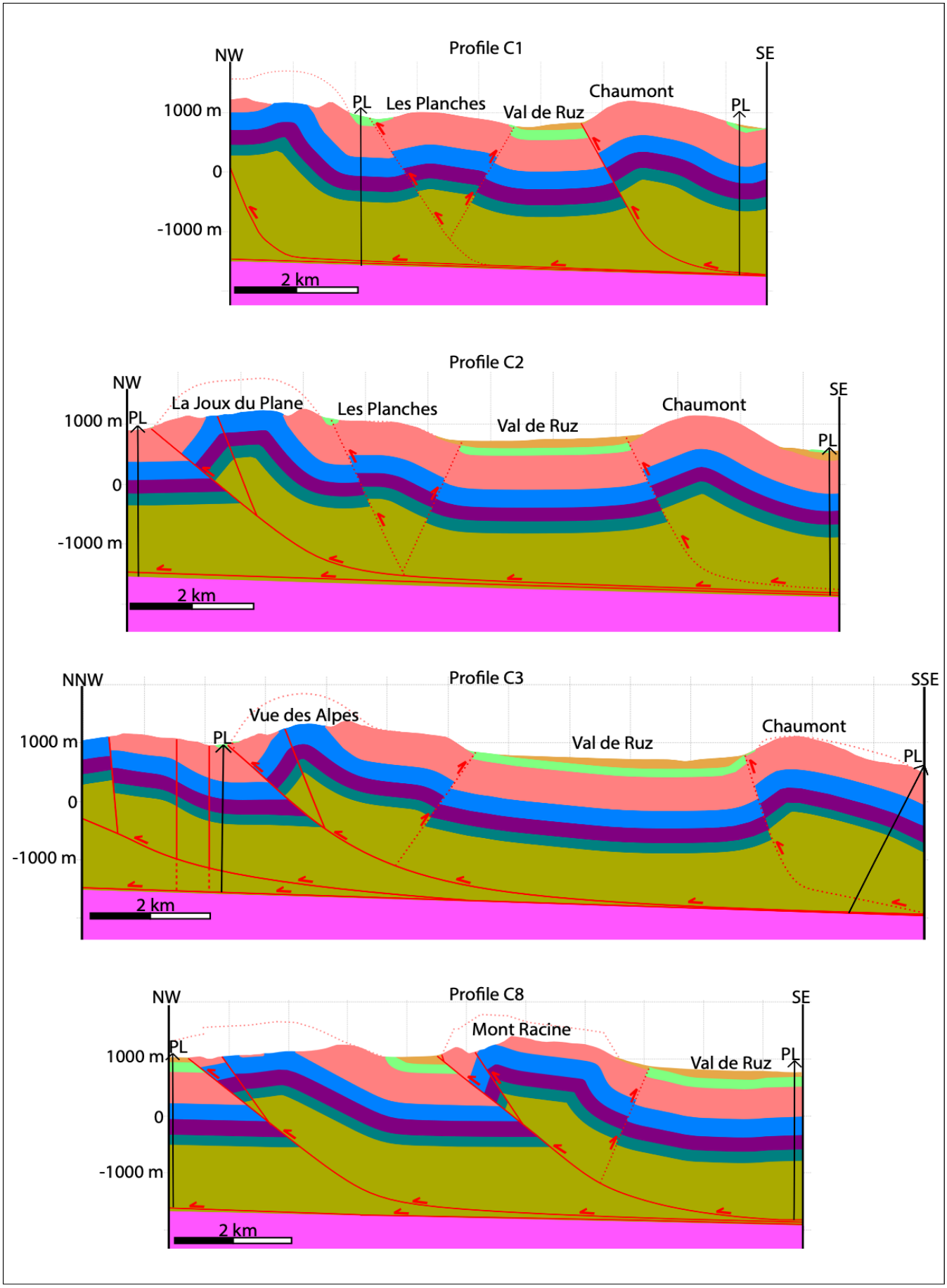

Figure 2.4: Input profiles. Location of the profiles: see Fig. 2.2. PL: Pin lines for line balancing. Thrusts exposed at the surface are shown as solid red lines, blind thrusts are dashed. Tear faults are subvertical and dashed in the lower part since their extension is uncertain. Colours: See Fig. 2.3.

The construction of line-balanced cross-sections as such sections typically assume constant layer thicknesses.

To the northwest of the Val-de-Ruz syncline follows the dominating anticline on the map sheet, which widely exposes Middle Jurassic strata in its core. The southwestern part of this anticline (Mont Racine, Tête de Ran) trends northeast to north-northeast, the northeastern part (Mont d'Amin, Joux du Plane) trends east-northeast. In the area where the trend changes, the anticline is offset by a system of minor, en-échelon strike-slip faults, which form the southern tip of the major sinistral La Ferrière strike-slip fault (Tschanz 1990; Sommaruga 1997). These strike-slip faults are located between the profile traces C4 and C7 shown in Fig. 2.2. Similarly oriented, small strike-slip faults occur also in other parts of the area, e.g. at Chaumont and Mont Racine. The Mont d'Amin - La Joux du Plane anticline on the eastern side of the strike-slip zone is not directly adjacent to the Val de Ruz syncline. A tight syncline with Cretaceous in the core and a gentle anticline (Les Planches Anticline) exposing Malm appear in between. Hence, anti- and synclines are discontinuous across the strike-slip fault system and not only rigidly displaced, suggesting that the faults were active as tear faults during folding and thrusting. In the northwestern corner of the map sheet, there is another couple of complex anticlines (Les Roulets and Pouillerel) separated by synclines. The structurally deepest syncline is that of La Chaux-de-Fonds containing Tertiary beds up to Late Middle Miocene age. The geometries of these folds outside the map sheet to the north are actually substantially different to both sides of the La Ferrière fault (Sommaruga 1997). The particular shape of the Val-de-Ruz syncline results from the southwestward divergence of the Les Planches anticline and the Chaumont anticline and the

following convergence outside the study area to the southwest (Fig. 2.1, 2.2). Such truly 3-dimensional structures are seen at several places in the Jura Mountains, exposing further rhomb-shaped synclines such as the Delémont syncline (Keller and Liniger 1930). This architecture may partly result from simultaneous distributed buckling and subsequent lateral growth of anticlines into a non-cylindrical pattern (Grasemann & Schmalholz 2012). On the other hand, pre-existing faults inherited from Rhine Graben rifting also play an important role (Laubscher 1972).

The exposed Mesozoic-Tertiary succession is an alternation of competent limestone and incompetent marl and shale layers (Fig. 2.3; Bourquin et al. 1968; Sommaruga 1997, 1999). Thin Tertiary sediments of the Molasse rest unconformably on the Lower Cretaceous strata consisting of alternating marls and limestones. The underlying Middle and Upper Malm formations are formed by massive limestones, which represent the major competent unit and define local fold geometry and topography. The lithologies of the Lower Malm are thick marls ("Argovian"). Below a brief sedimentary gap follow dominantly thick, oolitic limestones with some intercalations of marls in the Dogger strata. Lower Dogger (Aalenien) and the uppermost Liassic are represented by a prominent black shale, the Opalinus clay (Fig. 2.3). The latter is the lowermost unit in the study area, which is exposed in structural continuity. It occurs only in small outcrops in the core of the Mont d'Amin anticline and also, together with some slivers of Liassic rocks, along the La Ferrière fault. The deeper units do not reach the surface. Their thickness and the thickness of the Opalinus clay in the study area are only inferred from seismic interpretation and correlation with well logs outside the study area (Sommaruga 1997). Sommaruga (1997, 1999)

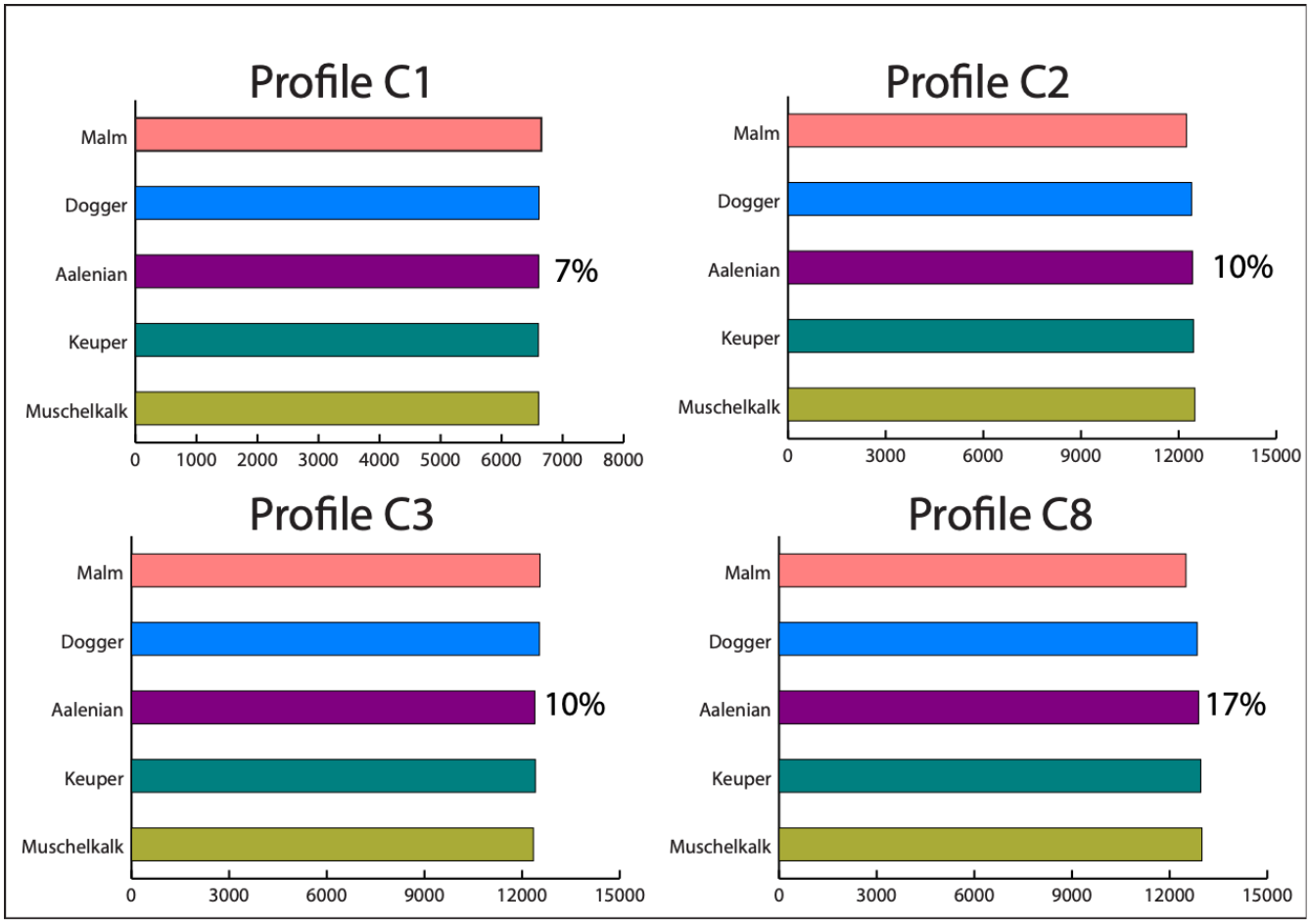

Figure 2.5: Line balancing for the input profiles in Fig. 2.4. The bars show the length of the top of the respective stratigraphic units, e.g. "Malm" means the length of the top of the Malm. Numbers on the horizontal axis are meters. Average percentage of shortening of the layers is indicated for each profile. All profiles are well balanced, i.e. differences in bed length are small.

distinguishes a Triassic Unit I (corresponding to Keuper in the Germanic facies) and a Triassic Unit II (corresponding to Muschelkalk). Both units are extremely ductile and can contain significant portions of evaporites (rock salt and/or gypsum) besides dominantly shallow marine limestones in the Muschelkalk and terrestrial clastic sediments in the Keuper series. Sommaruga (1997) interprets a distinct reflector (reflector H) within the Triassic series as dolomites typically found in the uppermost Muschelkalk. Because of the indirect evidence, however, she uses the terms Triassic Unit 1 and 2. I adopt the thickness of Triassic series I and II from her correlation but for simplicity use the terms Muschelkalk and Keuper, respectively. The main décollement horizon/floor thrust in this part of the Jura Mountains is assumed to be at the base or within

the Muschelkalk strata, although few well data in the wider vicinity suggest considerable deformation and internal stacking also in the Keuper formations (Sommaruga et al. 2012). The view that there is little thrusting within the Keuper in the study area, is supported by the identification of the above mentioned reflector H.

This reflector appears consistently deformed with the younger strata and involved in the ramp-flat architecture. Units below the floor thrust are Lower Triassic fluvial sandstones (Buntsandstein), possible Permo-Carboniferous graben fill, and Variscan basement, lumped here together as mechanical basement. Surfaces below reflector H, in particular the very important top of the mechanical basement, are not very clearly resolved in seismic sections; hence some uncertainty remains about its actual depth.

2.3. Three-dimensional model

2.3.1. Data and building strategy

I constructed nine cross-sections as input constraints for the 3D-model (Fig. 2, 4) (to see all nine cross-sections, see Appendix 1). Four of these are in the vicinity of the La-Ferrière fault and oriented north south, parallel to the fault, in order to define the geometry in this structurally complicated zone. The other cross-sections are oriented perpendicular to the local strike of bedding and fold axial planes, i.e. broadly northwest-southeast (Fig. 2.2). Using geological

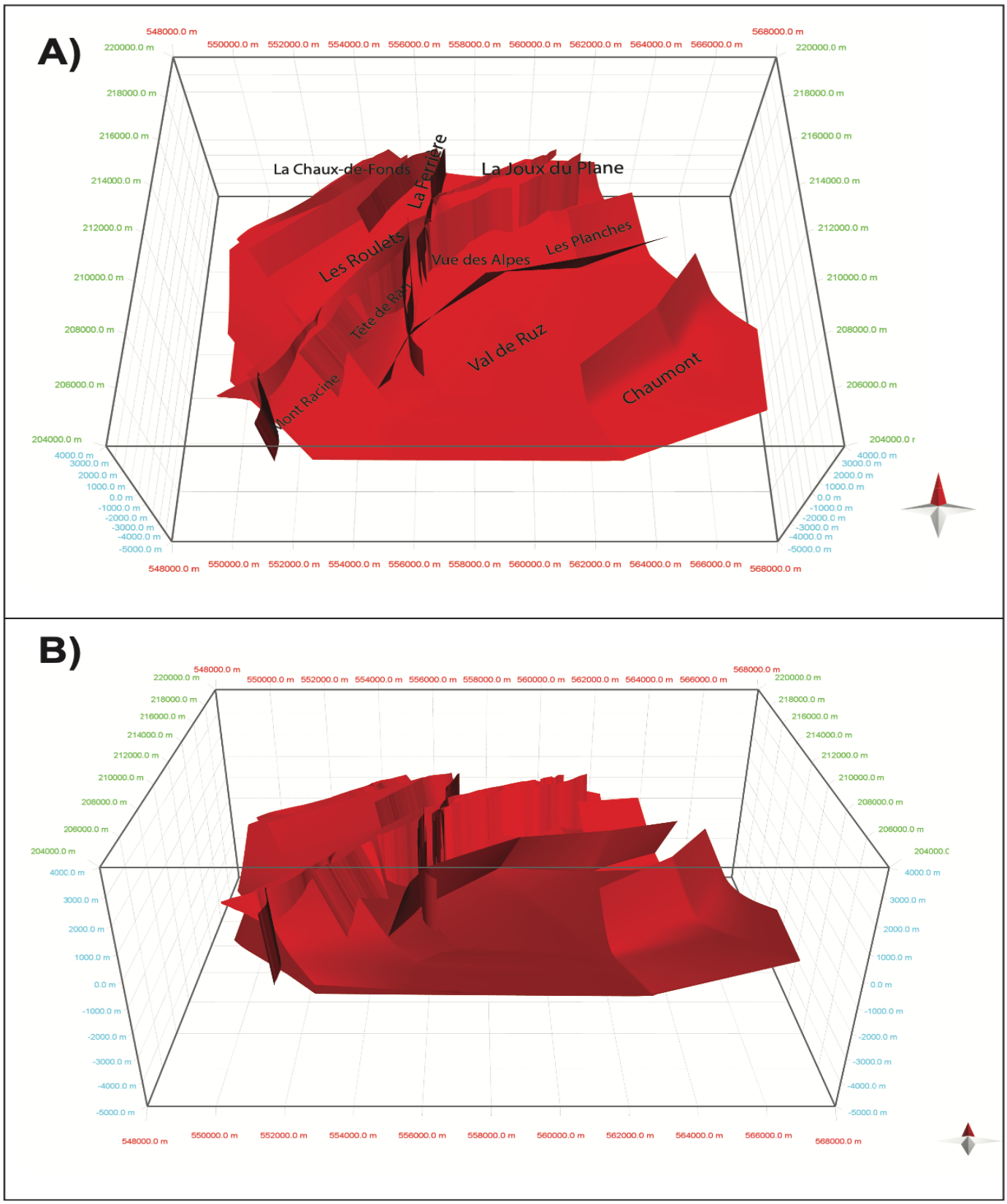

Figure 2.6: Fault surfaces of the model, viewed in two different directions. North-south oriented faults are parts of the La Ferrière strike-slip fault system. North direction indicated by red peak of the compass rose. Green and red numbers around the box are Swiss coordinates, blue numbers depth.

surface information (Bourquin et al. 1968) and assuming a floor thrust at the top of the contoured mechanical basement at the base of the Muschelkalk series (Sommaruga 1999), the construction follows concepts of ramp-flat thrusting

and associated fault-bend folding (e.g. Suppe 1983; Suppe and Medwedeff 1990). We used classic “thrust-belt rules” allowing e.g. to predict the ramp dip from back limb orientation or to infer the lower end of a ramp using the axial plane of the syncline at the bottom of the back limb (Suppe 1983). The lithological column is somewhat simplified (Fig. 2.3). However, as I assume coherent deformation from the Tertiary down to the top of the Muschelkalk series, lithological boundaries in figure 2.4 are merely passive markers. The thickness of the strata from the Cretaceous series down to the Keuper series were taken from the depth conversion of Sommaruga and Burkhard (1997; their figure 7.1-4), which for the exposed units in the study area are very similar to thicknesses estimated in the field (Guellec et al. 1990). Parallel folding with constant layer thickness was assumed for the construction. The location of the floor thrust was taken from Fig. 20 of Sommaruga (1999), a regional contour map based on depth conversion of seismic sections and drill-hole data. According to this map, the top of the mechanical basement dips shallowly southward in the model area, ranging from ca. 1600 m below sea level in the North to ca. 1900 m below sea level in the South. However, as mentioned above, this surface is rather poorly imaged on the seismic lines. A caveat about the accuracy of this contour map in the study area is posed by the fact that the only nearby well that reaches the Lower Triassic sandstones, the well

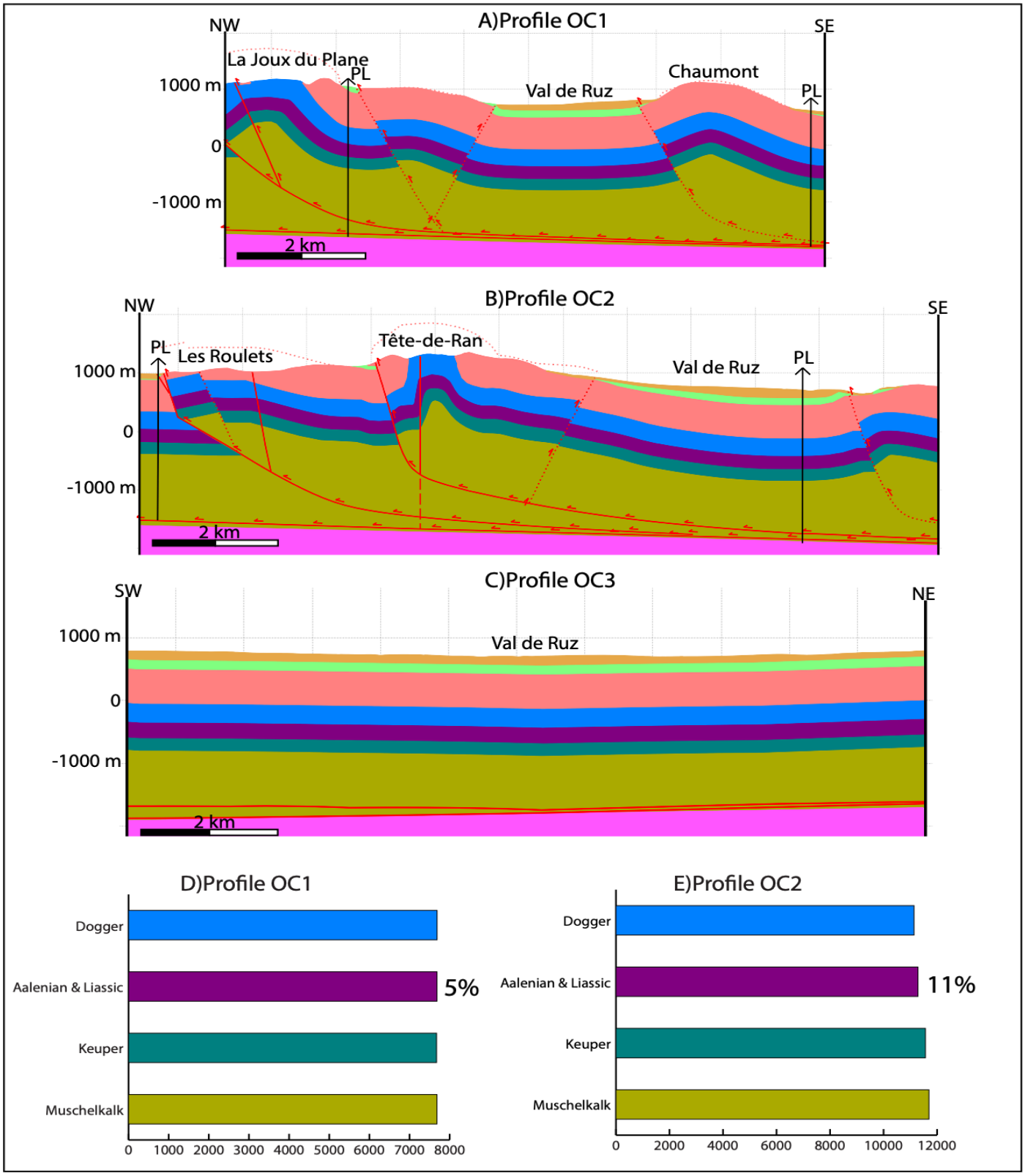

Figure 2.7: ***a-c*** *Profiles extracted from the model. Location of the profiles: see Fig. 2. PL: Pin lines for length balancing.* ***d,e*** *line balancing for two profiles (A and B). The extracted profiles are well line-balanced. Colours as in Fig. 3.*

"Treycovagnes-1" (Fig. 2.1; Sommaruga et al. 2012), enters the Lower Triassic ca. 300 meters higher than the general trend of the contour lines would predict,

which causes the proposition of a local basement high in the map of Sommaruga (1999). The well is located outside the map sheet southwest of Lake Neuchatel at the boundary between Molasse and folded Jura (Fig. 2.1), but it is the only well in a wider area that penetrates the Muschelkalk series. Also well “Laveron-1” located some 50 kilometres west of Lake Neuchatel in the Plateau Jura corresponds to a local basement high in the contour map (Sommaruga 1999). Hence, the actual depth of the mechanical basement may be somewhat shallower, and consequently also the thickness of the Muschelkalk series smaller than in the profile constructions (Fig. 2.4).

Seismic lines and interpreted geological cross-sections presented in Sommaruga (1997) were considered in my construction. My sections are quite similar to Sommaruga’s and the ones presented recently in a report on the geothermal potential of the area (Groupe de travail PGN 2008). During profile construction I assumed that the southeast-dipping fore-thrusts continue through the Muschelkalk series and curve into parallelism with the top of the mechanical basement, but they might as well root within the Muschelkalk series or even dissipate in distributed deformation. The northwest-dipping back-thrusts are interpreted to terminate when reaching more prominent fore-thrusts. The NW-SE-oriented profiles C1, C2, C3 and C8 were checked for plausibility by line balancing between pin lines placed in the synclines. The line length is well

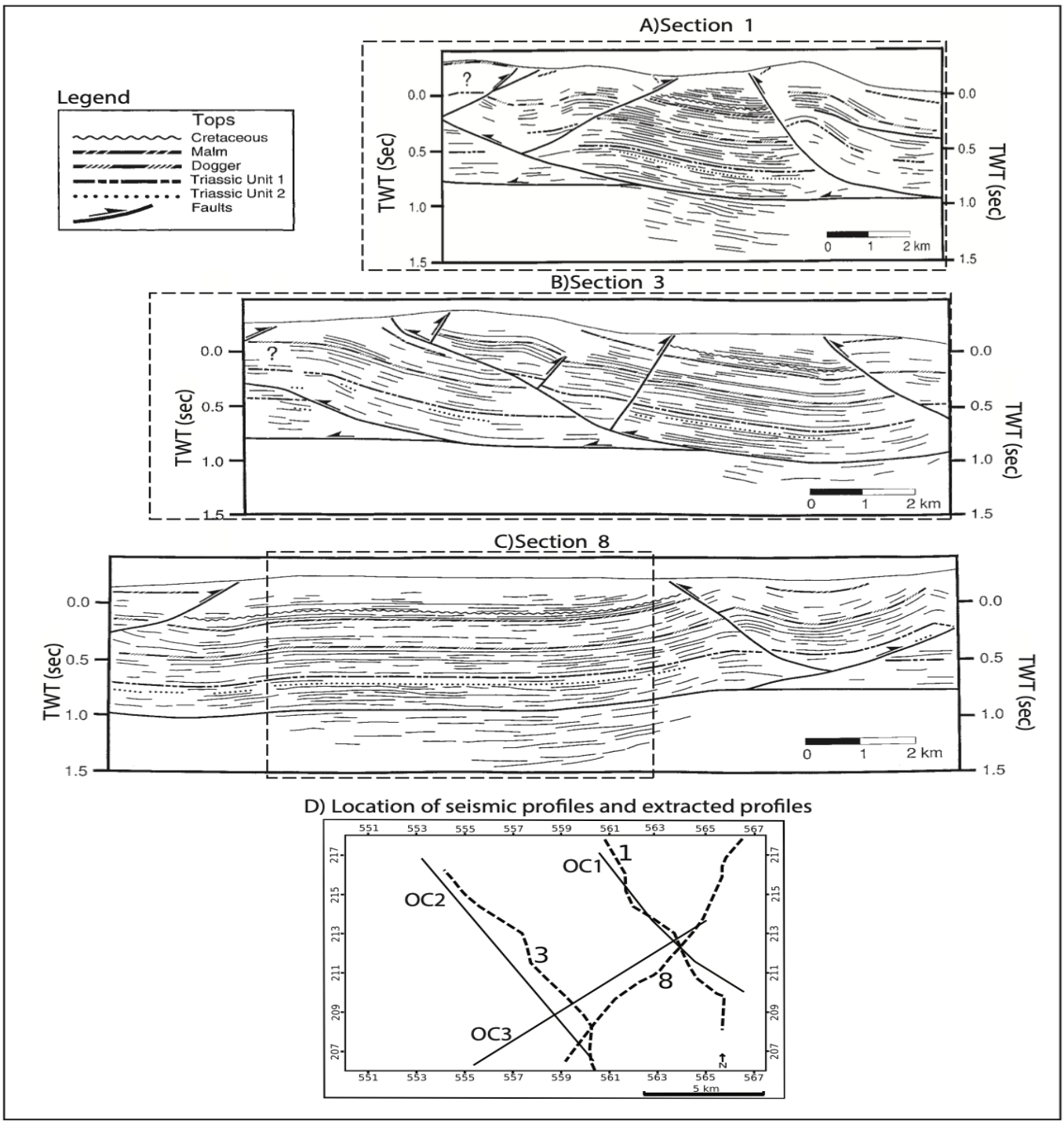

Figure 2.8: ***a-c*** *Seismic profiles along extracted cross-sections, from Sommaruga (1997). Dashed frames refer to the profiles as shown in Fig. 2.7.* ***d*** *Location of the seismic profiles (dashed lines) and extracted profiles (solid lines). Note close correspondence between seismic profiles and profiles extracted from the model.*

balanced for all cross-sections (Fig. 2.5). The thickness of the Muschelkalk in the profiles is variable; it results from the distance between the base of Keuper and the top of the basement. I allowed distributed deformation (flow) in this unit at locations where flow explains observations at the surface better than a pure

ramp-flat geometry. For example, the saucer shape of some synclines (e.g. Profile C1), with a variable thickness of the Muschelkalk under the syncline, is a feature that would not occur if the folds were pure fault bend or fault-propagation folds; if they were, synclines would be defined as lower flats and the bedding would remain perfectly parallel to the dip of the floor thrust in southeastward direction until being cut off by the next, structurally higher thrust below the adjacent anticline (Suppe 1983; Suppe and Medwedeff 1990).

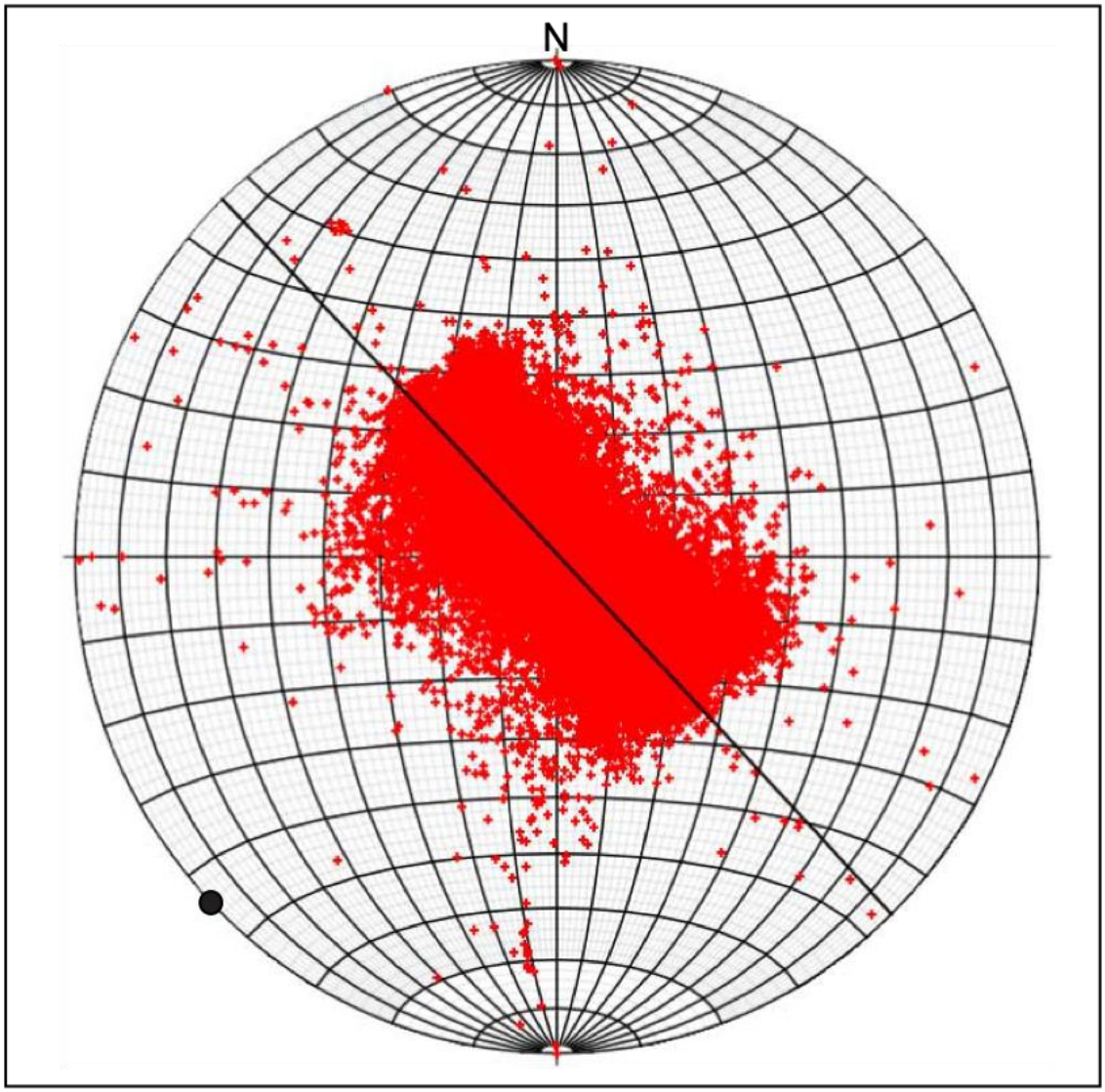

Figure 2.9: Schmidt net (lower hemisphere) showing 82382 poles to the Earth's surface as calculated from the digital elevation model, for the entire model area. Best-fit great circle of the orientation distribution is indicated. Filled circle indicates calculated "topographic fold axis" oriented SW-NE, i.e. parallel to the average fold orientation in the area.

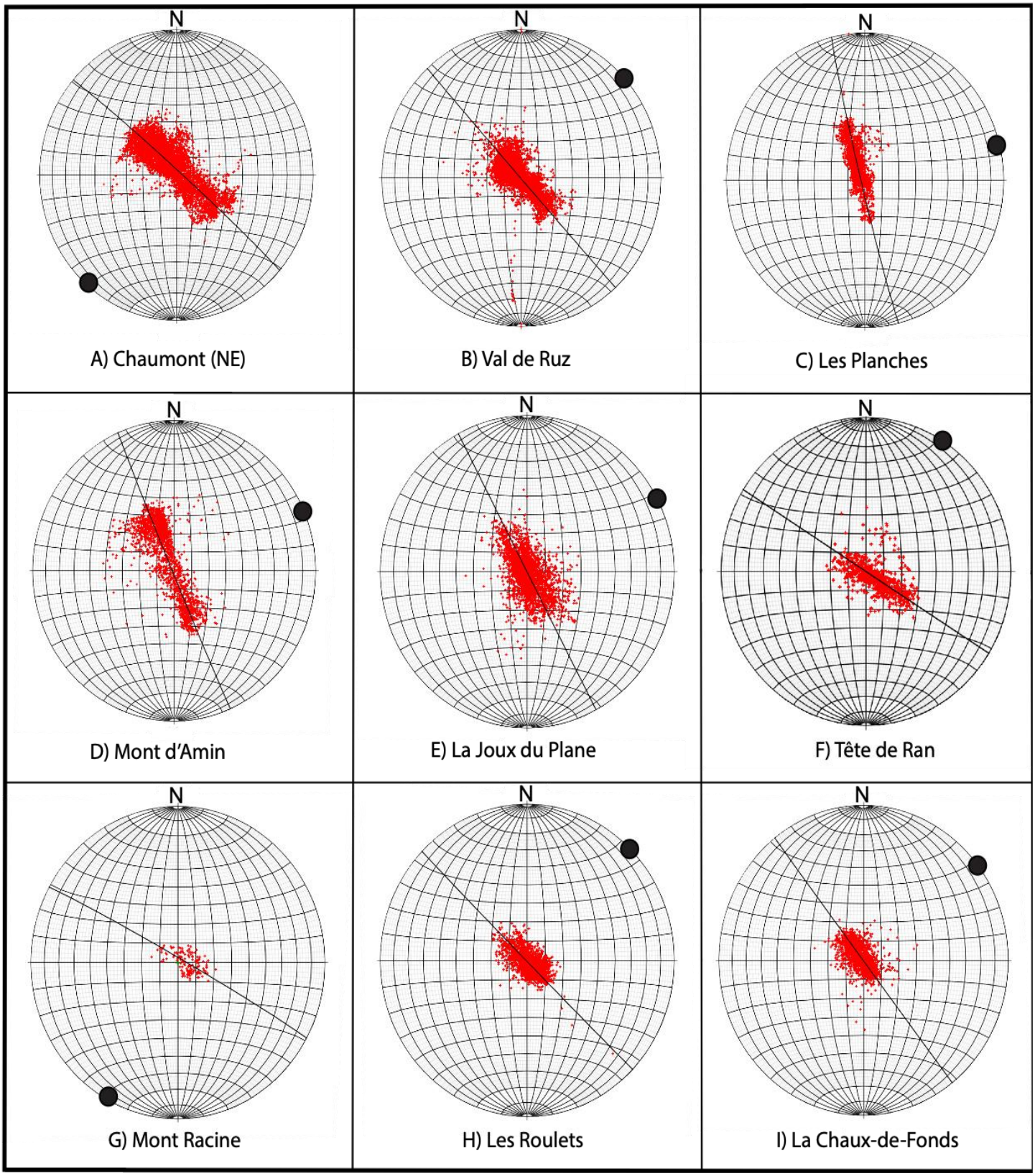

Figure 2.10: Schmidt nets (lower hemisphere) showing orientation distribution of Earth's surface, determined from digital elevation model, for parts of the area. Great circles and filled circles as in Fig. 9. See Fig. 2 for location of the subareas, and Tab. 1 for comparison of the "topographic fold axes" with structural fold axes from Sommaruga and Burkhard (1997). The difference in trend is small for ENE-trending anticlines (e.g., Mont d'Amin) and partly large for NNE-trending anticlines (e.g., NE part of Chaumont).

However, in several places in the Jura Mountains, the domains immediately below thrusts appear to be structurally lifted, suggesting a continuation of the forelimb of the antiform below the thrust. A prominent example is the

Weissenstein anticline in the northern Jura Mountains, where this observation has led to the rather far-fetched proposition of a series of small blind backthrusts beneath the ramp (Laubscher 2003). The saucer shape of synclines illustrates that the folds originally formed as detachment folds.

Buckling of the higher Mesozoic succession under horizontal compression was accommodated by lateral flow of Muschelkalk evaporites from synclinal to anticlinal areas, leading to the observed thickness changes under the synclines even before thrusting started (Sommaruga 1999; Mitra 2003). Folds subsequently developed into fault-propagation folds and where then broken and imbricated by the northwest-directed thrusts. This scheme is also supported by the fact that in the entire Jura Mountains, cross-sections constructed in a pure ramp-flat approach, i.e. using constant thickness also in the Triassic strata, systematically run into balancing problems, if the applied sediment thicknesses are derived from the lower flats in the synclines (see above). Since the assumed thickness of the sedimentary pile is too small, cross-sections have difficulties filling the space between the folded higher units and the floor thrust and often propose large offset thrusting of lower units (e.g. Laubscher 2008; Sommaruga 1997) or other poorly constrained shortening structures in the deep subsurface. The detachment fold model adopted here results in a larger average thickness of the Muschelkalk series and smaller associated amounts of shortening.

The 3D geometrical model was constructed using MOVE (version 2014) developed by Midland Valley Corporation. First the digital elevation model (DEM) and the geological map (1:250000) of the area were implemented as a reference. In the next step, the key features of the area such as tear faults and

thrust faults and also unit boundaries (called “horizons” in MOVE) on the surface were digitized according to the surface data and the geological map. Nine vertical cross-sections, which had been newly constructed and/or modified from Sommaruga (1997), were entered, and the structural architecture of each profile was digitised by using the Fault and Horizon tool. Finally, the synthetic three-dimensional model of the fold-and-thrust belt was constructed using the interpolation algorithm of MOVE between serial cross-sections. Thrust surfaces were constructed in the same way. For those surfaces (horizons, thrusts and faults) not defined between two adjacent cross sections (e.g. at the side of the model), the Extrusion Method of the software was used, which extrapolates lines based on the original specification in the desired trend or plunge direction.

	A	B	C	D	E	F	G	H	I
Topographic fold axis data	221/04	047/01	076/03	247/01	062/01	212/01	209/04	045/02	052/02
*Structural fold axis data	242/13	-	070/00	246/07	068/03	223/02	212/08	-	-

*from Sommaruga 1997

Table 2.1: Comparison of “topographic fold axes” (plunge direction / dip angle) determined from orientation analysis of the digital elevation model with “structural fold axes” from Sommaruga and Burkhard. (1997). Letters A to I refer to areas as indicated in Fig. 10.

The geometries of tear faults were designed in the following way. The two largest tear faults cut and offset the underlying ramp below the Tête de Ran anticline at shallow depth but root into them in the deeper parts of the section. Hence, the thrust is zipped by the tear faults down to a certain depth below which there is no offset (3D file in the supplementary material). In this way, the tear faults account for the offset of the thrust faults at the surface, but still preserve a continuous branch line with the major floor thrust. Minor tear faults

were modelled as mere surfaces that produce no offset or only a small flexure in the horizons.

Figure 2.6 shows two views of the fault surfaces in three dimensions (for more surface and subsurface views of the model, I refer to the 3D file in the supplementary material). Once the 3D model (both surface and subsurface layers) has been completed, the software permits to examine it from various directions. In particular, it allows the extraction of cross-sections in order to check the model against other available data and geological concepts. Corrections were made where the model showed inconsistencies, especially for tear-fault surfaces, where in some cases the interpolation algorithm resulted in dip angles contradicting the surface data.

2.3.2. Results and implications

Three cross-sections extracted from the 3D model, OC1, OC2, and OC3, are shown in figure 2.7 (for additional sections see electronic supplementary material). They are oriented approximately parallel to existing reflection seismic sections (Fig. 2.8). Two are perpendicular and one is parallel to the overall strike of fold axial planes. All three appear geologically plausible, except for very minor inconsistencies. Profile OC2 crosses the Tête de Ran anticline in the area where it is most strongly affected by the faults of the La Ferrière fault system. The thrust in the northwestern limb of this anticline is surprisingly steep in the profile; this may be a mistake in the model or, alternatively, result from interference with the strike-slip faults. One of the minor faults of the La Ferrière system appears as a vertical fault in the core of the Tête anticline and roots in

the thrust. It displays a small apparent offset, which is modelled as a flexure. All three cross-sections are consistent with seismic observations (Fig. 2.8), and the two sections perpendicular to the strike direction (Profile OC1 and OC2) are well-balanced (Fig. 2.7 D, E).

The model also allows the extraction of statistical data on surface orientations including the topography and the illustration of this data in Schmidt nets, using the Vertex Attributes tools of MOVE. I applied this to the entire DEM of Val de Ruz and to specific anticlinal and synclinal areas in order to analyse the orientation of surfaces. Fig. 2.9 and Fig. 2.10 show orientations of topography as

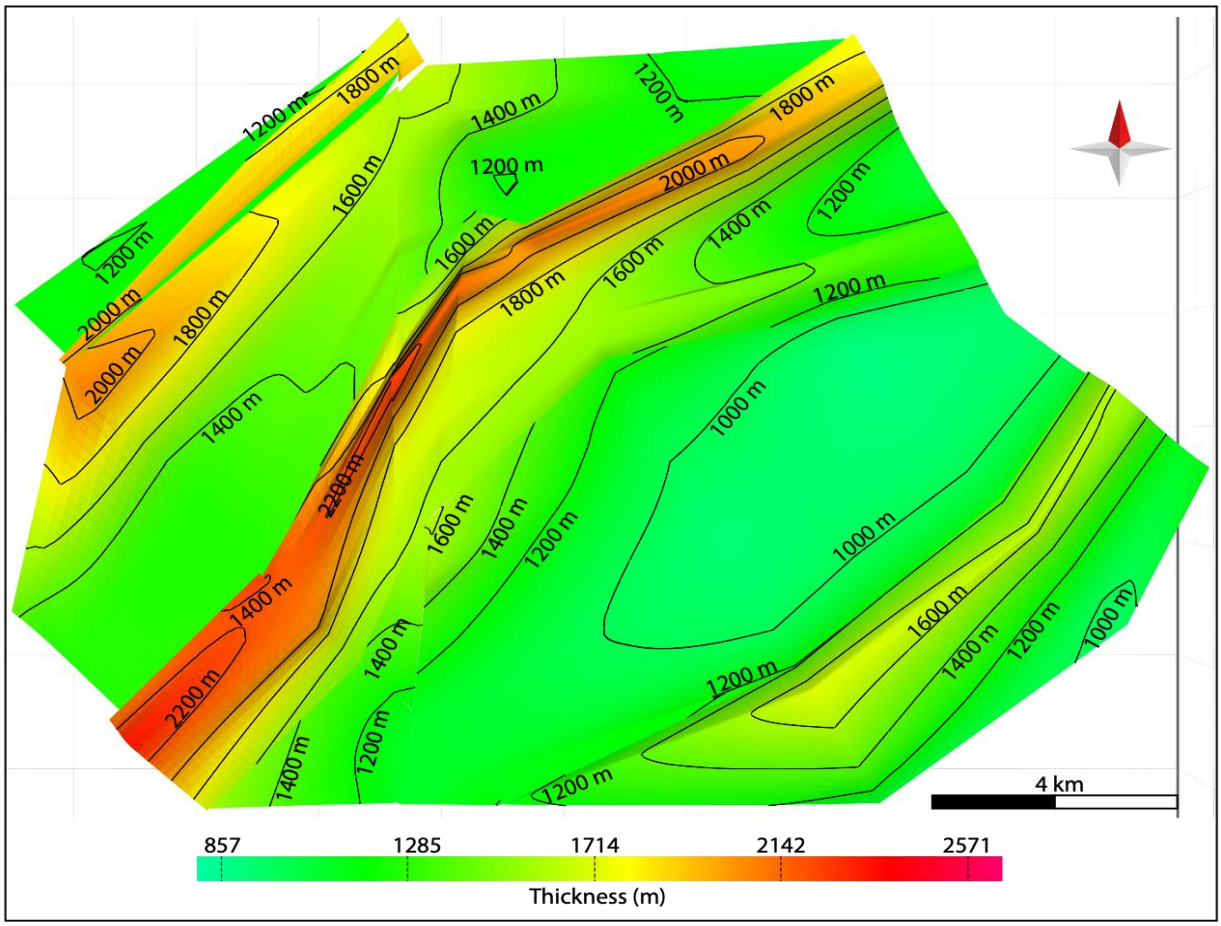

Figure 2.11: "Tectonic" thickness of Muschelkalk, measured in a vertical direction from the top of the Muschelkalk down to the top of the basement, and shown in an oblique view. This thickness includes layer repetition by thrusting, leading to high thickness in anticlines. Red compass needle indicates north.

lower-hemisphere poles to the DEM in the entire area and in local areas, respectively. Fig. 2.9 for the entire area shows a broad girdle distribution. The dip directions of the steep slopes are predominantly northwest- and southeastward. The pole to the best-fit great circle of the orientation distribution defines a “topographic fold axis” in the same way as a fold axis is constructed for a girdle distribution of folded geological surfaces. This topographic fold axis is horizontal and trends SW (226°). Its orientation is similar to the average trend of fold axes in the area, showing that topography is strongly controlled by the folds. This reflects the fact that deformation in the Jura Mountains is rather young, most anticlines still coinciding with mountain ridges and synclines with valleys. The lithological succession with alternating limestone and marl layers leads to the top of limestone layers often forming the Earth’s surface. The girdle in Fig. 2.9 is rather wide, which results partly from the variation in trend of the folds between north-northeast and east-northeast.

Some local-area Schmidt nets (Fig. 2.10 C, F) display the asymmetry typical for fault-bend and fault-propagation anticlines: forelimbs of the folds and the associated topography are steeper than the back limbs and this structural asymmetry is reflected also in the topographic slope. The Schmidt net for the Chaumont anticline (Fig. 2.10A) shows a subordinate girdle representing west- and east-directed slopes, which are related to north-south-oriented strike-slip faults. Comparison of the topographic fold axes with “structural” fold axes determined from the analysis of bedding orientation measurements (Sommaruga and Burkhard, 1997; Tschanz and Sommaruga 1993) shows deviations of 21º and 11º for the Chaumont and the Tête de Ran anticlines, respectively (Tab. 2.1). In both areas, the topographic fold axis trends more

northerly than the structural fold axis. Both anticlines are significantly influenced by north-south striking strike-slip faults. These anticlines can be imagined as arrays of small, more easterly-striking anticline fragments displaced by sinistral north-south strike-slip folds into an overall more northerly-striking alignment. This was also concluded by Sommaruga and Burkhard (1997) when they compared their structural fold axes with “map scale fold axis trends”. To explain the wrenching of the NNE-trending anticlines, Sommaruga and Burkhard (1997) proposed that these anticlines were influenced by fault zones related to pre-Jura-folding, i.e. Oligocene normal faults that formed due to WNW-ESE-directed stretching of the Upper Rhine Graben system.

An example of thickness analysis derived from the final model is shown in figure 2.11 that shows the thickness of the Muschelkalk strata, measured in a vertical direction from the top to the base of the series. It shows values around 1000 m in the synclines and locally reaches more than 2000 meters in the anticlines. I will discuss thickness variations in detail in the following.

2.4. Discussion

I briefly discuss a few aspects of the model: the implied thickness of the Muschelkalk strata, thickness variations within the Muschelkalk, and finally fault offset and deformation style.

The Muschelkalk strata have an average sedimentary thickness of around 1000 meters according to my model (see detailed discussion below). Though relatively large, this thickness is perfectly reasonable in view of seismic and well data in- and outside the Jura Mountains and is also in line with other studies

on the western Jura Mountains (Sommaruga 1997; Affolter and Gratier 2004). However, the top of the basement in the study area is not constrained by drilling and not imaged beyond doubt by reflection seismics. The Triassic formations might well be 200-300 meters thinner if top basement would be shallower. The nearest well that penetrates the Triassic rocks, the above-mentioned well Treycovagnes-1 (Fig. 2.1), yielded more than a thousand meters of Triassic rocks. Most of these were actually imbricated Keuper sediments. Hence, it seems that at a regional scale the strata of the Keuper experience the same style of decoupled deformation as those of the Muschelkalk. In the Val de Ruz area, coherent deformation of Keuper and the overlying sequence is merely suggested by the regionally occurring reflector H (Sommaruga 1997).

It appears that thickness variations of the Triassic succession within and in the vicinity of the study occur at different scales and that they have different origins: (1) At the regional scale, the average thickness of Triassic strata continuously decreases by an order of magnitude from the Jura Mountains towards the Helvetic domain of the Alps and this variation is clearly of sedimentary origin (e.g. Sommaruga 1997). (2) Within the Jura Mountains, there are pronounced local thickness increases related to ramp-flat thrusting at the kilometre scale. (3) This thrusting appears to be superimposed on broader anti- and synclines at the scale of 5-10 kilometres, which are related to lateral flow in the soft Triassic sediments and this deformation might at least partly be older than the thrusting. The wide Val de Ruz basin corresponds to a syncline of this sort. The average pre-deformation (pre-thrusting and pre-flowing) sedimentary thicknesses of the Muschelkalk strata along a cross section can be estimated by dividing the cross sectional area of the Muschelkalk between two pinlines by

the original (retro-deformed) length of the now folded and thrusted sedimentary pile. Note that this length is well constrained by the length of the younger Mesozoic strata near the surface. Thicknesses of the Muschelkalk series derived by this approach are between 1010 and 1130 meters for four NW-SE-oriented cross sections (Fig. 2.4; D1: 1010 m, D2: 1025 m, D3: 1095m, D8: 1130 m). This is 100-250 meters thicker than the minimum thickness of the Muschelkalk below the Val-de-Ruz syncline. Hence, the thickness below the Val-de-Ruz syncline is significantly lower than the average pre-deformation sedimentary thickness and I interpret this deviation to be the result of horizontal flow from the syncline into the adjacent anticlines. The presence of salt leads to extremely weak detachment horizons and typically causes flow into anticlines during incipient deformation, as has been shown for several examples of fold-and-thrust belts, including the Jura Mountains (Davis and Engelder 1985).

Strictly law-abiding balancing assuming a constant thickness for the Triassic has led to far-reaching interpretations about the subsurface architecture such as local basement highs or complicated shortening geometries at depth (e.g. Laubscher 2003) as the thickness has typically been inferred from the wide synclines where the original sedimentary thickness of the Triassic might be underestimated.

More than one thrust can nucleate from a flow-related larger-scale anticline leading to the occurrence of structurally high, narrow synclines in between. In order to explain a wide structural high, Schori et al. (2015) have proposed doubling of the older part of the stratigraphic succession along a detachment with several kilometres offset in the lower Middle Jurassic Opalinus clay for the map sheet “Chasseral” northeast of the study area. However, where the lower

Middle Jurassic rocks reach the surface, e.g. on the next map sheet to the Northeast ("Moutier"), the Opalinus clay is coherently folded together with the older and younger Mesozoic successions and no detachment is present (Pfirter 1997). Also in tunnels the Opalinus clay has typically been found in stratigraphic succession (see Buxdorf 1916; Laubscher 2008; Caer et al. 2015). Large-wavelength folding at amplitudes of a few hundred meters accommodated by lateral flow in the Triassic is well documented by drilling and seismics in the Molasse Basin (Sommaruga 1997) but also in the more external Plateau Jura. The above-mentioned well Laveron-1 (Fig. 2.1) penetrates more than 1400 meters of Triassic rocks, and reflection seismic data show a corresponding antiform with a wavelength of 10 kilometres below the reflector H (Sommaruga 1997). Such folding under the Internal Jura can explain structural highs more naturally than discrete fault-related structures. My model also shows a gradual variation of structural level rather than discrete steps, which would be expected if highs and lows were controlled by faults. The observed upward bend of strata towards the anticlines even beneath the thrust ramps (Fig. 2.4, e.g. southern anticline in sections C1, C2, and C3) is in my view a further argument for lateral flow in the Triassic. Finally, thrust faults in the study area show at most a few hundred meters offset at the surface. In traditional balancing approaches, such thrusts often are displayed with kilometres of offset at depth since the rather wide back-limbs of antiforms are explained by the doubling of strata rather than by horizontal flow. Accordingly, my model predicts moderate shortening between 7% and 17%, which is less than typical reconstructions that assume an on the average thinner Triassic succession. The initial buckling stage may be associated with an unknown amount of distributed layer-parallel shortening and associated thickening (e.g. Frehner et al. 2012; Ghassemi et al. 2010). For

this reason my shortening estimates are minimum values. I consider, however, distributed deformation to be limited since little or no internal deformation is found outside tectonized zones in the Jura (Tschanz 1990).

2.5. Conclusions

3D geometrical modelling resulted in a plausible subsurface model from which new kinematically balanced cross-sections can be extracted. The folds are decoupled from the basement in the evaporite-bearing Muschelkalk series. The Muschelkalk appears to show significant pre-thrusting thickness variations. This variation is at least partly due to lateral flow of the Triassic evaporites during the early phase of detachment folding, away from synclines and towards anticlines. Assuming a second decoupling horizon in the Dogger or involvement of the basement in the Jura tectonics is unnecessary for explaining the geology of the study area. Due to the young tectonics of the Jura Mountains, topography closely correlates with tectonic structure. Comparing “topographic” fold axes derived from orientation statistics of the Earth’s surface with published “structural” fold axes confirms earlier suggestions that the trend of the NNE-trending folds was modified by small-scale NS-striking sinistral strike-slip faults similar to regional tear faults like the La Ferrière fault.

This page intentionally left blank.

Chapter 3

Quantitative shortening calculation for the eastern part of the Alps (Eastern Alps+Southern Alps)

Abstract

The tectonic evolution of the Eastern Alps involved subduction and collision processes during the Mesozoic and Cenozoic and resulted in a complicated structure at the surface where tectonic nappes are exposed, but also at depth where subduted lithospheric slabs appear to dip in different directions. The structure is highly three-dimensional and not completely understood. In this research I have tried to integrate all available data such as DEMs, geological maps, profiles from different sources as well as 30 newly constructed cross-sections in order to build a comprehensive 3D model for this copmplex area by using a GIS data base and the modelling software MOVE (Midland Valley Co.). The model allows us extracting cross-sections in any desired orientation, determining volumes of tectonis units, line and area balancing for all the profiles, and geophysical modelling. In the first step, I have analysed the profiles and calculated the amounf of shortening for all the profiles. I have considered top of the European and Adriatic Basement as a reference for calculating the amount of shortening for European and Adriatic continents. Line balancing of the European basement shows about 100 km shortening in the West (NFP20 East), a decrease to about 50 km in the Engadine Window, an increase towards east to a maximum of about 140 in the western Tauern Window and a decrease

to rather constant values of about 80-90 km further east. Area balancing assuming constant pre-collisional crustal thickness gives generally lower values for shortening than line balancing and even negative values east of the Tauern Window (i.e. stretching), which may reflect, among other processes, pre-orogenic thinning of the continental margins as well as east-west stretching of the crust during Miocene tectonic extrusion. Line balancing of shortening of the South Alpine basement gives values of about 50 km in the West (NFP 20), a maximum of about 65 km, close to the western end of the Tauern Window., and a strong decrease towards east reflecting the transfer of shortening of Adria from Southern Alps to the Dinarides. The added shortening of European and South Alpine basements is at a maximum at the western end of the Tauern Window, probably reflecting pre-Alpine margin geometry (Dolomites indenter). Although the model carries large uncertainties, partly due to the scarcity of information about deep crustal structure away from the seismic sections, these results are in good accordance with the tectonic evolution as inferred from other methods.

3.1. Introduction

3.1.1. Alpine orogeny and Eastern Alps

The Alps resulted from a long and still ongoing tectonic evolution which started with the opening of the Atlantic Ocean in the Early Jurassic, around 180 Million years ago. This mountain chain developed at the boundary between the Eurasian Plate to the North and the Adriatic microplate to the South. The Alps are geographically divided into Western, Central, Southern andEastern Alps. The boundary between the Eastern and CentralAlpsruns from Bodensee along the Rhine Valley and over the Splügen Pass to Lago di Como (Fig.3.1). The Eastern Alps are surrounded by different tectonic units. These are the Central Alps to the West, the European platform and the Molasse Basin in the North, the Carpathians and the Pannonian basin in the east, and the Dinarides and

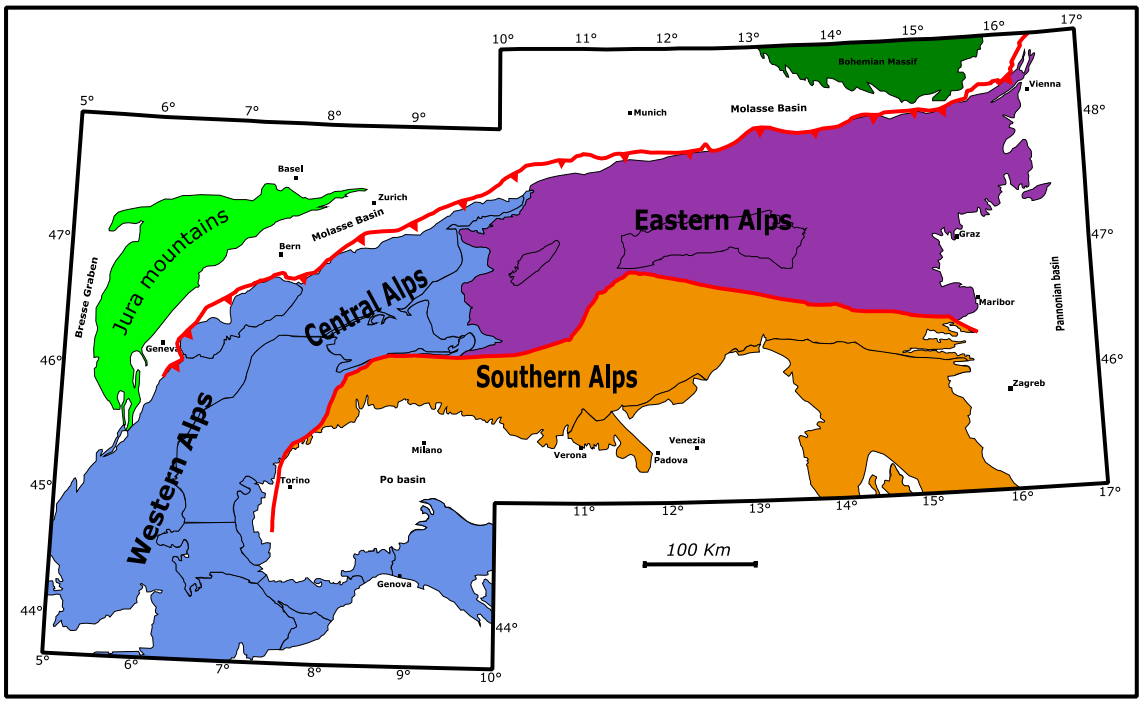

Figure 3.1: Geographic subdivision of the Alps (Western, Central, Eastern and Southern Alps) and surrounding basins.

Adriatic foreland in the south. Although the development of these units is very close to the Eastern Alps a detailed explanation of these units is beyond the scope of this study. In contrast to the strongly arc-shaped Western and Central Alps, the Eastern Alps are straighter. They are also wider and less high. The distribution of tectonic units at the surface is also different. The Western Alps are mostly formed by the Helvetic/Dauphinois superunit, derived from Mesozoic Europe, and the Penninic superunit, derived from Mesozoic ocean basins, continental fragments, and continental margins. In contrast, the Eastern Alps are largely covered by the Austroalpine superunit which comes from the former Adria continent. The Penninic and Helvetic are only exposed in windows in the central part of the Eastern Alps (Tauern Window, Engadine Window) and in a narrow stripe along the northern margin.

3.1.2. The Eastern Alps

The main structures of the Eastern Alps were built in Upper Cretaceous and Lower Tertiary (Tollmann 1980). This part of the Alps is mostly covered by the Austroalpine units. These consist of smaller nappes (Tollmann 1980) which will be explained in more detail in the following paragraphs (Fig. 3.2).

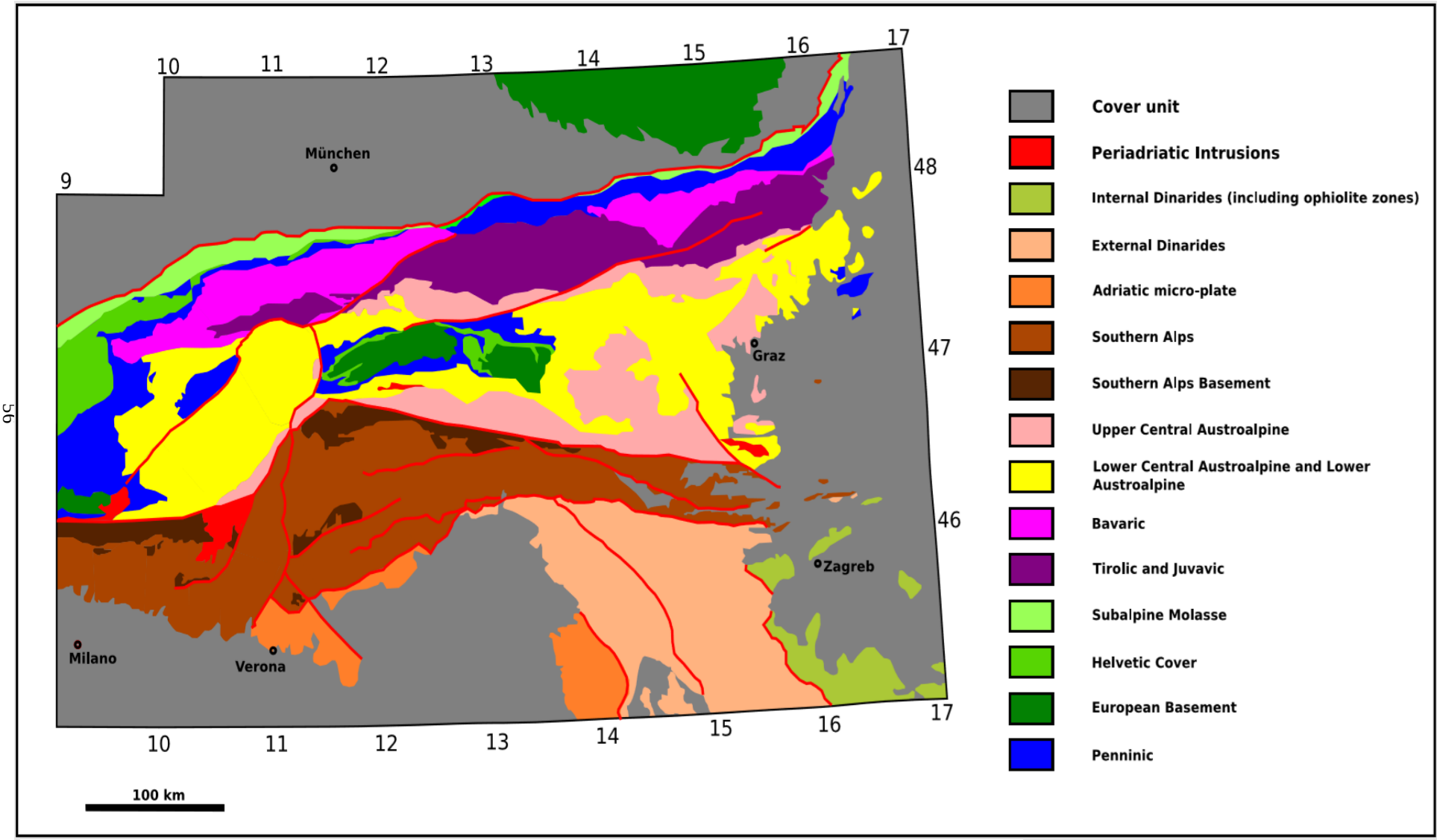

Figure 3.2: Simplified tectonic map of the Eastern part of the Alps (Eastern Alps and Southern Alps) (Schmid et al. 2004).

The Eastern Alps are a composite orogen in that the Austroalpine was mainly shaped by thrusting and subsequent extensional tectonics in the Late Cretaceous. In the Tertiary, it was emplaced as one large thrust sheet northward over the Penninic and Helvetic (Fig. 3.3). The Tertiary tectonics of the Austroalpine are dominated by renewed orogen-parallel extension together with north-south shortening, and strike-slip faults accommodating extrusion towards east. One of these strike-slip faults is the dextral Periadriatic Line which forms the boundary against the South Alpine superunit. In the South Alpine, south-directed thrusting evolved through the Tertiary and continues today at the southern front of the orogen. At the northern front, thrusting has stopped. Tertiary strike-slip fault systems affected the development of the Eastern Alps as well as the topography.

The tectonic units in the Eastern Alps may be grouped into 5 main groups based on their paleogeographic evolution (Schuster et al. 2013). These five units are:

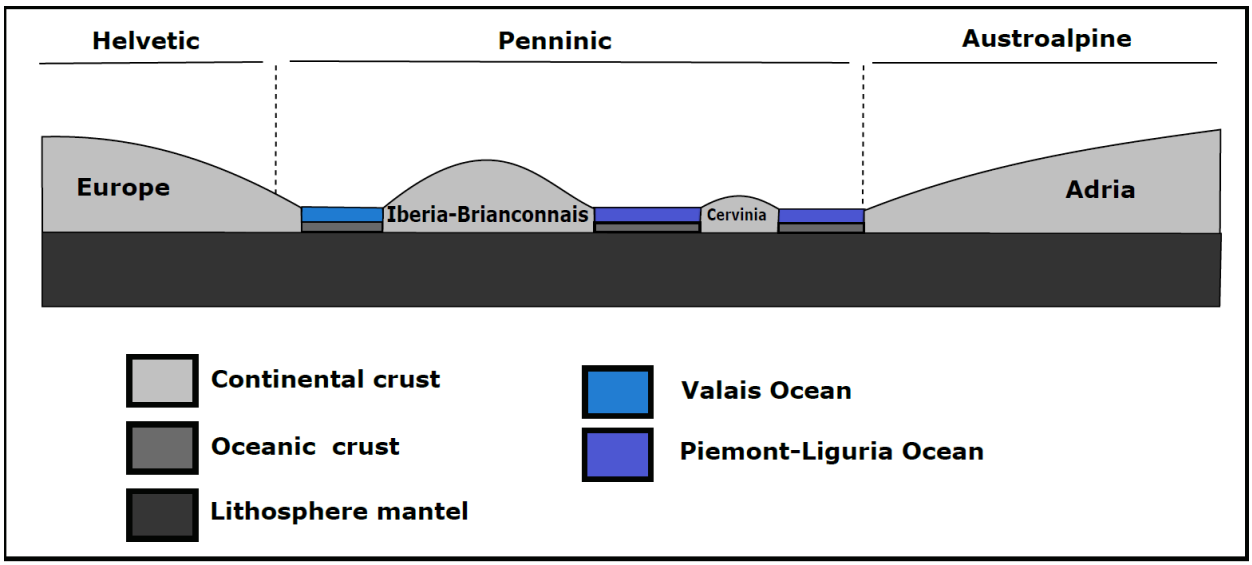

Figure 3.3: Schematic paleogeographic profile of the Alps at the end of the Early Cretaceous.

1. Units derived from the European continent

2. Penninic nappes

3. Adriatic microcontinent

4. Meliata unit

5. Eocene to Miocene magmatic rocks.

The structure at depth is as complicated as the surface structure and it is difficult to understand how the two are coupled. Seismic tomography revealed that a south-dipping lithospheric slab exists under the Central Alps, and a north-dipping one under the eastern part of the Eastern Alps (Lippitsch et al., 2003) (Fig. 3.4). Subduction of the north-dipping one may be coupled with the active southward thrusting at the southern border of the Eastern Alps. The coupling of crustal and lithospheric deformation is a subject of high scientific relevance that is currently discussed and not yet completely understood (e.g. Handy et al. 2014).

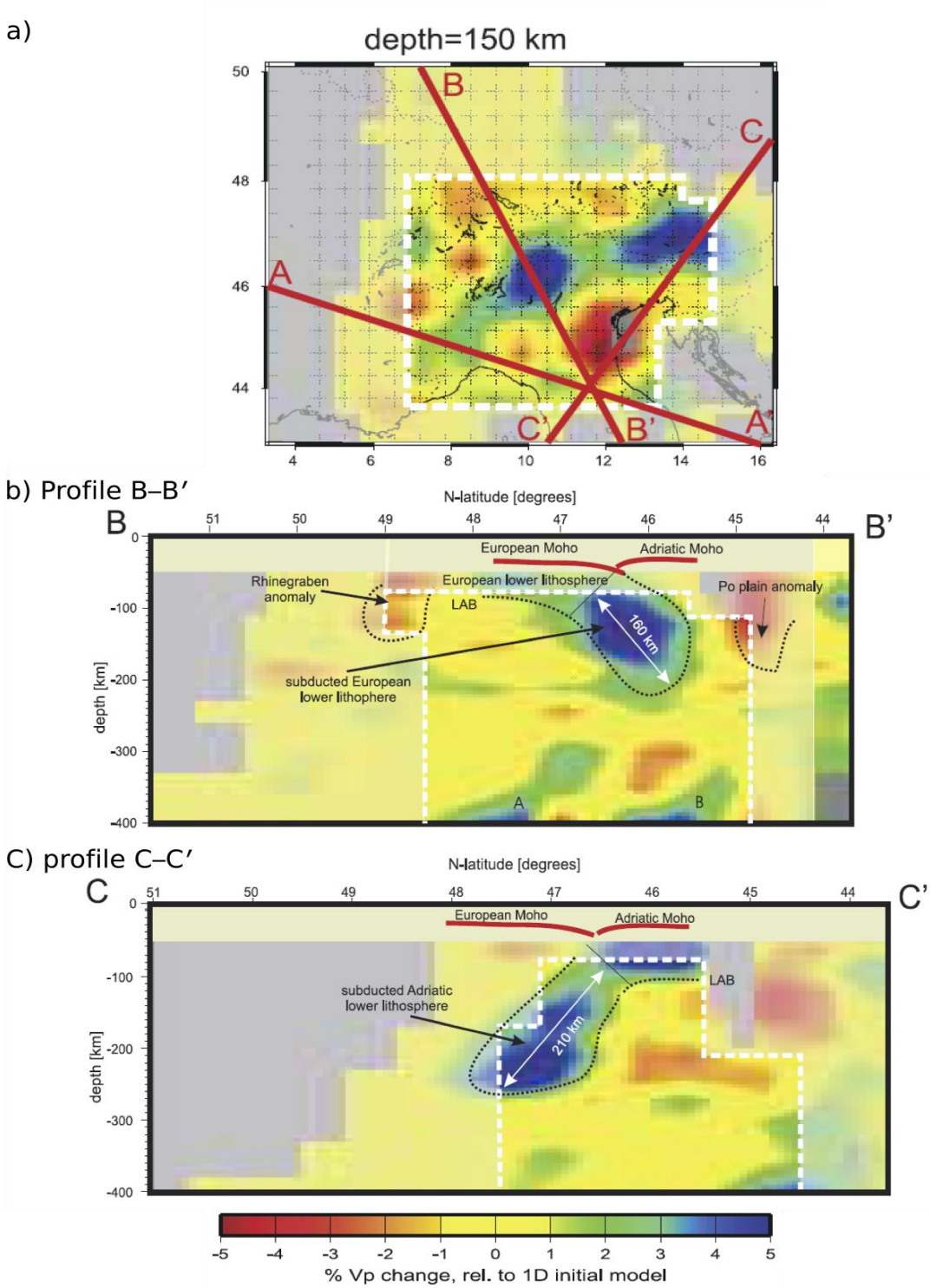

Figure 3.4: Results of seismic tomography in the Alps from Lippitsch et al., 2003. ***a*** *Tomographic map of the 135-165 km depth range showing slab anomalies and slab gap beneath the Alps.* ***b*** *Profile B-B' and* ***c*** *profile C-C' showing inclined slab anomalies with opposite polarities beneath the Central and Eastern Alps.*

3.1.3. Previous 3D subsurface models of the Alps and aims of this study

Three-dimensional models of the Alpine subsurface were for a long time produced graphically by projection techniques, making use of the excellent geological surface information (e.g. Argand 1911, Argand 1916). With the development of geological modeling software in the last decades, more and more attempts were made to apply such tools to Alpine geology. Maxelon and Mancktelow (2005) produced a model of the complicated nappe geometry in the Lepontine Dome, resulting from the overprinting of several phases of folding. Marquer et al. (2006) modelled a part of the French Western Alps. Vouillamoz et al. (2012) constructed an orogen-scale model of the Western Alps, including the MOHO as the deepest interface. These authors used software developed by the French Geological Survey BRGM. D'Ambrogi et al. (2010) used the software package Move to model the subsurface of Italy down to the lithosphere-asthenosphere boundary (LAB). This includes the southern part of my target area, the Eastern Alps.

One of the aims for my research is to provide a subsurface model of the Eastern Alps. Such a model does not exist yet. It may be used for various purposes, like generating cross sections of any desired orientation, determining the volume of tectonic units, kinematic modeling (stepwise restoration), and geophysical modeling (e.g. gravity, seismics). On the other hand, the modeling process will help to better understand the deep structure of the Eastern Alps and their kinematic evolution. The subsurface structure of the Eastern Alps is particularly puzzling and highly 3-dimensional because the dip direction of lithospheric slabs is probably reversed along strike of the orogen. This part of my research mainly is trying to answer the following questions:

How much coupling exists between deformation in the crust and the mantle?

How do the volumes of cover and basement rocks relate to each other?

How are oppositely dipping lithospheric slabs under the Eastern Alps related to crustal deformation?

3.2. Tectonic windows in the Eastern Alps

A tectonic window in a geological sense is a place where autochthonous rocks or deeper thrust sheets reach the surface, surrounded by higher thrust sheets.

Two famous tectonic windows, the Tauern and Engadine window are located in the Eastern Alps (Fig. 3.5). These tectonic windows provide an opportunity to take a close look at the deep structures and lower nappes of the Alps and understand the crustal-scale collisional accretion of the Alps (Schmid et al. 2013). These two tectonic windows also allow studying the Penninic nappes besides the northern front of the Alps (the Rhenodanubian Flysch Zone), since the Penninic nappes in these areas are not covered by the Austroalpine nappes.

3.2.1. Tauern Window (Hohe Tauern Window)

The Tauern Window is the largest tectonic window in the Alps. It is located in Austria and northern Italy and almost in the middle of the eastern Alps. It was first recognized by P.Termier in 1903. The first map for this area was published

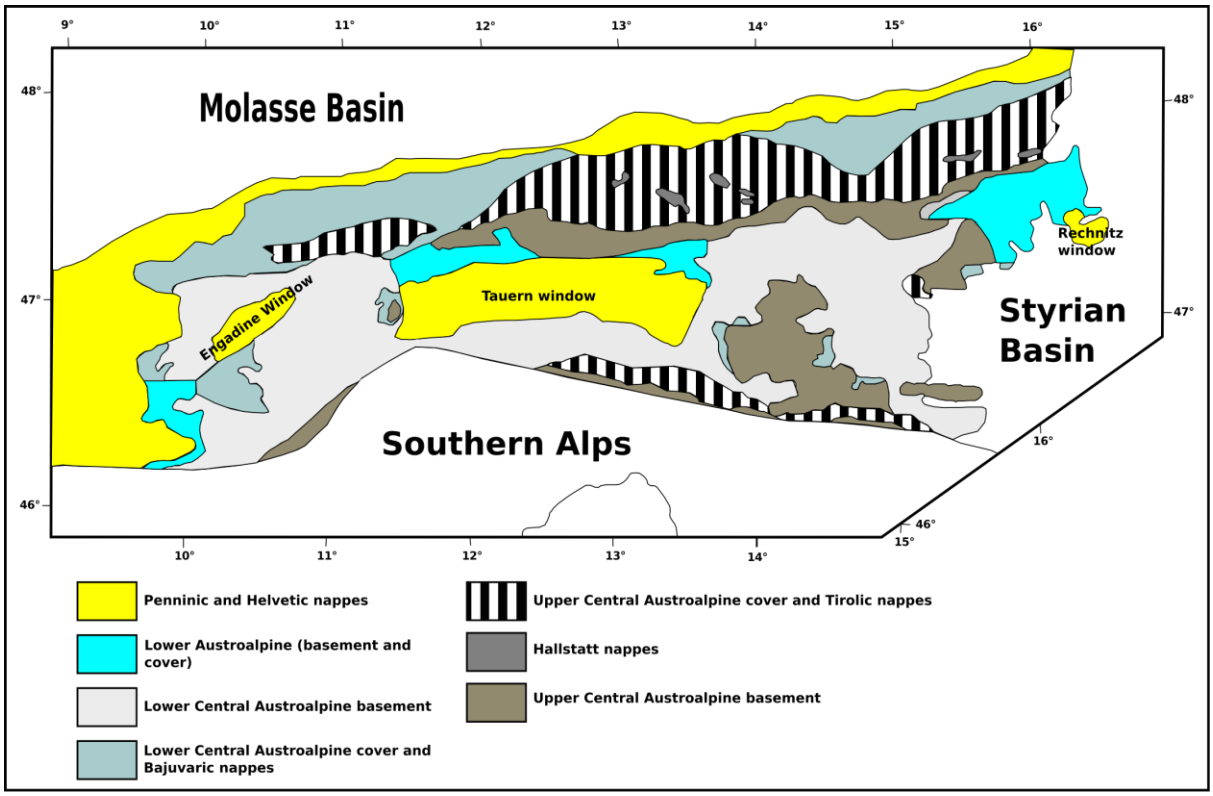

Figure 3.5: Simplified tectonic map of the Eastern Alps (Janák et al. 2009).

in 1844 (Geognostische Karte von Tirol) and research is still going on. The Tauern window is about 160 km long and about 30 km wide (Fig. 3.5) and strikes sub-parallel to the orogen of the Eastern Alps. It reveals a stack of nappes derived from the distal European continental margin as well as Alpine Tethyan oceans (Schmid et al. 2013, Bertrand et al, 2017). This window exposes metamorphic rocks of the Penninic nappes.

The Tauern window consists of different nappes but in general, the rocks can be grouped into two main units:

1. Units derived from the distal European margin (Subpenninic nappes).

These units form the lower part of the Tauern window.

2. Ophiolite-bearing units (Penninic nappes).

These units compose the higher parts of the Tauern window. They were derived from the continental-ocean transition and from the Penninic- oceanic basin (Lammerer et al. 2008; Lammerer & Weger. 1998).

3.2.2. Engadine Window

The Engadine window is the second largest tectonic window in the Eastern Alps and located west of the Tauern window in Switzerland and Austria (Fig. 3.5). Compared to the Tauern window, the Engadine window is much smaller, about 55 km long and 17 km wide.

The Engadine window consists mainly of weakly metamorphosed deep-sea sediments of middle Jurassic to Eocene age. Most of these are explained as turbidite deposits (Waibel and Frisch1988). The sediments are seen as part of the Penninic units. The units of the Engadine window are assigned to the Valais Ocean, the Briançonnais microcontinent, and the Piemont-Liguria Ocean (*Schmid et al. 2004).* Closure of two oceans (Valais and Piemont-Liguria) caused metamorphic overprinting during the Paleogene. The rocks in this part of the eastern Alps experienced low-temperature-high-pressure overprint which reached the blueschist facies (Bousquet, 2008).

3.2.3. Rechnitz Window Group

The Rechnitz Window Group is located in the most eastern part of the Alps at the edge of the Pannonian Basin (Alpine-Pannonian border). This Window Group consists of four small windows between the Rechnitz and Köszeg area

and again Penninic nappes crop out. The area is partly covered by Neogene sediment. Different metamorphic events have been recorded for the Rechnitz Group. The metamorphic rocks comprise ophiolite remnants and sedimentary rocks (Dunkl and Demeny1997).

3.3. Main tectonic units in the Eastern Alps

In this research I have grouped all the existing tectonic units and nappes in the eastern part of the Alps into 17 units based on their origin and tectonic evolution. These 17 units come mainly from the detailed map of Schmid et al. 2004 and the names of the units in our research are are as follows (Fig. 3.6):

Cover, Periadriatic Intrusions, Internal Dinarides, External Dinarides, Southern Alps Basement, Southern Alps Cover, Adriatic microplate, Tirolic and Juvavic, Bavaric, Upper Central Austroalpine, Lower Central Austroalpine and Lower Austroalpine, Penninic, European Basement, Helvetic Cover, Subalpine Molasse, Lower crust (European) and Lower Crust (Southern Alps).

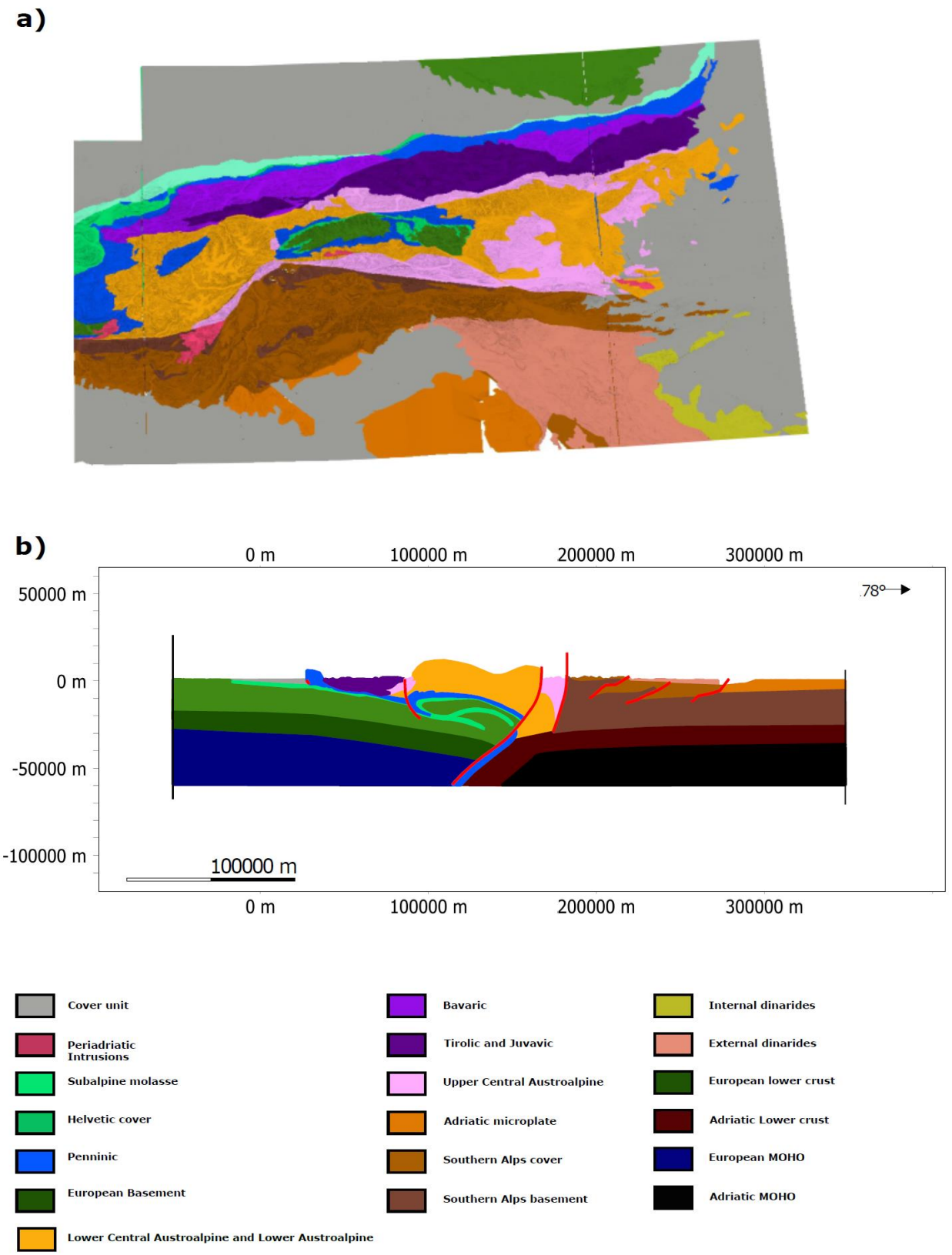

Figure 3.6: ***a*** *Simplified tectonic units and nappes in the Eastern Side of the Alps from Schmid et al. 2004.* ***b*** *Eastern Alps profile showing the major tectonic units which were used in the model.*

For simplicity these units (except Periadriatic Intrusions) are grouped into three main groups according to their origin and tectonic background as follows and each group will be explained in detail in the following paragraphs:

1. **European units**

   1.1 European cover

   1.2 Subalpine Molasse

   1.3 European Basement

   1.4 Helvetic cover

   1.5 European Lower crust

2. **Oceanic units**

   2.1 Penninic unit

3. **Adriatic units**

   3.1 Southern Alps Basement

   3.2 Southern Alps Cover

   3.3 Adriatic microplate

   3.4 Tirolic and Juvavic

   3.5 Bavaric

   3.6 Upper Central Austroalpine

   3.7 Lower Central Austroalpine and lower Austroalpine

   3.8 Internal Dinarides

3.9 External Dinarides

3.10 Adriatic Lower crust

1. European units

This group consists of all the rocks derived from the European continent and is subdivided into smaller units that will be explained in the following paragraphs.

1.1 European cover

This unit, which corresponds to the Tertiary cover in general in Schmid et al. (2004), consists of two different basins: Molasse Basin in the North and Pannonian Basin in the East.

The Molasse Basin is the northern Alpine foreland basin. It is limited by the northern border of the Alps. The length of this basin is about 1000 km with a maximum width of 130 km. It extends from the west to the most eastern part of the Alps. The Molasse Basin developed mainly from the Eocene (55 Ma) to Pliocene (5 Ma) and represents the non or less-deformed Oligo-Miocene sediments (Veron 2005).

The Pannonian Basin which is also called Carpathian Basin, east of the Eastern Alps, is a classical back-arc basin, underlain by thinned continental lithosphere and formed during Miocene times as a result of fast rollback of a slab attached to the European continent as well as the related upper mantle flow (Balla, 1986; Horváth et al., 1986; Horváth, 1993; Horváth et al., 2015; Matenco & Radivojević. 2012; Handy et al., 2010).

1.2 Subalpine Molasse

The Subalpine Molasse unit consists of congolomeratic Molasse thrust slices, which dip south and root underneath the external massifs in eastern Switzerland (Pfiffner 1986, Pfiffner et al. 1997a, Schmid et al. 2004). The Subalpine Molasse unit is exposed along the northern edge of the Eastern Alps. The thickness of the Subalpine Molasse varies between 900 and 2500m based on drilling data in different areas (Ortner et al. 2015). These units form the northern front of the Alpine thrust sheets (Schmid et al. 2004). In the Western Alps, these thrust sheets are more scattered and partly missing (Lickorish and Ford 1998).

1.3 European Basement

This unit in our research includes three subunits of the map by Schmid et al (2004). These units are: (1) Non-eclogitic Sub-Penninic basement nappes including “Gotthard Massif”, (2) Eclogitic Sub-Penninic basement units, and (3) External massifs of the Alps and Variscan basement of the Northern Alpine foreland. The first two categories are part of the Sub-Penninic nappes which come from the distal European margin and the last category (External massifs of the Alps) comes from the European continent. The European basement unit is exposed in a large area NNE of the Eastern Alps (Bohemian Massif; Fig. 3.6), in the Tauern Window, and in a small area at the western end of the map.

The Non-eclogitic Sub-Penninic basement nappes and Eclogitic Sub-Penninic basement units especially in the Tauern window are subdivided into Zillertal Nappe, Riffl Nappe, Sonnblick-Romate Nappe, Mureck gneissic slice and Storz Nappe, Tux Nappe, Granatspitze Nappe, Hochalm Nappe, Ahorn Nappe and Göss Nappe (Schmid et al. 2013), although separation of these nappes from each other is locally not possible. These nappes in this part of Alps reached

temperatures of 500 to 600ºC during the Alpine metamorphism (Schmid et al. 2013; Oberhänsli et al. 2004; Schuster et al. 2004).

The External massifs of the Alps and Variscan basement of the Northern Alpine foreland are part of the European continent that is unaffected (unmetamorphosed) or only weakly deformed and metamorphosed during the Alpine orogeny (Schmid et al. 2004). The Bohemian Massif in the NE part of the map is one of the largest continuously outcropping fragments of the Variscan orogen.

1.4 Helvetic cover

Based on the paleogeography in the Early Cretaceous, the Helvetic cover represents the southern shelf of the European continent. This unit occurs as the cover of the Sub-Penninic nappes, in the Northern Alpine foreland, and in the Helvetic nappes. It is equal to three subunits: Mesozoic cover of Sub-Penninic basement nappes (including cover of Gotthard), Helvetic and Ultrahelvetic nappes (including Combeynot and Tavetsch Massif), and Helvetic flysch (Schmid et al. 2004).

The Helvetic cover appears in three parts of the Eastern Alps. The first is along the northern margin of the Eastern Alps in Central and Eastern Austria. These are only few thin Helvetic slices because of the Mesozoic erosion of passive margin sediments (Ziegler 1992).

The Helvetic units that occur in the Tauern Window represent the Mesozoic cover of the Sub-Penninic basement nappes which stayed attached to the metamorphic cores of the Alps and experienced metamorphism during the Alpine orogeny (Schmid et al.2004; Frey et al. 1999).

The third area covered by the Helvetic units is the northwestern part of the map. The Helvetic units in this part of the Eastern Alps comprise Helvetic and

Ultrahelvetic nappes and Helvetic flysch. The latter constitutes predominantly Late Eocene to Early Oligocene flysch including limestone at its base which was deposited in an internal part of the Alpine foreland basin (Schmid et al. 2004).

1.5 European Lower crust

European Lower crust represents the lowermost unit in the profiles (Fig. 3.6 b) and is not exposed at the surface at all. The composition and physical properties of this unit are difficult to determine and generally remain little known, because it is inaccessible. The mineral composition, origin, age, chemical composition vary from one part of the continent to another (Downes 1993). Some studies have reconstructed the Lower crust using the volcanic rocks in Europe and show the wide range of rock types from eclogites to high-grade metasediments (Downes 1993).

2. Oceanic units

2.1 Penninic unit

In this research, I have grouped all the oceanic units into one group and called them Penninic unit for simplicity. This group includes former oceanic crust from the Alpine Tethys Ocean (Fig. 3.6) in the eastern part of the Alps. This ocean opened in the Middle Jurassic (about 165 ma) between Europe and Adria and was closed during the late Cretaceous and Tertiary as a result of movement of Adria towards Europe.

The Penninic units in the Eastern Alps are mostly covered by the Austroalpine nappes and exposed in three areas: The narrow Rhenodanubian Flysch Zone

in the northern front of the eastern Alps, the Engadine window, and the Tauern Window (Pfiffner 2010). The Penninic units are traditionally divided into three subgroups based on the paleogeographic evolution and origin of these nappes: Upper Penninic, Middle Penninic, and Lower Penninic nappes, which come from the former Piemont-Liguria Ocean, Brianconnais terrane, and Valais ocean, respectively (Schmid et al. 2004). Each of these parts consists of different nappes (Froitzheim et al. 2008, Schmid et al. 2004).

The precise paleogeographical locations of these ancient oceans and even the existence of branches of these oceans (Valasian) are still a matter of debate.

The Piemont-Ligurian Ocean (Alpine Tethys) opened in the Middle Jurassic and the Valais Ocean probably opened in the Early Cretaceous (Froitzheim 1994, Schmid 2004).

The Lower Penninic nappes consist mostly of Bündnerschiefer sediments from the Valais Ocean (Pfiffner 2010). These nappes make up large parts of the Engadine window, Tauern window and slim nappes along the northern front of the Alps. The Middle Penninic nappes are mainly derived from the Brianconnais microcontinent and cover only a small area in the Engadine window. East of this window, no remnants of the Brianconnais microcontinent are known. Finally the Upper Penninic nappes are predominantly ophiolitic rocks and oceanic sediments derived from the Piemont-Ligurian ocean and cover small areas in the westernmost part of the Eastern Alps, Engadine Window , Tauern Window, and Rechnitz Window (Schmid et al. 2004; Pfiffner 2010; Schuster et al. 2013).

3. Adriatic units

This group consists of all the units and nappes derived from the former Adriatic or Apulian continent. The Southern Alps are the part of the Adriatic units located south of the Periadriatic fault. The Southern Alps are tectonically characterized by large scale thrusting and folding; the dominant direction of thrusting and fold asymmetry is southward. In this research the Southern Alps are subdivided into Lower Crust, Basement and Cover.

3.1 Southern Alps Basement

The Southern Alps Basement unit in my study includes two subunits of the map by Schmid et al (2004). Lower crust of the Southern Alps (Ivrea zone) and Upper crustal basement of the Southern Alps. The Lower crust unit which corresponds to the Ivrea zone (or Ivrea-Verbano zone) is not exposed in the eastern Alps. The Upper crustal basement of the Southern Alps in the Eastern Alps comprises former Paleozoic sediments of variable Variscan metamorphic grade (Castellarin et al. 2006, Schmid et al. 2004).

3.2 Southern Alps Cover

This unit corresponds to the “Post-Variscan volcanic and sedimentary cover of the Southern Alps” in Schmid et al. (2004). The Southern Alps Cover generally includes a continuous Late Carboniferous to Oligocene cover succession. Southern Alps Cover and parts of the Upper crustal basement of the Southern Alps are affected by Neogene top-south thrusting over the southern units, i.e. the Adriatic micro-plate and external Dinarides (Schmid et al.2004).

3.3 Adriatic micro-plate

The Adriatic micro-plate unit is the undeformed part of the former Adriatic (Apulian) plate which is located south of the frontal thrust of the Southern Alps. This unit covers a small area in the map south of the Eastern Alps. It represents the weakly deformed autochtonus foreland of the Southern Alps, Apennines and External Dinarides (Schmid et al. 2004) which comprises continental lithosphere (Le Breton et al. 2017; Munzarová et al., 2013) and is covered by Mesozoic sedimentary rocks (mostly limestones).

3.4 Tirolic and Juvavic unit

The Tirolic and Juvavic nappes constitute groups of Mesozoic cover nappes and represent the higher nappes in the Northern Calcareous Alps. They belong to the Upper Austroalpine. The uppermost unit (Juvavic) is traditionally divided into two sub-units: “Tiefjuvavikum” and “Hochjuvavikum” which are characterized by Hallstatt facies and Dachstein facies, respectively (Schmid et al. 2004). The origin of the Juvavic nappes still remains a matter of debate. Some authors propose an origin of this unit from the southern margin of the Meliata ocean (i.e. Neubauer et al. 2000). Others suggested an origin from the northern margin of the Meliata Ocean (Gawlick et al. 1999, Mandl 2000). The lower nappes (Tirolic) also comprise 3 subunits (Inntal, Krabachjoch and Staufen-Höllengebirge nappes) and are formed by Mesozoic sediments. These nappes had a paleogeographic position within the passive margin north of the Meliata Ocean (Schmid et al. 2008).

3.5 Bavaric unit

The Bavaric unit is the lowermost unit within the Northern Calcareous Alps nappe system and covers a large area in the northern part of the Eastern Alps.

Like the Tirolic and Juvavic unit, the Bavaric unit also consists of detached Mesozoic cover but the palaeogeographic origin is more distal with respect to the passive margin of the Piemont-Ligurian Ocean. The Bavaric unit is divided into Tiefbavarikum and Hochbavarikum and includes 3 main nappes from base to top: Cenomanian sliver, Allgäu Nappe and Lechtal Nappe (Schmid et al. 2004). The Cenomanian sliver is the lowermost nappe in the Bavaric unit and overlain by the Allgäu Nappe. The western part of the Northern Calcareous Alps is covered by Allgäu Nappe and Lechtal Nappe and to the east the Tirolic nappe advances north and as a result the Bavaric unit does not crop out in the middle part of the Northern Calcareous Alps. Further east the front of the Tirolic nappe swings back to the south and thus Bavaric nappes crop out again.

3.6 Upper Central Austroalpine

This unit is equal to three subunits in Schmid et al (2004), Grauwackenzone (Paleozoic, stratigraphic base of Tirolic nappes), Mesozoic cover of Upper Austroalpine basement and Drauzug-Gurktal nappe system (Steinach nappe, Gurktal nappe, basement of Drauzug). The Grauwackenzone (Schönlaub 1980) or Greywacke Zone represents the basement of the Tirolic nappe system in the Northern Calcareous Alps and consists of the Veitsch, Silbersberg, Vöstenhof-Kaintaleck and Noric nappes from base to top (Neubauer et al. 1994b, Froitzheim et al. 2008). The origin of this nappe is assumed to be north of the Meliata Ocean (Schmid et al. 2004). Mesozoic cover of Upper Austroalpine basement indicates the cover of Upper Austroalpine basement nappes south of the Northern Calcareous Alps.

Finally, the Drauzug-Gurktal nappe system is the tectonically highest nappe system amongst the Upper Austroalpine basement nappes, positioned south of

the Northern Calcareous Alps. It is partly located between the Southern border of Alpine metamorphism, called SAM by Hoinkes et al. (1999), and the Periadriatic fault. It is derived from the Apulian plate with the Southern Alps and the Dinarides and represents the southern margin of the Meliata Ocean during the Eo-alpine nappe stacking according to Schmid et al. (2004).

3.7 Lower Central Austroalpine and Lower Austroalpine

This unit here groups five units of Schmid et al. (2004). These are: Öztal-Bundschuh nappe system, Korale-Wölz high pressure nappe system, Silvretta-Seckau nappe system, Lower Austroalpine nappes and Nappes derived from the Sesia-Margna fragment.

The Öztal-Bundschuh nappe system represents a transition zone between the upper (Drauzug-Gurktal nappe) and lower nappe system (Koralpe-Wölz high pressure nappe system). The Öztal nappe includes the Brenner Mesozoics and the Bundschuh nappe includes the Stangalm Mesozoics (Tollmann 1977). Both of these nappes exhibit a metamorphic gradient concerning Eoalpine metamorphism, for example the metamorphic imprint increases within the Öztal nappe from lower greenschist-facies to amphibolite conditions from north to south (Schuster et al. 2004).

The Koralpe-Wölz high-pressure nappe system contains a succession of units showing remarkable pressure-dominated Eoalpine metamorphic overprint (Hoinkes et al. 1999, Schuster et al. 2001, Schuster. 2003, Schmid et al. 2004). It includes mostly basement units, among them the Schneebergzug, Millstatt, Wölz, and Saualpe-Koralpe.

The Silvretta-Seckau nappe system represents the lowermost Upper Austroalpine tectonic unit which overlies the Lower Austroalpine units. This nappe system includes Languard, Campo-Sesvenna and Silvretta nappes in the west, Lasörling complex south of the Tauern Window and different complexes like Schladming, Speik etc. in the east (Froitzheim et al. 2008). From a paleogeographic point of view, the Silvretta-Seckau nappe system shows rifting-, subduction-, and collision-related magmatic rocks from Precambrian to Ordovician and Permian and Mesozoic cover rocks (Neubauer 2002).

The Lower Austroalpine nappe system contains the nappes from the distal Jurassic-age passive margin of Apulia close to the Piemont-Liguria Ocean. These units are widespread in eastern Switzerland, particularly along the southwestern margin of the Austroalpine nappes (Froitzheim et al. 2008, Schmid et al. 2004). This nappe system includes Err Nappes at the base and Bernina Nappes at the top, as well as the Innsbruck Quartz Phyllite (Froitzheim et al. 1994, Froitzheim et al. 2008, Schmid et al. 2004).

Nappes derived from Sesia-Margna fragment: This fragment is supposed to be rifted off from the most distal part of the Apulian margin as an extensional allochthon during the mid-Jurassic (opening of the Piemont-Liguria Ocean). This unit includes the Sesia-Dent Blanche nappe in Northern Italy and Western Switzerland and the Margna-Sella nappes in Eastern Switzerland (Froitzheim et al 1996, Trümpy 1992).

3.8 Internal Dinarides

The Internal Dinarides include the ophiolite zone in the southeastern part of the model. The Internal Dinarides cover only a small area (Fig. 3.6). This unit involves the distal continental margin of Apulia and oceanic crust of Neotethys, as well as subduction-related mélange formations. The Internal Dinarides are divided in four different tectonic units (Tomljenovic et al. 2008). These are: (1) the Bosnian flysch zone (2) the zone composed of non- to low-grade metamorphic units derived from the distal Adriatic continental margin involved in the Late Jurassic ophiolite obduction (3) the Central Dinaridic ophiolite zone (CDOZ) which can be divided into two parts, i) ophiolite massifs, ii) Jurassic ophiolite mélange; and finally (4) the Sava zone or Sava-Vardar zone sensu Pamic (2002) located between CDOZ and Tisia. The Sava zone is interpreted as a Cretaceous-Palaeogene suture zone between the Dinarides and Tisia and is not exposed at the surface in the studied area (Tomljenovic et al. 2008, Pamic 2002).

3.9 External Dinarides unit

The External Dinarides include the tectonic units derived from the eastern part of the Adriatic (or Apulian) continent and are largely composed of Mesozoic to Tertiary shallow marine carbonate platform formations (Tomljenovic et al. 2008; Vlahovic et al. 2005). This unit covers a big area in the Southeastern part of Fig. 3.6. Since the external Dinarides and adjacent Southern Alps both belong to the former Apulian continent and are located south of the Periadriatic Fault (Doglioni & Bosselini 1987), defining the precise boundary is arbitrary. Both of these units are also characterised by an interference of Eocene (the main

deformational phase which is also known as “Dinaridic phase”) and Neogene to recent deformations (Vlahovic´et al. 2005; Schmid et al. 2008).

3.10 Adriatic Lower crust unit

The Adriatic Lower crust unit is the lowermost unit in the southern part of the profiles and lies above the MOHO. As mentioned above for the European Lower crust unit, it is not possible to determine the composition and physical properties of the Lower crust unit and it is only distinguished from the upper units by seismic properties. The Lower crust unit crops out only in the Ivrea zone, west of the study area.

3.4. MOHO discontinuity

The MOHO horizon in all the profiles corresponds to the boundary between the crust and the mantle. MOHO was first introduced in 1909 by the Croatian seismologist Andrija Mohorovičić and is well imaged by refraction seismics due to the different seismic velocities (McLeish 1992). The depth of the MOHO varies between 28 km and 56 km in the Eastern Alps and was mapped by Spada et al. (2013). This map is used here as a reference for constructing the profiles for my modelling.

3.5. Main Fault systems in the Eastern Alps

Normal faults as well as strike-slip faults formed after the collision of Adria and Europe (Behm et al. 2007; Ratschbacher et al. 1991). These faults affected the formation of topography in the Eastern Alps in Miocene time (Bartosch et al.

2017; Frisch et al. 1998; Frost et al. 2009; Linzer et al. 2002; Ratschbacher et al. 1991a, 1991b; Robl et al. 2008b; Sachsenhofer et al. 2003; Wölfler et al. 2011). Most of these faults became inactive in the late Miocene (about 10 Ma) except the Periadriatic faults and the eastern part of the Salzach-Ennstal-Mariazell-Puchberg Fault (SEMP) (Bartosch et al. 2017; Fig. 3.7). In the following, the major strike slip fault systems will be described in detail.

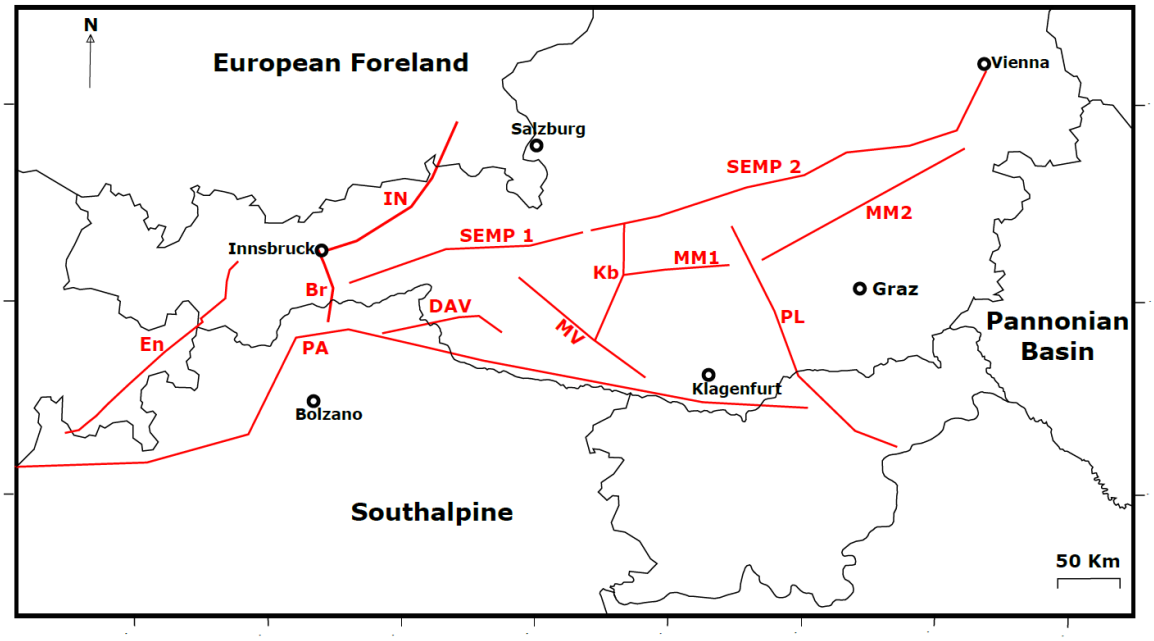

Figure 3.7: Simplified map of the Eastern side of the Alps showing the seven major faults in the study area (Bartosch et al. 2017).PA: Periadriatic fault, IN: Inntal fault, SEMP: Salzach-Ennstal-Mariazell-Puchberg fault , DAV: Defreggen-Antholz-Vals fault , PL: Pöls-Lavanttal fault, MM: Mur-Mürztal fault, MV: Möll valley, En: Engadine fault, Kb: Katschberg fault.

3.5.1. Inntal fault

The Inntal fault is located northwest of the Tauern Window and separates the western from the central part of the Northen Calcareous Alps. This fault played a key role in the E-W stretching process during lateral extrusion. The total offset (displacement) of the Inntal fault is about 80 km (Frisch et al. 2000) and it is recognised as a NE trending sinistral strike-slip fault. The Brenner fault caused

transformation from the sinistral into normal displacement at the western termination of the Inntal fault (Fig. 3.7) (Frisch et al. 2000).

3.5.2. Salzach-Ennstal-Mariazell-Puchberg fault

The Salzach-Ennstal-Mariazell-Puchberg (SEMP) fault system is one of the largest fault systems of the Alps and extends 400 km through the Eastern Alps. It is located south of the Northern Calcareous Alps and forms the northern boundary of the Tauern window in the west (Ratschbacher et al., 1991a, 1991b; Linzer et al., 2002). This fault system is divided into two parts (SEMP1 and SEMP2) (Bartosch et al. 2017) but here it is considered as one fault system. It comprises different segments. The Salzachtal fault is the westernmost part, forming the northern boundary of the Tauern window. This part was active from 35 to 28 Ma (Linzer et al., 2002). Towards the east, the Ennstal part is a ENE trending segment with a sinistral offset of about 60 km. The Mariazell-Puchberg segment cuts through the Northern Calcareous Alps and the offset decreases towards east (Linzer et al.2002; Frisch et al.2000). The tectonic activity took place during Oligocene to Miocene and there is evidence that it is still partly active, especially SEMP 1 (Bartosch et al. 2017).

3.5.3. Pöls-Lavanttal (PL) fault

The Pöls-Lavanttal (PL) fault system east of the Tauern window is a NNW trending, mainly dextral fault system. It divides the Murtal fault system into two parts, Upper Mur Valley and Mürz valley. The total displacement of PL fault is

about 20 km and divided into almost two same equal parts (8 to 10 km). The northern part of this fault was active from 18 to 12 Ma (Reinecker 2000) and the southern part was active from 11 to 5.5 Ma (Reischenbacher and Sachsenhofer, 2013). At the southern end, the PL cuts and offsets the Periadriatic fault by 20 km (Fig. 3.7) (Frisch et al, 2000).

3.5.4. Mur-Mürztal (MM) fault (west and east)

The Mur-Mürztal (MM) fault is as complex EW to SW-NE trending sinistral fault system. It is divided into a western (Upper Mur Valley) and an eastern part (Mürz valley) by the PL fault system (Fig. 3.7). This fault is surrounded by transtensional (pull-apart) basins (e.g. Vienna basin). It was active from 17 to 13 Ma and major subsidence occurred between 17 and 14 Ma (Bartosch et al. 2017; Ratschbacher et al. 1991b).

3.5.5. Defreggen-Antholz-Vals (DAV) fault

The Defreggen-Antholz-Vals fault is another EW-trending fault in the Eastern Alps. It is located south of the Tauern Window and was active as a sinistral fault system. The DAV was partly active as a ductile shear zone and partly as a brittle fault (Mancktelow et al. 2001). The Defreggen-Antholz-Vals fault was active from 46 to 25 Ma (Bartosch et al. 2017).

3.5.6. Periadriatic fault

The Periadriatic fault is the most prominent fault line through the Eastern Alps and is also expressed in the topography of the Eastern Alps (Schmid et al. 2012). It extends about 700 km from the northwestern border of the Po basin to the eastern border of the Eastern Alps (Slovenia). This fault separates two different tectonic units, the Southern Alps with a weak Alpine metamorphic overprint, and the variably metamorphosed Northern Alps (Frisch et al. 2000; Bartosch et al. 2017; Mancktelow et al. 2001). The Periadriatic fault is subdivided into smaller fault lines. Some of them are sinistral (the Giudicarie Fault) but most of the fault system is dextral. The main fault is up to several hundred meters wide (Mancktelow, et al. 2001). The total displacement of the PL fault system is controversial. In some articles it is estimated at 200 to 300 km (Sprenger 1996; Schmid et al. 2004), in others, 30 to 100 KM (Pomella et al. 2011). This fault was active from 32 Ma until 13 Ma in different parts (Bartosch et al.2017; Wölfler et al. 2011; Zwingmann and Mancktelow 2004).

3.5.7 MV fault system

Möll-valley fault is a dextral fault which strikes along 80 km in a NW direction and cuts into the Tauern Window at its SE end. This fault shows an offset of about 2.5 km. The first main vertical kinematic tectonic activity of this fault zone was between 27 and 25 m.y. and second tectonic activity occurred at 21 m.y. (Bartosch et al.2017, Wölfler et al. 2011).

3.5.8. Engadine fault

The Engadine fault line is a sinistral strike-slip fault with lateral displacement varying between 3-6 km in the Upper Engadine window and also up to 20 km in the Lower Engadine window (Trümpy 1977). This fault line shows a major SW-NE trending steeply inclined discontinuity but the vectors of movement along this line rapidly chane along strike (Schmid and Froitzheim. 1993).

3.5.9. Katschberg fault

The katschberg fault system is located east of the Tauern window and developed dynamically in response to the strike-slip zone activity at 15 m.y. (Bartosch et al. 2017). This fault system is a north-south striking shallow angle detachment fault that is bound the eastern boundary of the Tauern window (Fügenschuh et al., 1997; Genser and Neubauer, 1989).

3.6. Methods, data and model building procedure

As discussed earlier, for the second part of my research I have built a model for the Eastern part of the Alps. Although the modeling is focused on structures within the crust, the model reaches from the Earth surface down to ca. 300 km depth in order to allow including the LAB (lithosphere-asthenosphere boundary) at a later stage. The geometry of the latter will be much better defined in the next few years by a passive seismic array in the framework of Alp Array, an international European research initiative. The western boundary of the model

is the NFP20 East transect. This section is well constrained by reflexion and refraction seismics and has been intensively studied (e.g. Schmid et al. 1996). It is also the eastern boundary of the model by Vouillamoz et al. (2012) for the Western Alps. The northern boundary of the model lies in the Alpine Foreland Basin in South Germany and Austria, the eastern boundary in the western Pannonian Basin, and the southern boundary in the Po Basin.

I included the following horizons in the model: Digital elevation model and simplified tectonic map of the Eastern Alps; base of Tertiary in the Northern Foreland Basin, Pannonian Basin, and Po Basin; boundary between pre-Tertiary cover and basement in the basins; boundaries between basement and cover in the Austroalpine nappes, base of the Austroalpine nappes, base of Penninic cover units (Rhenodanubian Flysch, sediment and ophiolite units in the Tauern Window and Engadine Window), base of Helvetic nappes, basement-cover contact in the Southern Alps; top of lower continental crust; Moho. In addition, major thrusts and faults transecting the nappe stack are defined as surfaces, including offset of the horizons that they cut: Salzach-Ennstal-Mariazell-Puchberg Fault (SEMP), Engadine Fault Periadriatic Fault, Katschberg Fault, etc.

The surface geological map is taken from Schmid et al. (2004) and simplified by merging the tectonic units into groups to fit the requirements of the model. In the Tertiary basins, very good constraints for the base of the Tertiary and the basement-sediment interface can be derived from numerous seismic sections and drillings. Well-studied reflection seismic traverses across the Alps are the NFP 20 East traverse, forming the western boundary of the model (Schmid et al. 1996), and minor E-W lines connected to this (Pfiffner & Hitz 1997). The

Transalp reflexion seismic section (Lüschen et al., 2004) is oriented north-south approximately in the middle of the model area. For the Italian (southern) part of the model, I adopted relevant horizons from the 3D model of the Italian subsurface (D'Ambrogi et al., 2010). The Moho topography was adopted from the map of Spada et al. (2013) which shows Moho topography according to controlled-source seismology and receiver function information. Furthermore, a wealth of cross sections have been constructed using projection of surface geology. The process of integrating all these input data into a model involves testing their compatibility and making corrections where necessary.

As mentioned before in chapter 1 and 2, the first step for building the three dimensional model in MOVE by Midland valley is to enter the digital elevation model of the area and to import the Geological map of the area which is georeferenced before by other software (Arc-GIS) in the model beneath the DEM. After implementing the DEMs and Geo-referenced maps, the different structural units and fault lines in the geologic map were digitized. The next step was to enter the parallel cross sections to the model. For this research 34 profiles were traced and inserted from west to east into the software as input profiles (Fig. 3.8). These profiles were drawn and edited from surface to about 60 km depth (until Moho). Four of these profiles, NFP-20 EAST, Engadine section, Transalp and Eastern Alps were available from the literature (Schmid et al. 2004, Rosenberg et al. 2015) and the rest I have newly constructed or completed. These 30 new cross-sections were mostly drawn based on the available data such as Moho maps, small scale profiles and seismic profiles and then completed down to the Moho.. For the parts where I could not find any

data, I have tried to follow the pattern of the available profiles and to gradually change the geometry between the profiles from most west (NFP 20) to east.

The steps that I have followed for building these profiles are as follows:

1. First, the location for all the profiles was determined and digitized parallel to the four main profiles (NFP-20, Engadine, Transalp and Eastern Alps).
2. In the next step, the topography was extracted from the inserted digital elevation model (DEM) and projected into the cross-sections.
3. Then like in the previous step, I have extracted the Moho line for each profile from the digitized Moho map in the model.
4. After that, the thicknesses of the European and Adriatic Basement where entered as constant values based on the available data. For the profiles located between the main profiles, I have assumed thickness values between thickness values of the profiles. For the profiles from Eastern

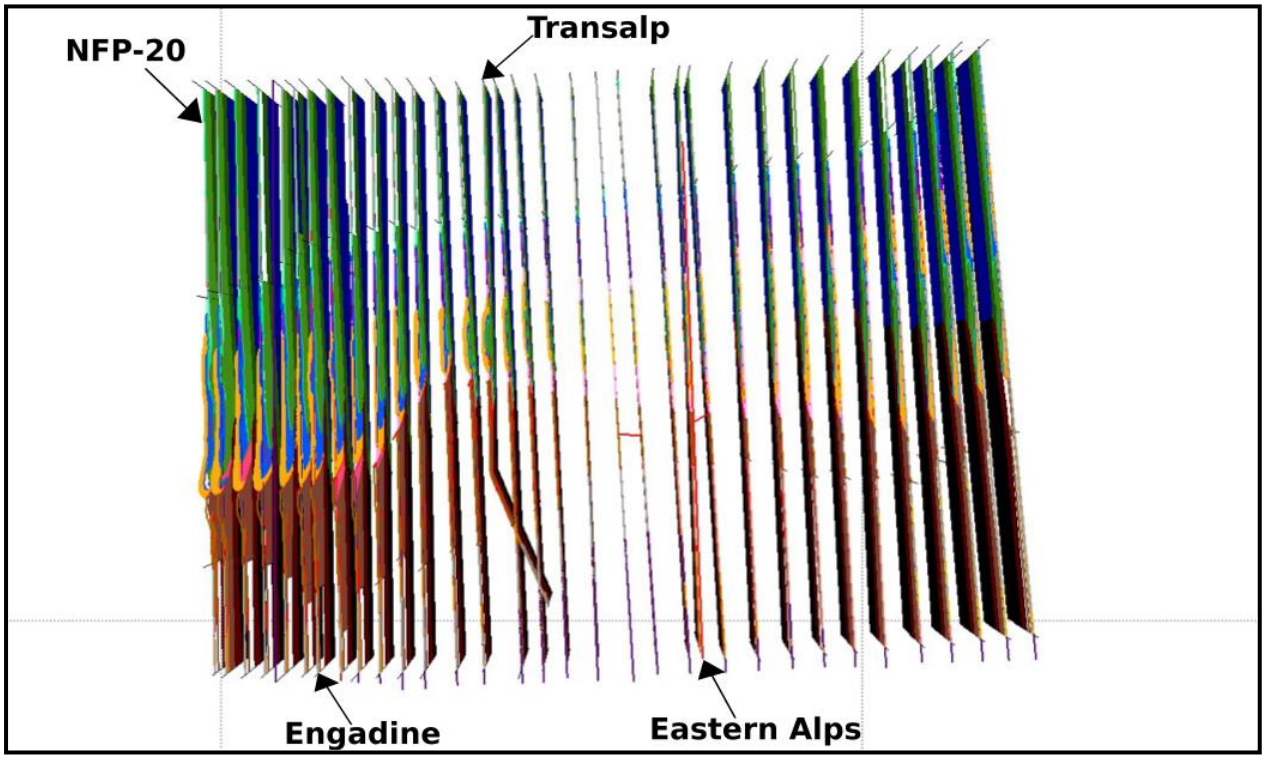

Figure 3.8: 34 input profiles which were inserted parallel to each other in the model. Please see Appendix B for the complete profiles.

Alps profile to east, I have assumed values decreasing towards to the East based on the available literature.

5. For the thicknesses of the other layers I have followed the same methods as described in previous steps as well as transitional geometries between the available profiles.

6. For the most eastern profiles C15 to C24 I have extracted the top of the Moho from the map and then tried to follow the trend of the layers from the Eastern Alps profile to the eastern end of the Alps (Fig. 3.8).

3.7. Quantifying the crustal shortening through the Eastern Alps by the input profiles

Since the Alps are the result of the collision between the two continents, the amount of shortening in different parts of the Alps is an interesting topic. Quantifying the shortening may help to understand the development of this

complicated mountain chains. The balanced cross-section concept was first discussed in detail by Dahlstrom in 1969 (Dahlstrom 1969; Woodward., et al. 1989). Crustal shortening is defined as the reduction of the length of the Earth's crust through tectonic activities such as those found at a convergent plate boundary. Different methods are used for calculating the amount of shortening. For example, 12 km of shortening of the TALP (Thickened Accreted Lower Plate) in the Engadine profile is calculated by Rosenberg & Kissling (2013). In contrast, 30 km shortening was calculated by Rosenberg et al (2015) for the same profile. In my research, I have calculated shortening by line length balancing and by area balancing since 30 Ma to present. It should be noted that for both of these methods the assumption is that the deformation happened in two dimensions and there is no lateral movement in or out of the profile (Woodward,1989).

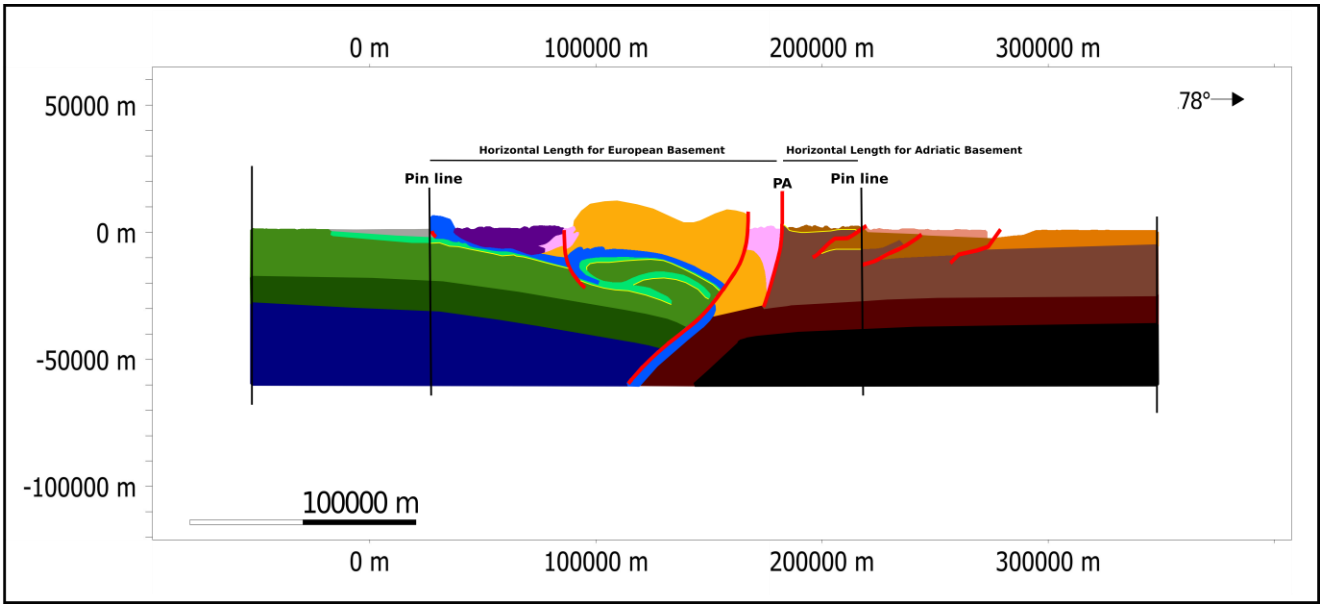

Figure 3.9: Eastern Alps profile as an example for showing the procedure for calculating the shortening with the line length balancing method. Yellow lines on top of the European and Adriatic basement indicate the length of the horizons which are used for calculating the shortening by the line balancing method. The total shortening by this method is equal to the total length of these yellow lines minus the Horizontal length of the horizon from the Pin line to the Periadriatic fault.PA: Periadriatic fault. Colours: See Fig. 3. 2.

For this purpose I have considered the same horizon in all the profiles (European Basement top and Adriatic Basement top) as a reference horizon

for calculating the collisional shortening and in order to have comparable data. For quantifying the shortening by line balancing and area balancing, pin lines are defined in the profiles. Pin lines were defined at the northern and southern borders of the Alps. In the following paragraphs, I will discuss the procedure which I used for calculating the shortening by line length and area balancing methods as well as amount of shortening that is calculated from the all input profiles. Finally I have compared the values that I found with the values and data from other studies.

3.7.1. Line length balancing

Line length balancing or line restoration is a common method for quantifying the shortening for horizons in a folded and/or faulted cross-section (Woodward

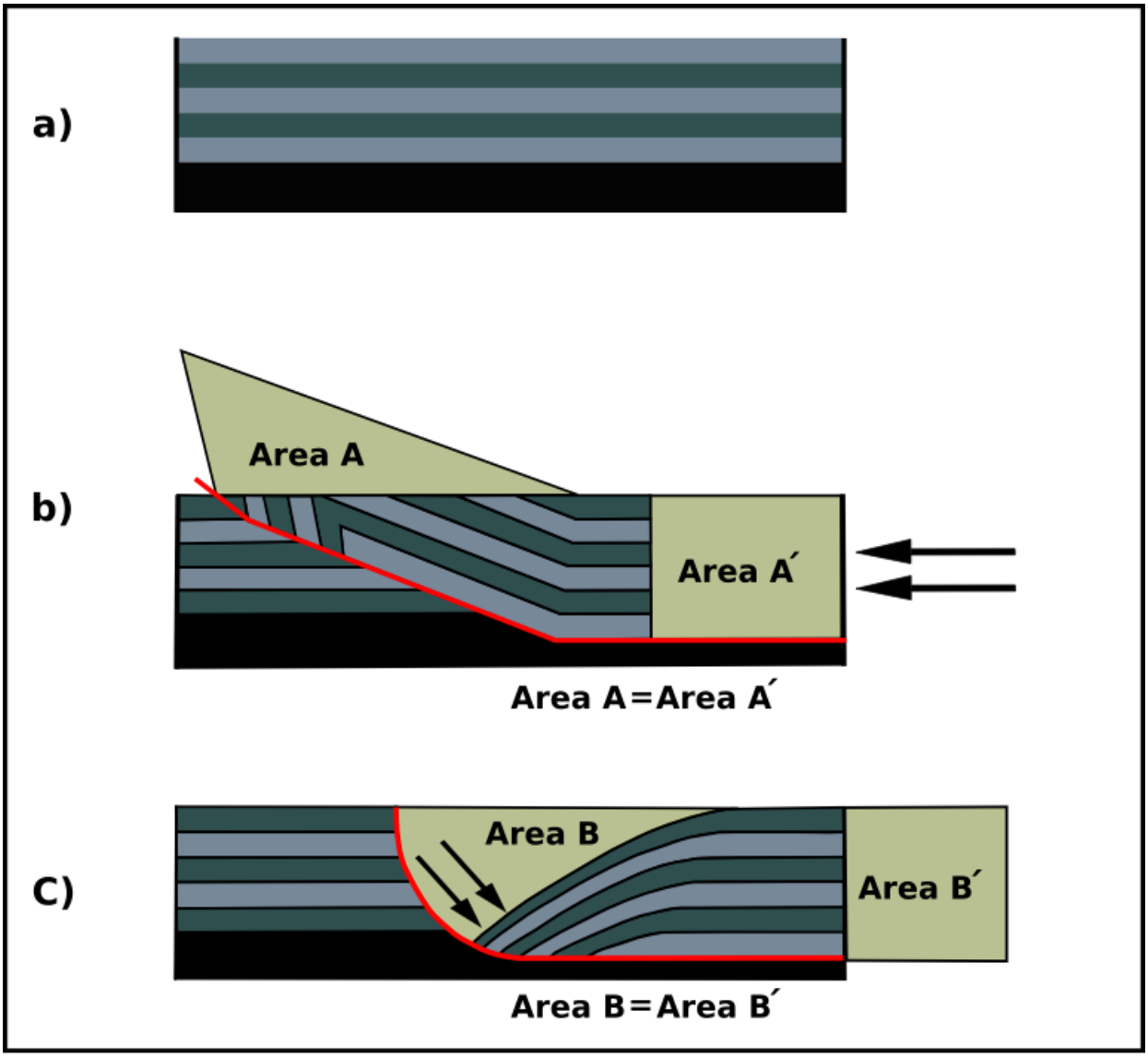

Figure 3.10: Constant area restoration of a profile in the transport direction, from Fossen 2016.

1989). This method measures the distance between end points after deformation and the horizontal length before deformation for a specific horizon in the profile.

I have only considered top of European basement and Adriatic basement horizons in the profiles (Fig. 3.9).

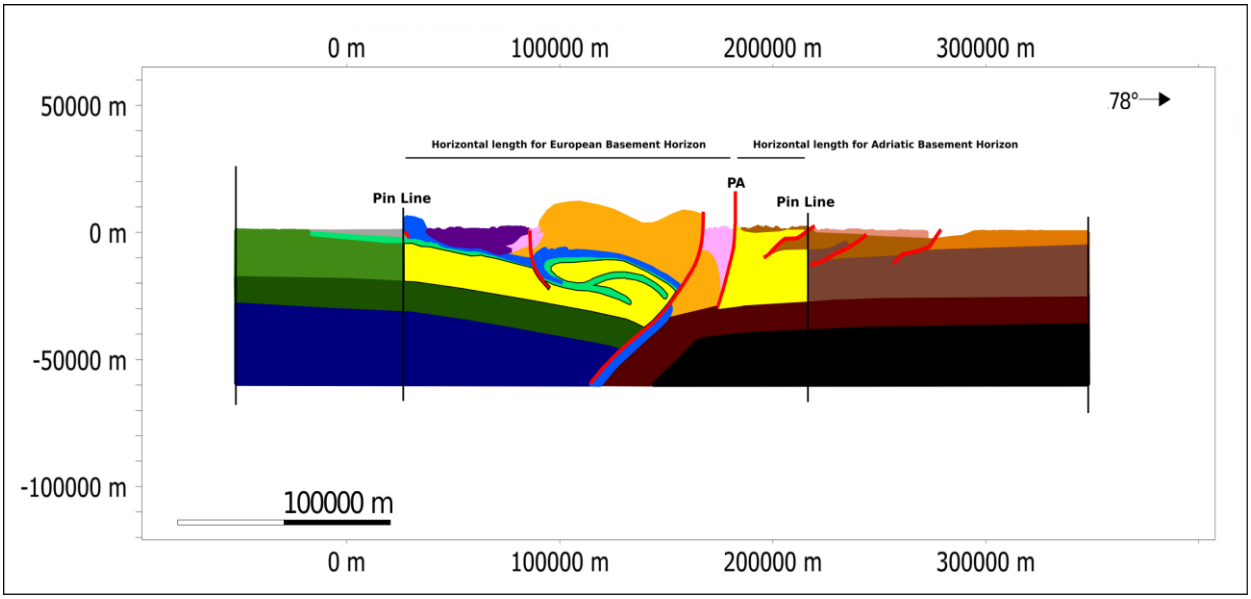

Figure 3.11: Eastern Alps profile as an example for showing the procedre for calculating the shortening based on the area balancing method. Yellow areas for the European and Adriatic basement horizons indicate the areas which are used for calculating the shortening by the area balancing method. The shortening by this method is equal to the horizon length which calculated by the Area divided by the pre-deformation thickness of the horizons minus the Horizontal length of the horizon from the Pin line to the periadriatic line. PA: Periadriatic fault. Colours: See Fig. 3. 2.

Fig. 3.9 shows an example of using the line restoration (length) method for a cross-section and this approach was applied to all cross-sections in order to get comparable results. The shortening results for all the profiles from 30 Ma to present are illustrated in Fig. 3.12 and 3.13.

3.7.2. Area balancing

Area balancing (restoration) method can also be used to quantify the shortening in a profile for a folded area. During deformation, the length of the horizon is not always preserved, but the area of the deformed rocks will remain constant. If deformation causes a rock to move out of one area by some volume, then the rock must move to another area by the same amount as seen in figure 3.10 where area A equals area B despite a change in layer length (Woodward, 1989). Calculating the shortening by the area balancing technique can allow us to reconstruct the rock deformation that is deformed by more than plane strain.

In this research, the area balancing method was also applied for all the profiles to get a better overview of the Alpine orogeny and also compare the results with the available data and test different hypotheses. The shortening values by the area balancing method in my research are calculated by the following formula;

Area balancing shortening= (Area of the Horizon/ Thickness before shortening)-Horizontal length after shortening

Fig. 3.11 shows an example for measuring the shortening by the area balancing method for the European and Adriatic basement horizons for one of the profiles in the model. These calculations were followed for all the other profiles and summarized in Tab. 2 and also plotted in Fig. 3.12 & 3.13.

3.8. Results and discussion

Fig. 3.12 shows the amounts of shortening calculated from the line balancing and area balancing as described before for the European basement top. The line-length shortening values vary between 52 and 148 km. They decrease first from NFP-east to Engadine profile and after that, they increase to the maximum of about 144 km for the Transalp profile. This extreme crustal shortening was mainly accommodated along the antiform of the Tauern window. After that, the shortening for European basement decreases again to about 93km for the Eastern Alps profile and remains almost constant until the easternmost profile (Profile C24) and the border of the model. These values in my data compared to other research (Linzer et al. 2002; Rosenberg & kissling. 2013; Rosenberg

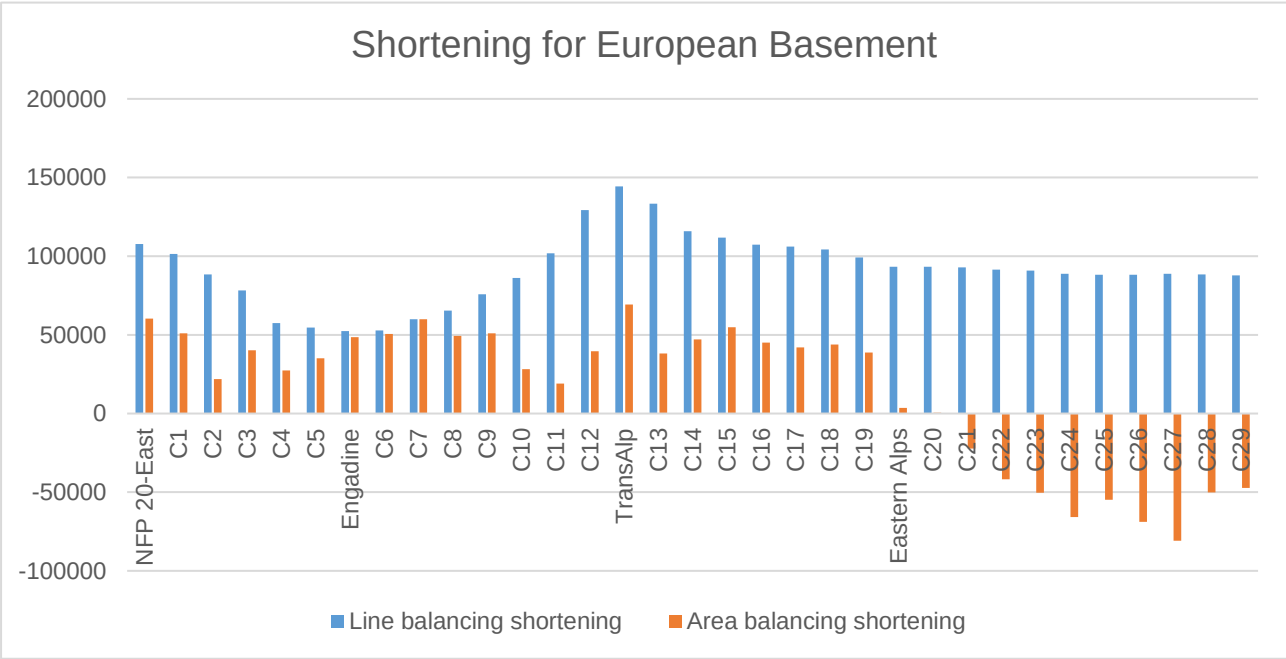

Figure 3.12: Line and area balancing shortening result for the European Basement horizon for all the profiles in the model.

et al. 2015) are much higher, for example for the Engadine Profile, it is about twice the amount calculated by Rosenberg et al. (2015).

For the shortening that is calculated from the area balancing of the European basement (second method), it should be noted that the amounts for all the profiles by this method are lower than by line balancing (Fig. 3.12). These lower values could result from two main reasons:

1. Pre-Alpine thinning of the upper crust,

2. E-W stretching together with N-S shortening during the Alpine collision.

The highest number of shortening by area balancing method, between all the profiles is about 69 km for the Transalp profile. Towards east, the shortening decreases to about 500 m for profile C15 and after that the values become negative. The negative values for the shortening in the easternmost Alps reveal that lateral extrusion (lateral material transport) occurred because of the extensional collapse and tectonic escape (Ratschbacher., L. et al. 1991; Linzer

et al,. 2002) during the late Oligocene-Miocene. The negative numbers vary between -20 km up to -75 km.

Fig. 3.13 represents the shortening results for the top of the Adriatic basement. It shows that shortening is about 42 km for the most western profile in the model (NFP-20) and increases to a maximum of 53 km for the Engadine profile. After that, the shortening decreases slightly until the Transalp profile and then continues to decrease sharper to the most eastern profile where it reaches the minimum amount of about 9 km, reflecting the transfer of shortening of Adria from the Southern Alps to the Dinarides. These crustal shortening amountsare about 30 km lower than the ones of Rosenberg & Kissling (2013) for the Southern Alps in the Engadine profile. This could be a result of neglecting the internal shortening in the Southern Alps basement.

Like for the European basement, the shortening that is calculated by the area balancing method for the Adriatic basement is lower than for line balancing (Fig. 3.13). The general trend of variation for shortening is also the same as for line balancing. The shortening in the west is about 38 km and towards the east, it increases slightly to about 42 km and then decreases and reaches about 8 km for profile 24.

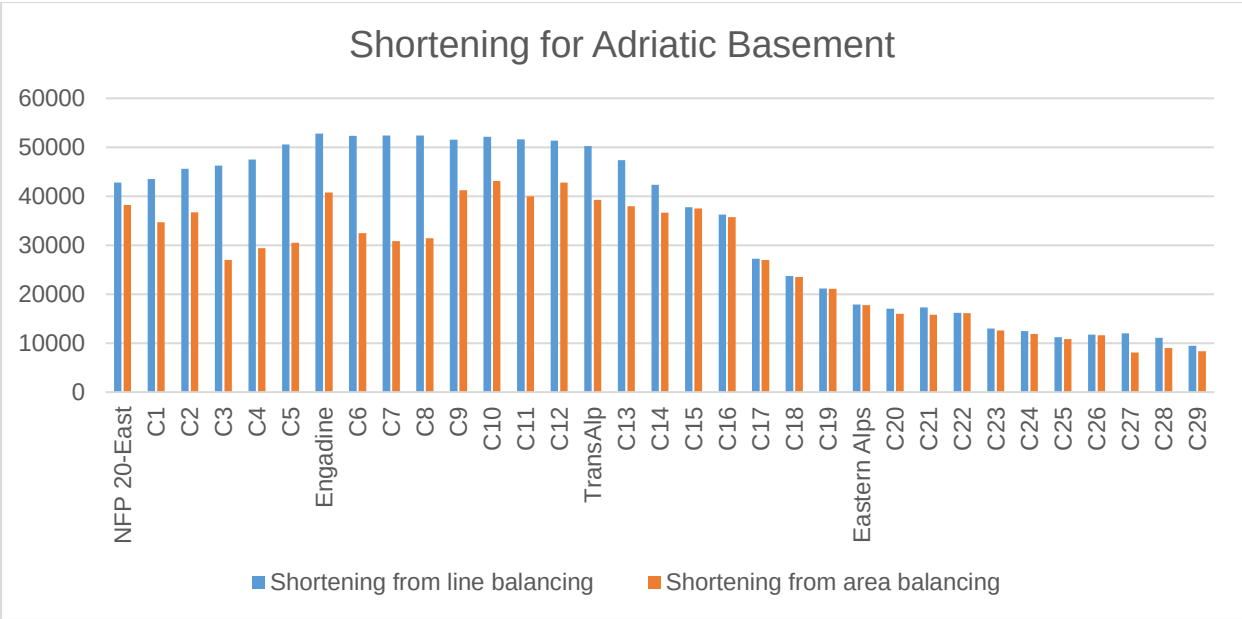

Figure 3.13: Line and area balancing shortening result for the Adriatic Basement for all the profiles in the model.

The total amounts of shortening by the line balancing method for all the profiles that are the sum of shortening for European and Adriatic horizons are shown in Fig. 3.14. The shortening values vary between 97 km and 180 km and reveal the different post-collisional shortening through the eastern Alps. The maximum amount is for the profiles in the Tauern window and could be the result of nappe folding in this window and probably reflecting pre-Alpine margin geometry (Dolomites indenter). The data for the eastern Alps (Fig. 3.15) also show that for the profiles in the Tauern window and also NFP-20 east profiles about 60% of the shortening are concentrated in the European units and 40% in the Adriatic units. For the Engadine profile shortening is almost equally distributed (50%/50%). In contrast, at the eastern side of the Tauern Window until the eastern end of the model, about 90% of shortening are concentrated in the European part and only 10% in the Southern Alps.

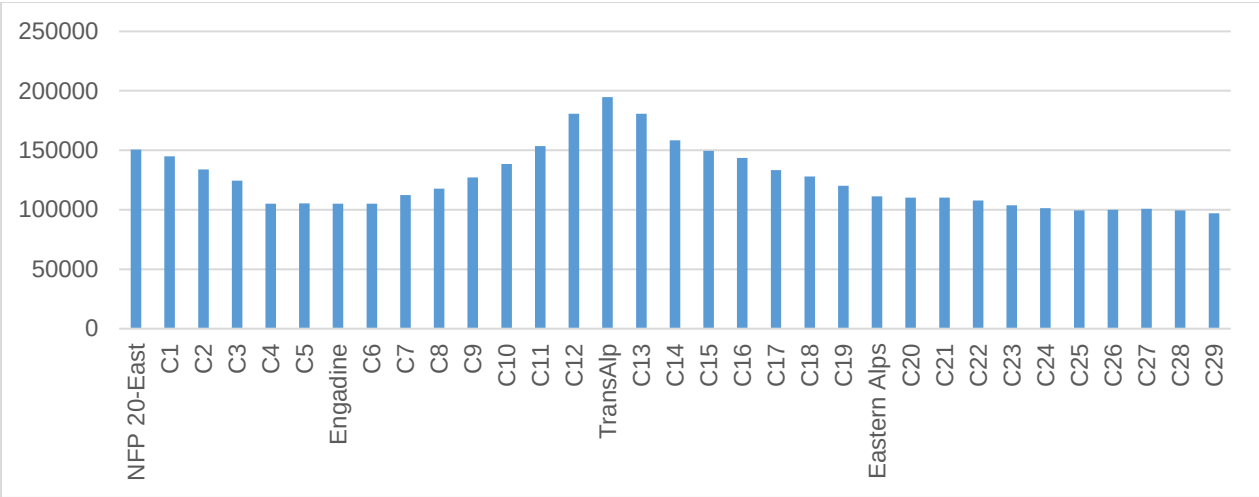

Figure 3.14: Total line length balancing result for the European and Adriatic Basement horizons for all the profiles in the model.

The crustal shortening that is calculated by the line-length balancing method is shown for both European basement and Adriatic basement horizons in Fig. 3.15. This figure shows the area that is destructed from the time of collision at 30 Ma untill the present. By connecting the fronts of these shortening lines, we can reconstruct the former front for the European continent and the front of the Adriatic continent (Fig. 3.15). By dividing the amount of shortening by 30 Ma it is possible to calculate the tectonic plate velocity.

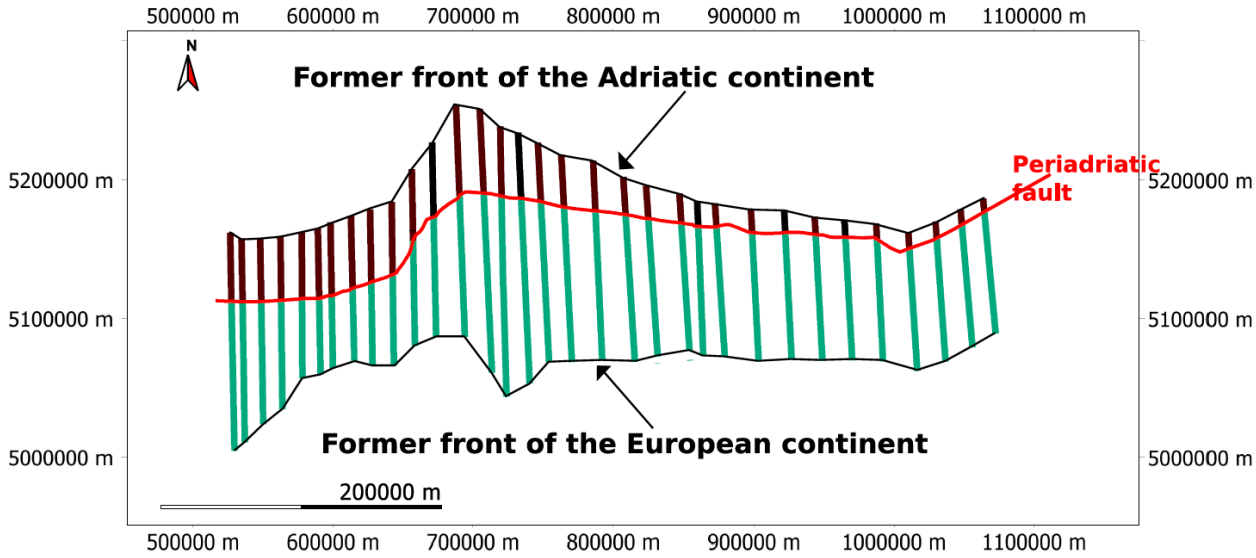

Figure 3.15: Line balancing result for the European Basement horizon for all the profiles in the model. The area represent the area whichwas destructed due to the collision of the Alps since 30 Ma.

Based on the total shortening data, the minimum tectonic plate convergence velocity is about 3 mm/year, and the maximum is 6 mm/year. These numbers from my data are in quite good range compared with the 3 - 4.5 mm/year N- S convergence between Adria and Europe and also the 2 - 3 mm/year N-S convergence between Eastern Alps and Adria that is calculated by Grenerczy et al. (2005) from GPS data. The plate velocities that are calculated by different researchers vary between 3 and 9 mm/year depending on different method (Geodetic data, GPS data, forward modelling data etc,) and remain still a matter of debate (Grenerczy, et al. 2005; DeMet et al. 1994; Sella et al. 2002; Nocquet & Calais 2003).

3.9. Conclusions

The area balancing assuming constant pre-collisional crustal thickness gives generally lower values for shortening than line balancing and even negative values east of the Tauern Window (i.e. stretching), which may reflect, among other processes, pre-orogenic thinning of the continental margins as well as east-west stretching of the crust during Miocene tectonic extrusion. The added shortening of European and South Alpine basements is at a maximum at the western end of the Tauern Window, probably reflecting pre-Alpine margin geometry (Dolomites indenter). These results are in good accordance with the tectonic evolution as inferred from other methods. By drawing the shortening data for the European and Adriatic basement it is possible to estimate the area that is missing due to the collision during the Alpine orogeny which is the area that was destructed by the movement of Adria towards Europe since 30 Ma. The data also shows the average tectonic velocity between 3 to 6 mm per year which is in a good range compared to other available data. Although the model carries large uncertainties, partly due to the scarcity of information about deep crustal structure away from the seismic sections, these results are in good accordance with the tectonic evolution as inferred from other methods.

This page intentionally left blank.

Chapter 4

Crust volume calculation for the eastern part of the Alps (Eastern and Southern Alps) based on the 3D Modelling and quantitative evaluation

Abstract

Many researches have been carried out regarding to the issues of subduction of continental crust, subsurface structures, and kinematics of the Alps but they have come to the inconsistent conclusions. Due to the scarce data and mass-balance calculations for the eastern Alps, in this research I have tried to build a valid three dimensional geometric model for the eastern part of the Alps in order to test different hypotheses in large scale and address some of the problems by numerical modelling and finally fill the gap that exists in literatures in this topic. The 3D model provides an opportunity to take a look at the deep structures of the eastern part of the Alps and measure the current amount of crust volume by forward modelling. I have also calculated the total amount of material which disappeared. This crust deficit could be explained as a result of different processes like subduction, east-west extension (thinning) and finally erosion. The results imply subduction of about 1*10^6 km^3 continental crust as a result of the collision since 30 Ma for both European and Adriatic continents in the eastern part of the Alps and the

subducted crust (material) from the European continent is almost twice the amount from the Adriatic continent.

4.1. Introduction

As mentioned before in the previous chapter, the Alps are the result of the continent-continent collision between the European and African continents since the Late Cretaceous. This convergence and tectonic plate collisions led to crustal thickening, erosion, subduction, and exhumation (Kuhlemann et al. 2001; Beamont et al. 1996) (Fig. 1). Although the Alps are well studied and despite the availability of many surface data (maps, profiles, P-wave velocities, topography data, tomographic images), many issues related to the deep structures and subjects regarding to the Alpine orogeny remain unsolved and matter of debate.

One of the important problems that still remained unknown and also crucial for understanding the Alpine orogeny as well as kinematic analysis of the Alps is the role of subduction and the volume of crust in the subsurface (Le Pichon et al. 1988; Butler 1986; Ingalls et al. 2016).

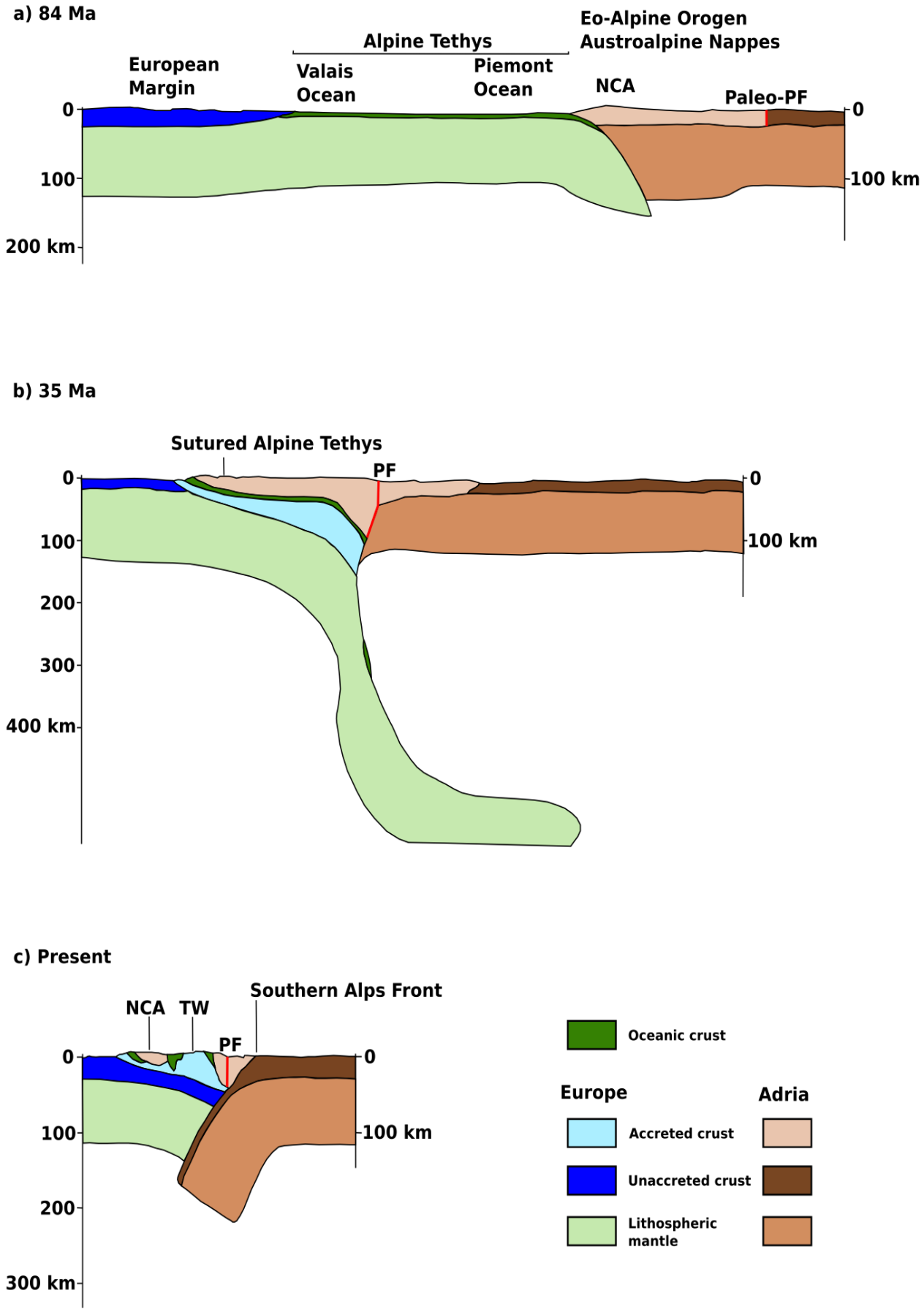

Figure 4.1: Simplified profiles across the eastern part of the Alpine orogen, from Handy et al. 2014. ***a*** *84 Ma : Initial subduction of Alpine Tethys;* ***b*** *35 Ma: Alpine orogenesis and incipient rupturing of European slab;* ***c*** *Present profile with north-dipping Adriatic slab beneath the Tauern Window.*

It is also proposed by some scientists (Coward & Dietrich; 1989) to restore the Alpine paleogeographic belts quantitatively especially in three dimensions to understand the crustal structure, structural history as well as collisional and post-collisional processes.

One of the key methods for quantifying the crust volume is the material balance method. The mass (material) balance for the continental crust helps us to calculate the amount which has been subducted from the start of the collision until now. This method also help us to understand the carbon cycle, the composition of the earth's mantle as well as understanding of volcanic and seismic hazards in subduction zones (Berner and Caldeira, 1997; Lyubetskaya and Korenaga 2007).

Since the beginning of the twentieth century, some scientists (Ampferer, 1906; Butler, 1986; Butler et al., 1986; Le Pichon et al., 1987) used the material balance method with the balanced cross-sections and tried to solve the problems related to the shortening and continental crust subduction in the Alps. The material balance concept also has been applied for understanding the complexity of the tectonic plate interactions especially in the Alps (Laubscher, 1988., Laubscher, 1990; Kuhlemann. et al., 2002).

For this part of my research I have used MOVE (Midland Valley Corporation) to build a consistent 3-D geometric model from the available data for the eastern part of the Alps in order to calculate the amount of continental crust which still exists both for the European and Adriatic continents, down to a depth of 60 km and compare the results from the 3D modelling with the material balance method.

More specifically, the main aim of this chapter is to answer three fundamental questions regarding the geodynamic evolution of the eastern side of the Alps. These are:

1. How much continental crust volume is still present in the Alps?
2. How much continental crust volume was subducted or destructed during the Alpine orogeny?
3. What is the subduction rate in the Alps?

By combining the data in this chapter with the data of the previous chapter, it is possible to calculate the crust which is still present and also the continental crust which was already subducted or destructed through the subduction zone since 30 Ma and finally calculate the subduction rate for this part of the Alps.

4.2. The Alps and the role of subduction zones

Subduction zones accommodated the convergence of the European and Adriatic plates in Mesozoic and Cenozoic (Wiederkehr. et al., 2009). The subduction process in the Alpine Tethys started in the Late Cretaceous, first with consumption of the Tethyan oceanic units (Piemont-Ligurian domain), followed by subduction of the lower part of the continental crust which continues to the present time (Handy et al., 2010; Bruckl, 2011; Schmid et al., 1996) (Fig. 4.1).

The tectonic evolution of the Alps is assumed to be controlled by two different subduction zones, an older subduction zone in the Neotethys

realm and a younger one in the Penninic domain (Froitzheim et al., 1996, Neubauer et al., 2000, Stüwe & Schuster, 2010).

Oceanic crust is denser than continental crust and as a result at the subduction zones, the oceanic crust usually sinks into the mantle whereas lighter continental crust stays at the surface. The initiation of subduction is a matter of debate (Stüwe & Schuster, 2010). Ampferer (1906), Argand (1916, 1924(a, b)), and Laubscher (1969, 1970) assumed subduction of continental crust based on the material balance results. There is now general agreement that assuming the subduction of continental crust is inevitable.

On one hand, based on the material balance a large volume of continental crust is missing (Butler et al., 1986; Butler, 1986; Laubscher, 1988; Le Pichon et al., 1988) and only small slices of the uppermost parts of the continental crust are preserved in the Alpine nappes. On the other hand high- and ultrahigh-pressure metamorphism is found in tectonic units which consist of continental crust. This cannot be explained without assuming the subduction and later exhumation of these units (Dal Piaz et al. 1972). In addition to the above mentioned reasons, continental crust subduction could also explain isostatic disequilibrium leading to the pattern of uplift in the Alps (Coward & Dietrich, 1989).

Studies of the subduction zone and crustal volume calculation in the Alps and Himalayas include Kuhlemann et al. (2002), Ingalls et al. (2016), and Merchant & Stampfli (1997). In addition to that many numerical studies have been carried out in order to investigate the subduction process

behaviour (e.g. Van Hunen et al., 2000; Funiciello et al., 2003; Kincaid & Hall, 2003; Hampel & Pfiffner, 2006).

Advancement in forward modelling especially with 3D applications opens a new window for geologists to go more into detail and build a valid geometric and kinematic 3D model of the research area and answer some of the issues which still remain unsolved. In the following, the volume and rate of continental crust subduction will be estimated for the eastern part of the Alps.

4.3. Geological setting and data

The studied area for this part of my research is the same as in chapter 3 and extends from N 45° to 47° and E 13° to 15°. The western boundary is the NFP-20 profile and the eastern boundary is the eastern transition of the Alps to the Pannonian Basin. This includes the entire eastern Alps as well as most of the Southern Alps (Fig. 3.2).

The data used for this chapter are mainly based on the new profiles that were drawn and already used in the previous chapter (chapter 3) for building the 3D model. As already mentioned in the previous chapter, it should be noted that my 3D kinematic model does not address strike-slip displacement.

4.4. Building the complete three dimensional model and calculation of the volume from the model

After implementing the digital elevation model (DEM), geo-referenced geological map, digitizing the fault and thrust lines on the surface, and inserting the input profiles in the digitized positions, the next step for building the 3D model is building the subsurface layers and connecting these profiles together by the surfaces. The surface in MOVE is built by the surface option in the model building menu. The surfaces in MOVE are built based on the interpolation algorithm between the parallel profiles (M.Yosefnejad et al. 2017). To build a surface between two profiles, I have followed the following steps:

First, I have opened the surface option from the model building panel.

Then, I chose two identical horizons from the adjacent profiles. In the next step, I have chosen one of the options that are available in the surface menu (linear, curved and …) and built a surface for the specific horizon. These different options allow the user to minimize the errors in the model and they depend on the horizon shape and characteristics. For instance, for a horizon that is straight and also has a sharp edge, the linear option for surface building gives a lower error and the surface matches better with the horizon lines.

These steps are repeated for all the horizons in all the inserted profiles to have a complete geological three dimension subsurface model for the studied area. When the subsurface layers are completed, the program allows to build a volume (blocks) between the surfaces. MOVE allows the user to build volumes using different options. I have tried different

options for my research but at the end, I have used the Geocellular volume option which is available in the model building menu since it reduced the error for our model compared to other options.

Another point about building a block volume between two surfaces is the mesh size which is also an important factor for reducing the error of the calculations. The error is decreased by decreasing the mesh size and width of the blocks since it also covers the small edges and the whole line curves can be covered between the two surfaces that are selected as the top and bottom horizons. However, I should also point out here that by decreasing the mesh size the size of the file will increase.

This option (Geocellular volume) is again using the interpolation algorithm for building the volume. In other words this option interpolates between the upper and lower surface and fills the space with a specific volume (block). This option has to be repeated for all the surfaces in order to have a complete volume for the whole model (Fig 4.2).

In my research, I have calculated the volume for only the units related to European and Adriatic continents and 4 specific layers. These layers are European and Adriatic lower crust and European and Adriatic basement (=upper crust). For instance in our case, the volume for European basement is built by interpolating between the European basement surface and the Lower crust surface.

The volumes created by this method can be used to determine how much volume from the European and Adriatic crusts is now present in the eastern side of the Alps down to the depth of 60 km and how much

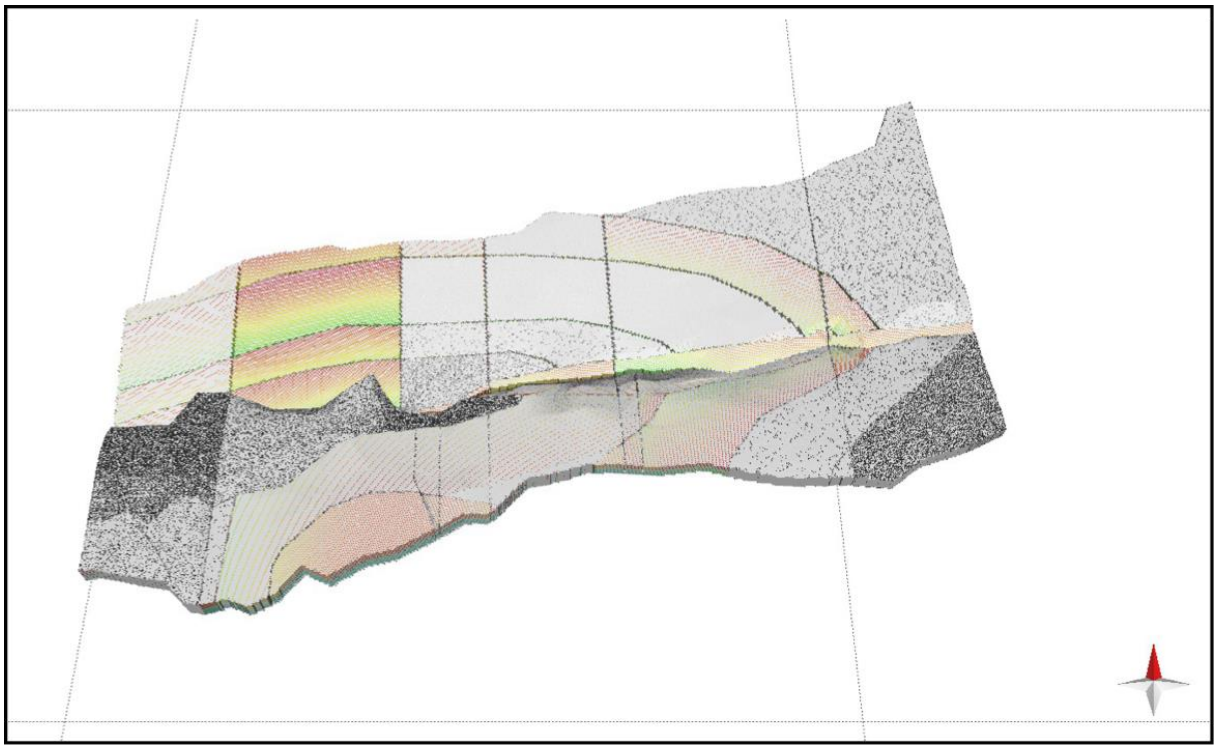

Figure 4.2: Block volumes resulted from the 3D model, for the European and Adriatic Lower crust.

has already been subducted into the mantle from the Cretaceous until today.

4.5. Results and discussion

As discussed earlier one of the great advantage of the 3D model is that it allows the user to extract surface as well as subsurface data. For this part of my research, I have extracted the total crust volume which still exists in the studied area for the four specific layers.

In addition to the current crust volume, I have also calculated the amount of continental crust that disappeared (eroded or subducted into the mantle) by using the data in chapter 3 since 30 Ma until now. As explained in the previous chapter, Fig 15 in chapter 3 shows the area that has been destructed (is missing) because of the collision of the European and Adriatic continents. By multiplying the pre-collisional area

at 30 Ma (destructed area + present area) for the European continent and Adriatic continent with the average thicknesses of each layer (European Lower crust, Adriatic Lower crust, European Basement and Adriatic Basement) that are derived from the 34 input profiles, the pre-collisional crust volume for each specific layer could be calculated. The difference between the pre-collisional crust volume with the present crust volume (derived from 3D model) could represent the destructed crust volume for each layer (Table.1). I have repeated this calculation for four mentioned layers to quantify the total destructed (missed) crust material due to the collision since 30 Ma.

The total amount of present crust volume which is stored in this part of the Alps, the average thicknesses, and also the destructed volume for the European and Adriatic basement units as well as the European and Adriatic Lower crust units are all summarized in table 1.

Table 1 shows that the total present crust volume in this part of the Alps is about 2.4*10^6 km^3 and 1.26*10^6 km^3 for the European and Adriatic continent, respectively.

Horizon name	Current volume (Km^3) extracted from 3D model[a]	Average Thickness (Km) from the input profiles[b]	Destructed volume (Km^3) due to the collision[c]
European basement	1 182 490	14.900	964 004
Adriatic basement	642 590	15.920	165 031
European lower crust	1 208 560	11.580	459 654
Adriatic lower crust	619 909	15.080	145 099

Table 4.1. European and Adriatic crust volume calculation. ***a.*** *These values are derived from the 3D model and represent the present amount of crust in the eastern part of the Alps. The total amount of present crust is about 2 391 050 km^3 for the European crust and about 1 262 499 km^3 for the Adriatic crust.* ***b.*** *These numbers show the average thickness of each horizon which is derived from the 34 input profiles and represents the pre-collision thickness for each layer.* ***c.*** *These numbers represent the total destructed volume for each layer and derived by multiplying the pre-collisional area at 30 Ma (destructed area due to the collision + present area) by the average thicknesses in the adjacent column minus current volume from coloumn one. The total destructed volume is 1 423 658 and 310 130 km^3 for the European and Adriatic continent respectively since 30 Ma.*

For checking the present crust volume data, first I have divided the current volume for the European lower crust (1 208 560 km^3) and Adriatic lower crust (619 909 km^3) which are extracted from the 3D

model by the average thicknesses of these two horizons and the result could represent the current surface area for the European and Adriatic continent. The results for both continents show 8 to 9% difference with the current actual surface that is presently covered by these two continental crusts (the total surface area that is covered by the European continent and Adriatic continents currently are around 94 500 km^2 and 33 300 km^2 respectively).

Based on published data (Le Pichon et al., 1988) the total amount of crust volume which is stored in the roots of the Alps is maximum 5*10^6 km^3 (considering only European crust). Since my studied area is about 60% of the total Alps area, by taking 60% of the number mentioned by Le Pichon et al. (1988) for the eastern part of the Alps, my data extracted from the 3D model for the European continental crust (2 391 050 km^3) shows about 20% of deviation and is in good agreement with the published data.

According to table 1, about 964 004 Km^3 of the European basement crust volume were destructed (or eroded), which is about 82% of the current volume for this layer (1 182 490 Km^3). Table 1 also shows the current amount of crust volume (642 590 Km^3) as well as eroded or subducted volume (165 031 Km^3) for the Adriatic Basement layer which implies destruction of about 25% crust material compared to the present crust volume for this horizon.

Table 1 also shows the data that are extracted from the model and also calculated data by using Fig 15 in the previous chapter, for the lower crust units (European and Adriatic Lower crust). For the European lower

crust, about 459 654 Km^3 of the crust volume was destructed since 30 Ma as a result of the collision and the total current amount of crust for this layer is about 1 208 560 Km^3 (38% compared to the current crust volume). For the Adriatic lower crust only about 145 099 Km^3 have been destructed and the current amount of the crust is about 619 909 Km^3 (23% compared to the current crust volume). For these two horizons almost all the material was subducted into the mantle and no erosion happened for them and as a result these values could represent the minimum subducted material for the eastern part of the Alps.

A low amount of subducted crust material from the Adriatic continent compared to the European continent is also mentioned by Pfiffner et al. (1991) and Marchant &. Stampfli (1997) for the Western Alps. According to my data for the eastern part of the Alps, at least 145 099km^3 crust volume from the former Adriatic continent were subducted and subduction of Adriatic crust should not be underestimated.

Table 1 shows that about 1 423 658 Km^3 from the European continent and about 310 130 km^3 from the former Adriatic continent were destructed or missed due to the collision since 30 Ma (the total destructed material is about 1.73 *10^6 km^3 for the eastern part of the Alps). This amount of continental crust from the European and Adriatic crust which disappeared could be explained as a result of the different processes like subduction, east-west extension (thinning) and finally erosion.

According to Kuhlemann et al (2000) the total amount of eroded sediment for the Eastern Alps is about 215 587 Km3 which is calculated

from the adjacent basins (see Kuhlemann. et al., 2000, for more details). As mentioned before, only upper crust is involved in the nappe stacking so we could conclude that most of these sediments came from the units above the European upper crust and mainly from the cover unit. Even by taking half of this number (107 794 km^3) it shows that only about 6% of the total missing crust material belongs to the erosion process and the rest (1 625 994 km^3) belongs to the other two processes (east-west extension and subduction).

Since it is difficult to quantify the amount of crust volume which moved out of the Alps as a result of the lateral extension, it is necessary to make some assumptions. Based on the work of Le Pichon et al. (1988) the shortening accounts in the Alps by the east-west extension since the Early Miocene (lateral expulsion) is about half of the total shortening (Le Pichon et al 1988). By taking this assumption we can say that the total amount of the continental crust that disappeared due to the east-west extension would be around 812 997 km^3 and the same amount would have been subducted into the mantle.

The total crust volume which was subducted into the mantle (812 997 km^3) shows about 26% of deviation from sum of the European and Adriatic lower crust material (604 753 km^3) that we can calculate from table 1. Based on the quantitative evaluation of Le Pichon et al. 1988, about half of the continental crust involved in the collision of the Alps was subducted into the mantle and the lower crust units did not take part in the nappe stacking. In order to be on the conservative side and since the 812 997 km^3 is less than half of the total material which was destructed,

our calculation could represent the minimum amount of subduction of material into the mantle since 30 Ma.

Based on the quantitative calculation in table 1 about 82% of the total destructed volume belongs to the European continent and 18% to the Adriatic continent. If we assume that this number also could be taken for the total subducted material (812 997 km^3) we can conclude that about .66*10^6 km^3 from the European continent is subducted into the mantle and the remaining material (.14 *10^6 km^3) belongs to the Adriatic continent.

According to Dercourt et al. (1985 and 1986), Savostin et al. (1986), Le Pichon et al. (1988), Marchant and Stampfli (1996), the material that was subducted for the whole Alps from the European continent into the mantle is at least 10*10^6 km^3 since the start of the collision. As mentioned above our studied area is about 60% of the total Alps area. Therefore we could assume that the volume that was subducted from the start of collision until now would be around 6*10^6 km^3 for the eastern part of the Alps. Our estimation implies material of about .66*10^6 km^3 which is missing from the European continent since 30 Ma which could be considered a minimum amount for the eastern part of the Alps.

This low number for the eastern part of the Alps compared to the total minimum amount that was estimated by the above mentioned scientists could also explain the fact that more material was subducted in the Western Alps than in the Eastern Alps. This result is also suggested by

Helwig (1976) that no significant subduction occurred in the eastern Alps and also mentioned by Marchant and Stampfli (1996).

Unfortunately there is no data available for the eastern part of the Alps to compare our method and data to the other methods and published data. However, comparing the calculated crust which disappeared due to the collision by our approach with other published data which were mentioned before, our number is relatively small (Menard et al.1991; Marchant & Stampfli 1996; ,Le Pichon et al., 1988). The possible reasons for such a discrepancy could be:

1) They have calculated the area (material) which disappeared from the start of the collision (late Mesozoic time) and I have calculated the subducted crust material since 30 Ma.

2) They have calculated the subducted crust material for the whole Alps since the start of the collision and my calculation is only for the eastern part of the Alps (Eastern Alps+ Southern Alps and about 60% of their area) since 30 Ma.

3) Their mass-balance calculations mostly depend on the location of the horizon that they have estimated and where they start their calculations. For example, in one research (Menard et al. 1991) they consider the European crust from the southern side of the Molasse basin and in the other one (Merchant and Stampfli. 1997) they started from the northern side of the Jura and as a result they came to the different conclusions.

4) In some papers there is a wide range between the minimum area and maximum area which was destructed as a result of the collision. For example Marchant and Stampfli in 1997 calculated the minimum area of a crustal root of about 2852 km^2. By multiplying this number by the length of the Alps (1000 km) our estimation for almost 60% of the Alps and since 30 Ma falls well within this minimum value and as mentioned before our calculation for the eastern side of the Alps could be considered as minimum value, so it depends which data I take as a reference to compare with.

The data in this chapter implies subducting a large amount of continental material (about 812 997 km^3) into the mantle since 30 Ma which is in line with the research of Butler (1986), LePichon et al. 1988, Laubscher (1988) and opposite to the Helwig´s (1976). As concluded also in these research (Butler et al. 1986, Butlet 1986, LePichon et al. 1988, Laubscher 1988) the Alps were built by the subduction of thick continental crust into the mantle beneath the Alps.

4.6. Conclusions

In this chapter it is tried to use MOVE to quantify the current crust material which still exists and also the amount which was subducted since 30 Ma. The result shows that about 59% and 25% of the current crust volume from the European and Adriatic continents respectively, have been destructed as a result of collision since 30 Ma. The results extracted from the 3D model and also from the calculations lead to the

conclusion that about 812 997 km^3 of the continental crust from the eastern part of the Alps were subducted into the mantle since 30 Ma. From this total destructed volume about 82% belonged to the European continent and 18% to the Adriatic continent and this amount of subducted crust could represent the minimum amount of material for this part of the Alps. My data in this chapter imply underthrusting and subducting a large amount of continental material into the mantle. Although my model does not include all the complexities of the Eastern and Southern Alps and despite many uncertainties regarding the reconstruction as well as evolution of the eastern part of the Alps, my data shed new light related to the 3D modelling of complex subsurface structures in details which could be used later as an input for further research and also preliminary data to compare with other data from the other methods.

Suggestions

It would be useful to continue the model into the Carpathians and Pannonian basin and calculate the amount of the continental crust that is present there and test the hypothesis of Ratschbacher et al. (1991) that the tectonic escape and material motion in the Eastern Alps was compensated in the Pannonian basin. It is also interesting for a next step to continue the model for the whole Alps to compare the results with other available research in this topic (Le Pichon, 1987; Butler, 1986).

Data availability

The complete 3D model of the Eastern part of the Alps that support the findings in this chapter is available from the author on request.

This page intentionally left blank.

Chapter 5

Summary and Conclusions

In this research, I have tried to integrate all available data (regional geological data, geological map, profiles as well as other data like seismic profiles) together, build a valid 3D geometrical models of the Val de Ruz area for the first part and then the eastern part of the Alps for the second part of my study, test different hypothesis and ideas to answer some of the open questions which remained unsolved for these two areas.

The following conclusions came as an output of this research study:

1. The study of the Val de Ruz area and the results of the 3D model shows significant pre-thrusting thickness variations for the Muschelkalk unit. This variation is at least partly due to lateral flow of the Triassic evaporites during the early phase of detachment folding, away from synclines and towards anticlines. The results also show that assuming a second decoupling horizon in the Dogger or involvement of the basement in the Jura tectonics is unnecessary for explaining the geology of the study area. Due to the young tectonics of the Jura Mountains, topography closely correlates with tectonic structure.

2. The results in **chapter 3** demonstrate that the area balancing assuming constant pre-collisional crustal thickness gives generally lower values for shortening than line balancing and even negative values east of the Tauern Window (i.e. stretching), which may reflect, among other processes, pre-orogenic thinning of the continental margins as well as

east-west stretching of the crust during Miocene tectonic extrusion. The added shortening of European and South Alpine basements is at a maximum at the western end of the Tauern Window, probably reflecting pre-Alpine margin geometry (Dolomites indenter). These results are in good accordance with the tectonic evolution as inferred from other methods. By drawing the shortening data for the European and Adriatic basement it is possible to estimate the area that was destructed by the movement of Adria towards Europe since 30 Ma. The data also shows the average tectonic velocity between 3 to 6 mm per year which is in a good range compared to other available data.

3. The modelling and quantitative calculation in **chapter 4** reveals that about half of the current crust volume from the European and Adriatic continents has been destructed as a result of collision since 30 Ma. The results also show that about 812 997 km^3 km^3 of the continental crust from the eastern part of the Alps were subducted into the mantle since 30 Ma. From this total destructed volume about 82% belonged to the European continent and 18% to the Adriatic continent and this amount of subducted crust could represent the minimum amount of material for this part of the Alps. The data implies underthrusting and subducting a large amount of continental material into the mantle since 30Ma.

This research provides geo-referenced models for the Val de Ruz area and eastern part of the Alps which could be use later as an input for further research by other scientists although the error of the models could be noticeable (especially for the eastern part of the Alps due to the size of this area and lack of enough information).

This page intentionally left blank.

References:

1. Affolter, T. & Gratier, J. P. (2004). Map view retrodeformation of an arcuate fold-and-thrust belt: The Jura case. Journal of Geophysical Research, 109, B03404, doi: 10.1029/2002JB002270.
2. Ampferer, O. (1906). Über das Bewegungsbild von Faltengebirgen. Jb. Geol. R.-A., 56, 539-622.
3. Andrew McLeish (1992). Geological science (2nd ed). Thomas Nelson & Sons. p. 122. ISBN 978-0-17-448221-5.
4. Argand, E. (1911). Les nappes de recouvrement dse Alpes Penines et leurs prolongements structuraux. Mat carte Geol Suisse n.s.31: 1-26.
5. Argand, E. (1916). Sur larc des Alpes Occidentales. Eclog Geol Helv 14: 145-191.
6. Argand, E. (1924a). La tectonique de L Asie. CR 13e Cong Geol Intl 1922, 171-372.
7. Argand, E. (1924b). Des Alpes et de l Afrique. Bull Soc Vaud Sci Nat 55, 233-236.
8. Aubert, D. (1945). Le Jura et la tectonique d'écoulement. Mémoire de la Société Vaudoise des Sciences Naturelles, 8, 217 –236.
9. Balla, Z., 1984, The Carpathian loop and the Pannonian Basin: a kinematic analysis: Geophysical Transactions, v. 30, p. 313-353.
10. Bartosch, T., Stüwe, K., Robl, J., 2017. Topographic evolution of the Eastern Alps: the influ-ence of strike-slip faulting activity. Lithosphere 9:384–398. https://doi.org/10.1130/L594.1.

11. Beaumont, C., Ellis, S., Hamilton, J., Fullsack, P. (1996). Mechanical model for subduction-collision tectonics of Alpine-type compressional orogens. Geology. V. 24 (no. 8), 675– 678.
12. Behm, M., E. Brückl, W. Chwatal, and H. Thybo, 2007. Application of stacking techniques to 3D wide-angle reflection and refraction seismic data of the Eastern Alps. Geophysical Journal International, 170 (1), 275-298, doi: 10.1111/j.1365-246X. 2007.03393.x.
13. Berner, R.A., Caldeira, K., 1997. The need for mass balance and feedback in the geochemical carbon cycle. Geology 1997; 25;955-956. doi: 10.1130/0091-7613(1997)025<0955:TNFMBA>2.3.CO;2
14. Bertrand, A., Rosenberg, C., Rabaute, A., Herman, F. and Fügenschuh, B., 2017. Exhumation mechanisms of the Tauern Window (Eastern Alps) inferred from apatite and zircon fission - track thermochronology: Exhumation of the Tauern Window Tectonics, 36, 207 -228.
15. Bitterli, P. (1972). Erdölgeologische Forschungen im Jura. Bulletin der Vereinigung Schweizerischer Petroleum-Geologen und –Ingenieure, 39, 13–28.
16. Bourquin, P., Buxtorf, R., Frei, E., Lüthi, E., Mühlenthaler, C., Ryniker, K., & Suter, H. (1968). Atlas géologique de la Suisse 1:25‘000, feuille 51 Val de Ruz. Commission géologique Suisse, Basel.
17. Brückl, E., Behm, M., Decker, K., Grad, M., Guterch, A., Keller, G.R., Thybo, H., 2010. Crustal structure and active tectonics in the Eastern Alps. Tectonics 29, TC2011. doi: 10.1029/2009TC002491.
18. Bundesamt für Wasser und Geologie (2005). Geologische Karte der Schweiz 1:500 000. Bern-Ittingen.

19. Burkhard, M. (1990). Aspects of the large-scale Miocene deformation in the most external part of the Swiss Alps (Subalpine Molasse to Jura fold belt). Eclogae geologicae Helvetiae, 83, 559-583.

20. Butler, R. W. H., Matthews, S. J., Parish, M. (1986). The NW external Alpine thrust belt and its implications for the geometry of the western Alpine orogen. In: Collision Tectonics (edited by Coward, M. P. & Ries, A. C.). Spec. Pubis geol. Soc. Lond. 19, 245-260.

21. Butler, R.W.H. (1986). Thrust tectonics, deep structure and crustal subduction in the Alps and Himalayas. Journal of the Geological Society, London, 143, 857–873.

22. Buxtorf, A. (1907). Geologische Beschreibung des Weissensteintunnels und seiner Umgebung. Beiträge zur Geologischen Karte der Schweiz (N.F.), 21.

23. Buxtorf, A. (1916). Prognosen und Befunde beim Hauensteinbasis- und Grenchenbergtunnel und die Bedeutung der letzteren für die Geologie des Juragebirges. Verhandlungen der Naturforschenden Gesellschaft in Basel, 27, 184–254.

24. Caer, T., Maillot, B., Souloumiac, P., Leturmy, P., Frizon de Lamotte, D., & Nussbaum, F. (2015). Mechanical validation of balanced cross-sections: The case of the Mont Terri anticline at the Jura front (NW Switzerland). Journal of Structural Geology, 75, 32-48.

25. Castellarin A., Vai G.B., Cantelli L. The alpine evolution of the Southern Alps around the Giudicarie faults: a Late Cretaceous to Early Eocene transfer zone. Tectonophysics. 2006;414: 203–223.

26. Coward, M., & Dietrich, D. (1989). Alpine tectonics - an overview. Alpine Tectonics, Geological Society Special Publication No. 45, 1-29.
27. D'Ambrogi, C., D. Scrocca, M. Pantaloni, V. Valeri and C. Doglioni. 2010. Exploring Italian geological data in 3D. In: (Eds.) M. Beltrando, A. Peccerillo, M. Mattei, S. Conticelli, and C. Doglioni, Journal of the Virtual Explorer, vol. 36, paper 33, doi: 10.3809/jvirtex.2009.00256.
28. Dahlstrom, C.D.A. Balanced cross sections: Canadian Journal of Earth Sciences, v. 6, p. 743-757, 1969.
29. Dal Piaz GV, Hunziker JC, Martinotti G (1972) La Zona SesiaLanzo e l'evoluzione tettonico-metamorfica delle Alpi nordoccidentali interne. Mem Soc Geol Ital 11: 433–466.
30. Davis, D.M & Engelder, T. The Role of Salt in Fold-and-Thrust Belts. Tectonophysics, 119 (1985) 67-88.
31. DeMets, C., Gordon, R.G., Argus, D.F., Stein, S., 1994. Effect of recent revisions to the geomagnetic reversal time scale on estimates of current plate motions. Geophys. Res.Lett. 21, 2191–2194.
32. Dercourt J, Zonenshain LP, Ricou LE, Kazmin VE, Le Pichon X, Knipper AL, Grandjacquet C, Sborshchikov IM, Boulin J, Sorokhtin O, Geyssant J, Lepvrier C, Biju-Duval B, Sibuet JC, Savostin LA, Westphal M, Lauer J-P (1985) Présentation de 9 cartes paléogéographiques au 1/20.000.000 s'étendant de l'Atlantique au Pamir pour la période du Lias à l'actuel. Bull Soc Géol France 1: 637–652.
33. Dercourt, J., Zonenshain, L. P., Ricou, L.-E., Kazmin, V. G., Le Pichon, X., Knipper, A. L., Grandjacquet, C., Sbortshikov, I. M., Geyssant, J., Lepvrier, C., Pechersky, D. H., Boulin, J., Sibuet, J.-C., Savostin, L. A.,

Sorokhtin, O., Westphal, M., Bazhenov, M. L., Lauer, J. P., and Biju-Duval, B., 1986, Geological evolution of the Tethys belt from the Atlantic to the Pamir since the Lias, in: Evolution of the Tethys (J. Aubouin, X. Le Pichon, and S. Monin, eds.), Tectonophysics 123:241-3 15.

34. Diebold, P. (1988). Der Nordschweizer Permokarbon-Trog und die Steinkohlenfrage der Nordschweiz. Vierteljahrsschrift der Naturforschenden Gesellschaft in Zürich, 133, 143–174.

35. Doglioni, C. & Bosellini, A., 1987: Eoalpine and Mesoalpine tectonics in the Southern Alps. - Geol. Rundschau, 76, 735-754.

36. Downes, H. (1993). The nature of the lower continental crust of Europe: petrological and geochemical evidence from xenoliths. Physics of the Earth and Planetary Interiors79, 195–218.

37. Dunkl, I., Demeny, A. (1997). Exhumation of the Rechnitz Window at the border of the Eastern Alps and Pannonian Basin during Neogene extension. Tectonophysics 272, Issues 2-4, 197-211.

38. Fischer, H. & Luterbacher, H. (1963). Das Mesozoikum der Bohrungen Courtion 1 (Kt. Fribourg) und Altishofen 1 (Kt. Luzern). Beiträge zur Geologischen Karte der Schweiz (N.F.), 115, 40 pp.

39. Frehner M., Reif D. & Grasemann B. (2012): Mechanical versus kinematical shortening reconstructions of the Zagros High Folded Zone (Kurdistan Region of Iraq). Tectonics 31, TC3002, doi: 10.1029/2011TC003010.

40. Frey, M., & Ferreiro Ma¨hlmann, R. (1999). Alpine metamorphism of the Central Alps. Schweizerische Mineralogische und Petrographische Mitteilungen, 79(1), 135–154.

41. Frisch W., Kuhlemann J., Dunkl I. & Brügel A. 1998: Palinspastic reconstruction and topographic evolution of the Eastern Alps during late Tertiary tectonic extrusion. Tectonophysics 297, 1—15.
42. Frisch, W., Dunkl, I., & Kuhlemann, J. (2000). Post-collisionalorogen-parallel large-scale extension in the Eastern Alps.Tectonophysics, 327, 239–265.
43. Froitzheim, N., Plasienka, D. & Schuster, R. (2008). Alpine tectonics of the Alps and Western Carapathians. In: T. McCann, T. (Ed.). The geology of Central Europe. Geological Society London, 1141-1232.
44. Froitzheim, N., Plašienka, D., Schuster, R., 2008. Alpine tectonics of the Alps and Western Carpathians. In: McCann, T. (Ed.), The Geology of Central Europe, vol. 2, Mesozoic and Cenozoic. Geological Society, London, pp. 1141–1232.
45. Froitzheim, N., S. M. Schmid, and P. Conti (1994), Repeated change from crustal shortening to orogen-parallel extension in the Austroalpine units of Graubunden, Eclogae Geologicae Helvetiae, 87(2), 559-612, doi:10.5169/seals-167471.
46. Froitzheim, N., S.M. Schmid, and M. Frey, Mesozoic paleogeography and the timing of eclogite-facies metamorphism in the Alps: A working hypothesis, Eclogae Geol. Helv., in press, 1996.
47. Froitzheim, N., Schmid, S. M., & Conti, P. (1994). Repeated changefrom crustal shortening to orogen-parallel extension in the Austroalpine units of Graubünden. Eclogae Geologicae Helvetiae, 87, 559–612.
48. Froitzheim, N., Schmid, S.M., Frey, M. (1996). Mesozoic paleogeography and the timing of eclogite-facies metamorphism in the Alps: a working hypothesis. Eclog Geol Helv 89:81–110.

49. Frost, E., Dolan, J., Sammis, C., Hacker, B., Cole, J., and Ratsbacher, L., 2009, Progressive strain localization in a major strike-slip fault exhumed from midseismogenic depths: Structural observations from the Salzach-Ennstal-MariazellPuchberg fault system, Austria: Journal of Geophysical Research, v. 114, B04406, doi: 10.1029/2008JB005763.

50. Fügenschuh, B., Seward, D., and Mancktelow, N., 1997, Exhumation in a convergent orogen: The western Tauern window: Terra Nova, v. 9, p. 213–217, doi: 10 .1046 /j .1365-3121 .1997 .d01 -33 .x.

51. Funiciello, F., Morra, G., Regenauer-Lieb, K., D. Giardini. (2003). Dynamics of retreating slabs: 1. insights from two-dimensional numerical experiments. Journal of Geophysical Research: Solid Earth (1978–2012), 108(B4). doi: 10.1029/2001JB000898.

52. Gawlick, H.J., W. Frisch, A. Vecsei, T. Steiger, F. Böhm 1999: The change from rifting to thrustingin the Northern Calcareous Alps as recorded in Jurassic sediments.–Geologische Rundschau, 87,pp. 644–657

53. Genser, J., and Neubauer, F., 1989, Low angle normal faults at the eastern margin of the Tauern window (Eastern Alps): Mitteilung der Österreichischen Geologischen Gesellschaft, v. 81, p. 233–243.

54. Ghassemi M.R., Schmalholz S.M. & Ghassemi A.R. (2010): Kinematics of constant arc length folding for different fold shapes. Journal of Structural Geology 32, 755–765,doi:10.1016/j.jsg.2010.05.002.

55. Gorin, G. E., Signer, C. & Amberger, G. (1993). Structural configuration of the western Swiss Molasse Basin as defined by reflection seismic data. Eclogae Geologicae Helvetiae, 86, 693–716.

56. Grasemann B. & Schmalholz S.M. (2012). Lateral fold growth and fold linkage. Geology, 40, 1039–1042, doi:10.1130/G33613.1.

57. Grenerczy, G., 2005, Crustal motions from space geodesy: A review from EPN, CEGRN, and HGRN data, in Fodor, L., and Brezsnyánszky, K., eds., Applications of GPS in Plate Tectonics in Research on Fossil Energy Resources and in Earthquake Hazard Assessment: Budapest, Hungary, Occasional Papers of the Geological Institute of Hungary, v. 204, p. 31–34.

58. Grenerczy, Gy., and Bada, G., 2005, GPS baseline length changes and their tectonic interpretation in the Pannonian Basin: Geophysical Research Abstracts, v. 7, no. 04808.

59. Groupe de travail PGN (2008). Evaluation du potentiel géothermique du canton de Neuchâtel (PGN). Vol.1: Rapport final, Vol.2: Annexes, CREGE 11-08/02,Neuchâtel;http://www.ne.ch/autorites/DDTE/SCAT/Documents/02_Plan_directeur_cantonal/Evaluation_potentiel_geothermique_canton_Neuchatel.pdf

60. Guellec, S., Mugnier, J. L., Tardy, M. & Roure, F. (1990). Neogene evolution of the western Alpine foreland in the light of ECORS data and balanced cross sections. In: Roure, F., Heitzmann, P. & Polino, R. (Eds.), Deep structure of the Alps. Mémoire de la Société Géologique Suisse, 1, 165–184.

61. Hampel, A., & Pfiffner, A. (2006). Relative importance of trenchward upper plate motion and friction along the plate interface for the

topographic evolution of subduction-related mountain belts. Geological Society, London, Special Publications, 253, 105-115.

62. Handy, M.R., Schmid, S.M., Bousquet, R., Kissling, E., Bernoulli, D.(2010) Reconciling plate-tectonic reconstructions of Alpine Tethys with the geological–geophysical record of spreading and subduction in the Alps. Earth Sci Rev 102:121–158

63. Handy, M. R., Ustaszewski, K., & Kissling, E. (2014). Reconstructing the Alps–Carpathians–Dinarides as a key to understanding switches in subduction polarity, slab gaps and surface motion. International Journal of Earth Sciences, 104, 1–26. Doi: 10.1007/s00531-014-1060-3.

64. Heitzmann, P., Müller, S., Steck, A. Deep structure of the Swiss Alps: results from the National Research Program 20 (NRP 20). Schweiz geol Komm. Birkhäuser, Basel, pp 139–153

65. Helwig, J., (1976). Shortening of continental crust in erogenic belts and plate tectonics. Nature, 260: 768-770.

66. Hoinkes, G., Koller, F., Rantitsch, G., Dachs, E., Höck, V., Neubauer, F., Schuster, R. (1999) Alpine metamorphism of the Eastern Alps. Schweiz Miner Petrogr Mitt 79:155–181.

67. Horva´th, F. (1993). Towards a mechanical model for the formation of thePannonian Basin.Tectonophysics, 226, 333 – 357.

68. Horva´th, F., Szalay, A´., Döve´nyi, P. & Rumpler, J. 1986. Structural and thermal evolution of the Pannonian basin: an overview. In: BURRUS, J. (ed.) Thermal Modeling in Sedimentary Basins, First IFP Exploration Research Conference, Carcans, France.Technip,Paris, 339 – 358.

69. Horváth, F., Musitz, B., Balázs, A., Végh, A., Uhrin, A., and Nádor, A., 2015, Evolution of the Pannonian basin and its geothermal resources: Geothermics, v. 53, p. 328–352.

70. Ingalls, M., B. Rowley, D., Currie, B., S. Colman, A. (2016). Large-scale subduction of continental crust implied by India–Asia mass-balance calculation. Nature Geoscience, Vol 9, 848-853.DOI: 10.1038/NGEO2806

71. Janák M, Cornell D, Froitzheim N, De Hoog JCM, Broska I, Vrabec M, Hurai (2009). Eclogite-hosting metapelites from the Pohorje Mountains (Eastern Alps): P-T evolution, zircon geochronology and tectonic implications. Eur J Miner 21:1191–1212

72. Jordan, P. (1992). Evidence for large scale decoupling in the Triassic evaporites of Northern Switzerland: an overview. Eclogae Geologicae Helvetiae, 85, 677–693.

73. Kälin, D. (1997). Litho- und Biostratigraphie der mittel- bis obermiozänen Bois de Raube – Formation (Nordwestschweiz). Eclogae Geologicae Helvetiae, 90, 97–114.

74. Keller, W.T. & Liniger, H. (1930). Geologischer Atlas der Schweiz, Blätter 92-95 Movelier–Soyhieres–Delemont–Courrendlin. Schweizerische Geologische Kommission.

75. Kincaid, C., & Hall, P.S. (2003). Role of back arc spreading in circulation and melting at subduction zones, J. Geophys. Res., 108(B5), 2240, doi: 10.1029/2001JB001174.

76. Kuhlemann, J., 2000. Post-collisional sediment budget of circum-Alpine basins (Central Europe). Mem. Sci. Geol. Padova 52 (1), 1–91.

77. Kuhlemann, J., Frisch, W., Dunkl, I., Szekley, B. (2001). Quantifying tectonic versus erosive denudation by the sediment budget: the Miocne core complexes of the Alps. Tectonophysics, 330, 1-23.

78. Kuhlemann, J., Frisch, W., Szekely, B., Dunkl, I., Kázmér, M., 2002. Post-collisional sediment budget history of the Alps: tectonic versus climatic control. Int. J. Earth Sci. 91 (5), 818–837.

79. Lammerer, B., & Weger, M. (1998). Footwall uplift in an orogenic wedge: the Tauern Window in the Eastern Alps of Europe. Tectonophysics, 285, 213–230.

80. Lammerer, B., Gebrande, H., Lüschen, E., Vesela, P. (2008). A crustal-scale cross-section through the Tauern Window (eastern Alps) from geophysical and geological data. In S. Siegesmund, B. Fügenschuh, N. Froitzheim (Eds.) Tectonic aspects of the Alpine-Dinaride-Carpathian system. Geological Society of London special publications 298, pp. 219–229.

81. Laubscher, H. (1988). Material Balance in Alpine orogeny. Geological Society of America Bulletin 100(9):1313-1328. DOI: 10.1130/0016-7606(1988)100<1313:MBIAO>2.3.CO;2

82. Laubscher, H. P. (1961). Die Fernschubhypothese der Jurafaltung. Eclogae Geologicae Helvetiae, 54, 221-280.

83. Laubscher, H. P. (1965). Ein kinematisches Modell der Jurafaltung. Eclogae Geologicae Helvetiae, 58, 231-318.

84. Laubscher, H. P. (1972). Some overall aspects of Jura dynamics. American Journal of Science, 272, 293-304.

85. Laubscher, H. P. (2003). Balanced sections and the propagation of décollement: A Jura perspective. Tectonics, 22, article 1063, doi: 10.1029/2002TC001427.

86. Laubscher, H.P. (1969). Mountain building. Tectonophysics 7, 551–563.

87. Laubscher, H.P. (1970). Bewegung und Wärme in der alpinen Orogenese. Schweiz. Mineral. Petrogr. Mitt. 50, 503–534.

88. Laubscher, H.P. (1990). Deep seismic data from the central Alps: mass distributions and their kinematics. In: F. Roure, P. Heitzmann and R. Polino (Editors), Deep Structure of the Alps. Mem. Soc. Geol. Fr., 156, Mem. Soc. Geol. Suisse, 1, Soc. Geol. Ital. Vol. Spec., 1: 335-343.

89. Le Breton, E., Handy, M. R., Molli, G., & Ustaszewski, K. (2017). Post-20 Ma motion of the Adriatic Plate: New constraints from sur-rounding orogens and implications for crust-mantle decoupling.Tectonics, 36, 3135–3154. DOI: 10.1002/2016TC004443

90. Le Pichon, X., Bergerat, F. and Roulet, M.-J. (1988). Plate kinematics and tectonics leading to the Alpine belt formation; a new analysis. Geol. Soc. Am. Spec. Pap., 218, 111-131.

91. Lickorish, W.H. & Ford, M. 1998: sequential restoration of the external Alpine Digne thrust system, SE France, constrained by kinematic data and syno-rogenic sediments. In: Mascle, A., Puidgefàbregas, C., Luterbacher, H.P. & Fernàndez, M. (Eds.): Cenozoic Foreland basins of Western Europe, Geological society London special Publication 134, 189–211.

92. Linzer HG, Decker K, Peresson H, Dell'Mour R, Frisch W (2002) Balancing orogenic float of the Eastern Alps. Tectonophysics 354:211–237.

93. Lippitsch, R., Kissling, E., and Ansorge, J. (2003). Upper mantle structure beneath the alpine orogen from high-resolution teleseismic tomography. Journal of Geophysical Research: Solid Earth, 108(B8).

94. Loup, B. (1992). Mesozoic subsidence and stretching models of the lithosphere in Switzerland (Jura, Swiss Plateau and Helvetic realm). Eclogae Geologicae Helvetiae, 85, 541-572.

95. Lüschen, E., Lammerer, B., Gebrande, H., Millahn, K., Nicolich, R., Group, T. W., et al.: Orogenic structure of the Eastern Alps, Europe, from TRANSALP deep seismic reflection profiling, Tectonophysics, 388, 85–102, 2004.

96. Lyubetskaya, T., Korenaga, J., 2007. Chemical composition of Earth's primitive mantle and its variance: 2. Implications for global geodynamics. JOURNAL OF GEOPHYSICAL RESEARCH, VOL. 112, B03212, doi: 10.1029/2005JB004224.

97. M.Yosefnejad, D., J.Nagel, T., Froitzheim, N. (2017). Three-dimensional modelling of folds, thrusts, and strike-slip faults in the area of Val de Ruz (Jura Mountains, Switzerland). Swiss Journal of Geoscience. DOI: 10.1007/s00015-017-0261-8

98. Madritsch, H., Fabbri, O., Hagedorn, E.-M., Preusser, F., Schmid, S. M. & Ziegler, P.A. (2010). Feedback between erosion and active deformation: geomorphic constraints from the frontal Jura fold-and-

thrust belt (eastern France). International Journal of Earth Sciences, 99 (Suppl. 1), S103–S122.

99. Madritsch, H., Schmid, S.M. & Fabbri, O. (2008). Interactions between thin- and thick-skinned tectonics at the northwestern front of the Jura fold-and-thrust belt (eastern France). Tectonics, 27, TC5005, doi:10.1029/2008TC002282.

100. Malz, A., Madritsch, H., Meier, B. & Kley, J. (2016). An unusual triangle zone in the external northern Alpine foreland (Switzerland): Structural inheritance, kinematics and implications for the development of the adjacent Jura fold-and-thrust belt. Tectonophysics, 670, 127–143.

101. Mancktelow, N. S., Stöckli, D. F., Grollimund, B., Müller, W., Fügenschuh, B., Viola, G., ... Villa, I. M. (2001). The DAV and Periadriatic fault system in the Eastern Alps south of the Tauern window. International Journal of Earth Sciences, 90, 593–622.

102. MANDL, G. W. & ONDREJICKOvA, A. (1991): Über eine triadische Tiefwasserfazies (Radiolarite, Tonschiefer) in den Nördlichen Kalkalpen - ein Vorbericht. - Jb. Geol. B.-A., 134, 309-318, Wien.

103. MANDL, G.W. & ONDREJICKOVA, A. (1993): Radiolarien und Cono-donten aus dem Meliatikum im Ostabschitt der Nördlichen Kalk-alpen (Österreich). - Jahrbuch der Geologischen Bundesanstalt,136: 841-871, Wien.

104. MANDL, G.W. (2000): The Alpine sector of the Tethyan shelf - Examplex of Triassic to Jurassic sedimentation and deformation from the Northern Calcareous Alps. – Mitt. Österr. geol. Ges., 92, 61–78.

105. Marquer, D., Calcagno, P., Barfety, J., Baudin, T., 2006. 3D modeling and kinematics of the external zone of the French western Alps (Belledonne and Grand Chatelard massifs, Maurienne valley, Savoie). Eclogae Geologicae Helvetiae 99, 211–222.

106. Marquer, D., Calcagno, P., Barfety, J.-C. & Baudin, T. (2006). 3D modeling and kinematics of the external zone of the French Western Alps (Belledonne and Grand Chatelard Massifs, Maurienne Valley, Savoie). Eclogae Geologicae Helvetiae, 99, 211–222.

107. Matenco, L., Radivojevic, ´ D., 2012. On the formation and evolution of the Pannonian basin: constraints derived from the structure of the junction area between the Carpathians and Dinarides. Tectonics 31. https://doi.org/10.1029/2012TC003206.

108. Maxelon, M. & Mancktelow, N. S. (2005). Three-dimensional geometry and tectonostratigraphy of the Pennine zone, Central Alps, Switzerland and Northern Italy. Earth Science Reviews, 71, 171–227.

109. Maxelon, M. and Mancktelow, N. S.: Three-dimensional geometry and tectonostratigraphy of the Pennine zone, Central Alps, Switzerland and Northern Italy, Earth-Sci. Rev., 71, 171–227, 2005.

110. Menard, G., & Molnar, P. (1991). Budget of crustal shortening and subduction of continental crust in the Alps. Tectonics, vol. 10, No.2, 231-244.

111. Merchant, R.H., Stampfli, G.M. (1997). Subduction of continental crust in the Western Alps. Tectonophysics, 269, 217-235.

112. Mitra, S. (2003). A unified kinematic model for the evolution of detachment folds. Journal of Structural Geology, 25, 1659–1673.

113. Munzarová, H., Plomerová, J., Babuška, V., & Vecsey, L. (2013). Upper-mantle fabrics beneath the Northern Apennines revealed by seismic anisotropy. Geochemistry, Geophysics, Geosystems, 14, 1156–1181. https://doi.org/10.1002/ggge.20092.

114. Neubauer, F., Genser, J., Handler, R. (2000) The Eastern Alps: result of a two-stage collision process. Mitt Öster Geol Ges 92:117–134.

115. Neubauer, F., Handler, R., Hermann, S., Paulus, G. (1994) Revised lithostratigraphy and structure of the eastern Graywacke Zone (EasternAlps). Mitt Österr Geol Ges 86:61–74

116. Neubauer, F. (2002): Evolution of late Neoproterozoic to early Palaeozoic tectonic elements in Central and Southeast European Alpine mountain belts: review and synthesis. Tectonophysics, 352: 87–103.

117. Neubauer, F., Genser, J. and Handler, R. (2000). The Eastern Alps: result of a two-stage collision process. Mitteilungen der Österreichischen Geologischen Gesellschaft, 92, 117–134.

118. Nocquet, J.M. & Calais, E., 2003. Crustal velocity field of Western Europe from permanent GPS array solutions, 1996–2001, Geophys. J. Int., 154, 72–88.

119. Oberhänsli, R., Bousquet, R., Engi, M., Goffe´, B., Gosso, G., Handy, M., et al. (2004).Metamorphic structure of the Alps 1:100000000. Paris: Commission for the Geological Map of the World.

120. Ortner, H., Aichholzer, S., Zerlauth, M., Pilser, R., & Fügenschuh, B. (2015). Geometry, amount, and sequence of thrusting in the Subalpine Molasse of western Austria and southern Germany, European Alps. Tectonics, 34(1), 1-30. https://doi.org/10.1002/2014TC003550.

121. Pamic´ J (2002). The Sava-Vardar Zone of the Dinarides and Hellenides versus the Vardar Ocean. Eclogae Geol Helv 95:99–113.

122. Pavoni, N. (1961). Faltung durch Horizontalverschiebung. Eclogae Geologicae Helvetiae, 54, 515-534.

123. Pfiffner, O.A., Sahli, S., Stäuble, M. (1997a) Structure and evolution of the external basement massif (Aar, Aiguilles Rouges/Mt. Blanc).

124. Pfiffner, O. A. 1986. Evolution of the north Alpine foreland basin in the Central Alps. Special Publication of the international Association of sedimentologists 8, 219-228.

125. Pfiffner, O. A., & Hitz, L. (1997). Geologic interpretation of the seismic profiles of the Eastern Traverse (lines E1–E3, E7–E9): Eastern Swiss Alps. In O. A. Pfiffner, et al. (Eds.), Deep structure of the Alps, results of NRP20 (pp. 73–100). Basel: Birkhäuser.

126. Pfiffner, O. A., Erard, P.-F. & Stäuble, M. (1997). Two cross sections through the Swiss Molasse Basin (lines E4-E6, W1, W7-W10). In: Pfiffner, O. A. et al. (Eds.): Deep structure of the Swiss Alps, results of NFP 20. Birkhäuser Verlag Basel, 73–100.

127. Pfiffner, O.A., 2010, Geologie der Alpen: Bern, Haupt Verlag, 360 p.

128. Pfiffner, O.A., Levato, L., Valasek, P. (1991). Crustal reflections from the Alpine orogen: results from deep seismic profiling. In: Continental Lithosphere: Deep Sesimic Reflections, Geodynamics, 22. American Geophysical Union, pp. 185-193.

129. Pfirter, U. (1997). Atlas géologique de la Suisse 1:25‘000, feuille 1106 Moutier. Commission géologique Suisse, Basel.

130. Philippe, Y., Colletta, B., Deville, E., Mascle, A. (1996). The Jura fold-and-thrust belt: a kinematic model based on map-balancing. In: Ziegler, P.A. & Horvath, F. (Eds.): Peri-Tethys Memoir 2: Structure and prospects of Alpine basins and forelands. Mémoires du Muséum National d'Histoire Naturelle, Paris, 170, 235-261.

131. Pomella, H.; Klötzli, U. et al. (2011). The Northern Guidicarie and the Meran-Mauls fault (Alps, Northern Italy) in the light of new paleomagnetic and geochronological data from boudinaged Eo-/Oligocene tonalites.

132. Ratschbacher, L., Frisch, W., Linzer, H.G., Merle, O. (1991) Lateralextrusion in the Eastern Alps, Part 2: structural analysis. Tectonics 10: 257-271.

133. Ratschbacher, L., Merle, O., Davy, R., Scobbold, P, 1991a: Lateral extrusion in the Eastern Alps, part 1: boundary conditions and experiments scaled for gravity. Tectonics, 10: 245-256.

134. Ratschbacher, L., Frisch, W., Linzer, H.-G. & Merle, O., 1991b: Lateral extrusion in the Eastern Alps, part 2: Structural analysis. - Tectonics, 10: 257-271.

135. Ratschbacher, L., Frisch, W., Linzer, H.-G. and Merle, O., 1991a. Lateral extrusion in the Eastern Alps, Part 2. Structural analysis. Tectonics, 10: 257-271.

136. Ratschbacher, L., Wenk, H.-R. and Sintubin, M., 1991b. Calcite textures: examples from nappes with strain-path partitioning. J. Struct. Geol., 13: 369-384.

137. Reinecker, J., 2000. Stress and deformation: Miocene to present-day tectonics in the Eastern Alps. Tübinger Geowissenschaftliche Arbeiten (TGA) Reihe A: Geologie, Paläontologie, Stratigraphie, pp. 128.

138. Reischenbacher, D. and Sachsenhofer, R., 2013. Basin formation during the post-collisional evolution of the Eastern Alps: the example of the Lavanttal Basin. International Journal of Earth Sciences, 102, 517-543.

139. Robl, J., Stüwe, K., Hergarten, S., and Evans, L., 2008b, Extension during continental convergence in the Eastern Alps: The influence of orogen-scale strike-slip faults: Geology, v. 36, p. 963–966, doi:10.1130/G25294A.1.

140. Rosenberg, C.L., Berger, A., Bellahsen, N., Bousquet, R., 2015. Relating orogen-width to shortening, erosion, and exhumation during Alpine collision". Tectonics, 34, 1306–1328, doi: 10.1002/2014TC003736.

141. Rosenberg, C.L., Kissling, E., 2013. 3D insight into Alpine collision: lower plate or upper plate indentation?. Geology 41,doi10.1130/G34584.1.

142. Sachsenhofer, R.F., Bechtel, A., Reischenbacher, D., Weiss, A., 2003. Evolution of lacustrine systems along the Miocene Mur-Mürz fault system (Eastern Alps, Austria) and implications on source rocks in pull apart basins. Marine and Petroleum Geology 20, 83–110.

143. Sala, P., Pfiffner, A. O. & Frehner, M. (2014). The Alpstein in three dimensions: fold-and-thrust belt visualization in the Helvetic zone, eastern Switzerland. Swiss Journal of Geosciences, 107, 177–195.

144. Savostin. L.A., Sibuet, J.C., Zonenshain. L.P., Le Pichon, X. and Roulet, M.J., 1986. Kinematic evolution of Tethys belt from the Atlantic Ocean to the Pamirs since the Triassic. Tectonophysics, 123 (this Vol.): l-35.

145. Schmid, S. M., & Froitzheim, N. (1993). Oblique slip and blockrotation along the Engadine line.Eclogae geolicae Helvetiae,86(2), 569–593.

146. Schmid, S. M., Fügenschuh, B., Kissling, E., & Schuster, R. (2004). Tectonic map and overall architecture of the Alpine orogen. Eclogae Geologicae Helvetiae, 97, 93–117.

147. Schmid, S.M., Bernoulli, D., Fügenschuh, B., Matenco, L., Schefer, S., Schuster, R., Tischler, M. & Ustaszewski, K. (2008) The Alpine-Carpathian-Dinaridic orogenic system: correlation and evolution of tectonic units. Swiss Journal of Geosciences, 101(1), 139-183.

148. Schmid, S.M., Pfiffner, O.A., Froitzheim, N., Schönborn, G. & Kissling, E. (1996) Geophysical geological transect and tectonic evolution of the Swiss-Italian Alps. Tectonics, 15, 1036-1064.

149. Schmid, S.M., Scharf, A., Handy, M.R. and Rosenberg, C.L., 2013. The Tauern Window (Eastern Alps, Austria): a new tectonic map, with cross -sections and a tectonometamorphic synthesis Swiss Journal of Geosciences, 106, 1 -32.

150. Schönlaub, H.P. (1980): Carnic Alps. Field Trip A. with contributions from Jaeger, H., House, M.R., Price, J.D., Göddertz, B., Priewalder, H., Walliser, O.H., Kříž, J., Haas, W. & Vai, G.B. – In: Schönlaub, H.P. (ed.): Second European Conodont Symposium, ECOS II, Guidebook,

Abstracts. – Abhandlungen der Geologischen Bundesanstalt, 35, 5–57, Wien.

151. Schori, M., Mosar, M. & Schreurs, G. (2015). Multiple detachments during thin-skinned deformation of the Swiss Central Jura: a kinematic model across the Chasseral. Swiss Journal of Geosciences, 108, 327–343.

152. Schuster R, Scharbert S, Abart R, Frank W (2001) Permo-Triassic extension and related HT=LP metamorphism in the Austroalpine–Southalpine realm. Mitt Ges Geol Bergbaustud Osterr 45: 111–141.

153. Schuster, R., Koller, F., Hoeck, V., Hoinkes, G., & Bousquet, R.(2004). Explanatory notes to the map Metamorphic Structure of the Alps. Mitteilungen der Österreichischen MineralogischenGesellschaft, 149, 175–199.

154. Schuster, R. (2003). Das eo-Alpidische Ereignis in den Ostalpen: Plattentektonische Situation und interne Struktur des Ostalpinen Kristallins. In M. Rockenschaub (Ed.), Arbeitstagung 2003 der Geologischen Bundesanstalt Trins im Gschnitztal (pp. 41–159). Wien: Geologische Bundesanstalt.

155. Schuster, R., Koller, F. & Frank, W. (2007): Pebbles of upper-amphibolite facies amphibolites in the Gosau Group of the Eastern Alps: relics of a metamorphic sole? Abstract 8th ALPSHOP Davos/Switzerland, 74.

156. Schuster, R., Kurz, W., Krenn, K., & Fritz, H. (2013). Introduction to the Geology of the Eastern Alps. Berichte der Geologischen Bundesanstalt Wien, 99, 121–133.

157. Sella, GF., Dixon, TH., Mao, A. (2002) REVEL: a model for recent plate velocities fromspace geodesy. J Geophys Res 107. Doi: 10.1029/2000JB000033.

158. Sommaruga, A. & Burkhard, M. (1997). Interpretation of seismic lines across the rhomb shaped Val-de-Ruz Basin (internal Folded Jura). In: Pfiffner, O.-A. et al. (Eds.), Deep structure of the Swiss Alps, results of NFP 20. BirkhäuserVerlag Basel, 45–53.

159. Sommaruga, A. (1995). Tectonics of the central Jura and the Molasse Basin. New insights from the interpretation of seismic reflection data. Bulletin de la Société Neuchatêloise des Sciences Naturelles, 118, 95–108.

160. Sommaruga, A. (1997). Geology of the Central Jura and the Molasse Basin: New insight into an evaporite-based foreland fold and thrust belt. Mémoire de la Société Neuchatêloise des Sciences Naturelles, 12, 1–176.

161. Sommaruga, A. (1999). Décollement tectonics in the Jura foreland fold-and-thrust belt. Marine and Petroleum Geology, 16, 111–134.

162. Sommaruga, A., Eichenberger, U. & Marillier, F. (2012). Seismic Atlas of the Swiss Molasse Basin. Beiträge zur Geologie der Schweiz—Geophysik, 44.

163. Spada, M., I. Bianchi, E. Kissling, N. Piana Agostinetti, and S. Wiemer (2013). Combining controlled-source seismology and receiver function information to derive 3-D Moho topography for Italy. Geophys. J. Int., 194 (2), 1050–1068.

164. Sprenger, W.L. (1996). Das Periadriatische Lineament südlich der Lienzer Dolomiten. Abhandlungen der geologischen Bundesanstalt, Band 52, p.1-220.

165. Stüwe, K., & Schuster, R. (2010). Initiation of subduction in the Alps: Continent or ocean? Geology, 38, 175–178. Doi:10.1130/G30528.1.

166. Suppe, J. & Medwedeff, D. A. (1990). Geometry and kinematics of fault-propagation folding. Eclogae Geologicae Helvetiae, 83, 409–454.

167. Suppe, J. (1983). Geometry and kinematics of fault-bend folding. American Journal of Science, 283, 684–721.

168. Tanner, D., Behrmann, J. & Dresmann, H. (2003). Three-dimensional retro-deformation of the Lechtal nappe, Northern Calcareous Alps. Journal of Structural Geology, 25, 737–748.

169. Termier, P., 1903: Les nappes des Alpes orientales et la Synthese des Alpes. Bull. Soc.geol. France, IV. Ser., 3, 711-765, Paris.

170. Tollmann, A. 1977. Geologie von Österreich. Band 1: Die Zentralalpen. Deuticke, Wien.

171. Tollmann, A. 1980. Geology and Tectonics of the Eastern Alps (Middle Sector). Geol, 34, P197-255.

172. Tomljenovic´ B, Csontos L, Márton E, Márton P (2008) Tectonic evolution of the northwestern Internal Dinarides as constrained by structures and rotation of Medvednica Mountains, North Croatia. Geol Soc Lond Spec Publ 298:145–167.

173. Trümpy R (1992) Ostalpen und Westalpen—Verbindendes und Trennendes. Jahrbuch der geologischen Bundesanstalt Wien 135(4):875–882.

174. Trümpy, R. 1980: Geology of Switzerland: a guide-book. Part A: An outline of the geology of Switzerland. Wepf, Basel.

175. Tschanz, X. & Sommaruga, A. (1993). Deformation associated with folding above frontal and oblique ramps around the rhomb shaped Val de Ruz basin. Annales Tectonicae, 7, 53-70.

176. Tschanz, X. (1990). Analyse de la déformation du Jura central entre Neuchâtel (Suisse) et Besançon (France). Eclogae Geologicae Helvetiae, 83, 543 –558.

177. Ustaszewski, K. & Schmid, S.M. (2006). Control of preexisting faults on geometry and kinematics in the northernmost part of the Jura fold-and-thrust belt. Tectonics, 25, TC5003, doi: 10.1029/2005TC001915.

178. Van Hunen, J., van den Berg, A.B., Vlaar, N.J., 2000. A thermo-mechanical model of horizontal subduction below an overriding plate. Earth Planet. Sci. Lett. 182,157- 169.

179. Véron, J. 2005. The Alpine Molasse Basin – Review of Petroleum Geology and Remaining Potential. Bull. Angew. Geol. vol. 10/1. 75-86.

180. Vlahovic, I., Tisljar, J., Velic, I. & Maticec, D. (2005): Evolution of the Adriatic Carbonate Platform: Paleogeography, mainevents and depositional dynamics. Palaeogeography, Palaeoclimatology, Palaeoecology, 220: 333-360, Amsterdam.

181. Vouillamoz, N., Sue, C., Champagnac, J. D. & Calcagno, P. 3D cartographic modeling of the Alpine arc. Tectonophysics 579, 131–143 (2012).

182. Vouillamoz, N., Sue, C., Champagnac, J., Calcagno, P., 2012. 3D cartography modeling of the Alpine Arc. Tectonophysics 579, 131–143. http://dx.doi.org/10.1016/j.tecto. 2012.06.012.

183. Waibel. A.F. & Frisch. W. 1989: The Lower Engadine Window: sediment deposition and accretion in relation to the plate-tectonic evolution of the eastern Alps. Tectonophysics 162, 229-241.

184. Wiederkehr, M., Sudo, M., Bousquet, R., Berger, A., & Schmid, S. M. (2009). Alpine orogenic evolution from subduction to collisional thermal overprint: The 40Ar/39Ar age constraints from the Valaisan Ocean, central Alps. Tectonics, 28, TC6009. https://doi.org/10.1029/ 2009TC002496.

185. Wölfler, A., Kurz, W., Fritz, H., Stüwe, K., 2011. Lateral extrusion in the Eastern Alps revisited: refining the model by thermochronological, sedimentary and seismic data. Tectonics 30, TC4006. doi:10.1029/2010TC002782.

186. Woodward, N.B., Boyer, S.E., Suppe, J., 1989. Balanced Geological CrossSections. American Geophysical Union, Short Course in Geology 6, 132.

187. Yosefnejad, D.M., Nagel, T.J. & Froitzheim, N. (2017): Three-dimensional modelling of folds, thrusts, and strike-slip faults in the area of Val de Ruz (Jura Mountains, Switzerland). Swiss Journal of Geosciences, 110, 613-630.

188. Zanchi, A., Salvi, F., Zanchetta, S., Sterlacchini, S., & Guerra, G. (2009). 3D reconstruction of complex geological bodies: examples from the Alps. Computers and Geosciences, 35, 49–69.

189. Ziegler, P. A. (1982). Geological Atlas of Western and Central Europe. Shell Internationale Petroleum Maatschappij B.V., Den Haag, 130 pp.

190. Ziegler,P. (1992). Plate tectonics, plate moving mechanisms and rifting. Tectonophysics, 215, 9–34.

191. Zwingmann, H., Mancktelow, N., 2004. Timing of Alpine fault gouges. Earth and Planetary Science Letters, 223, 415–425.

Appendix A: Additional information to chapter 2.

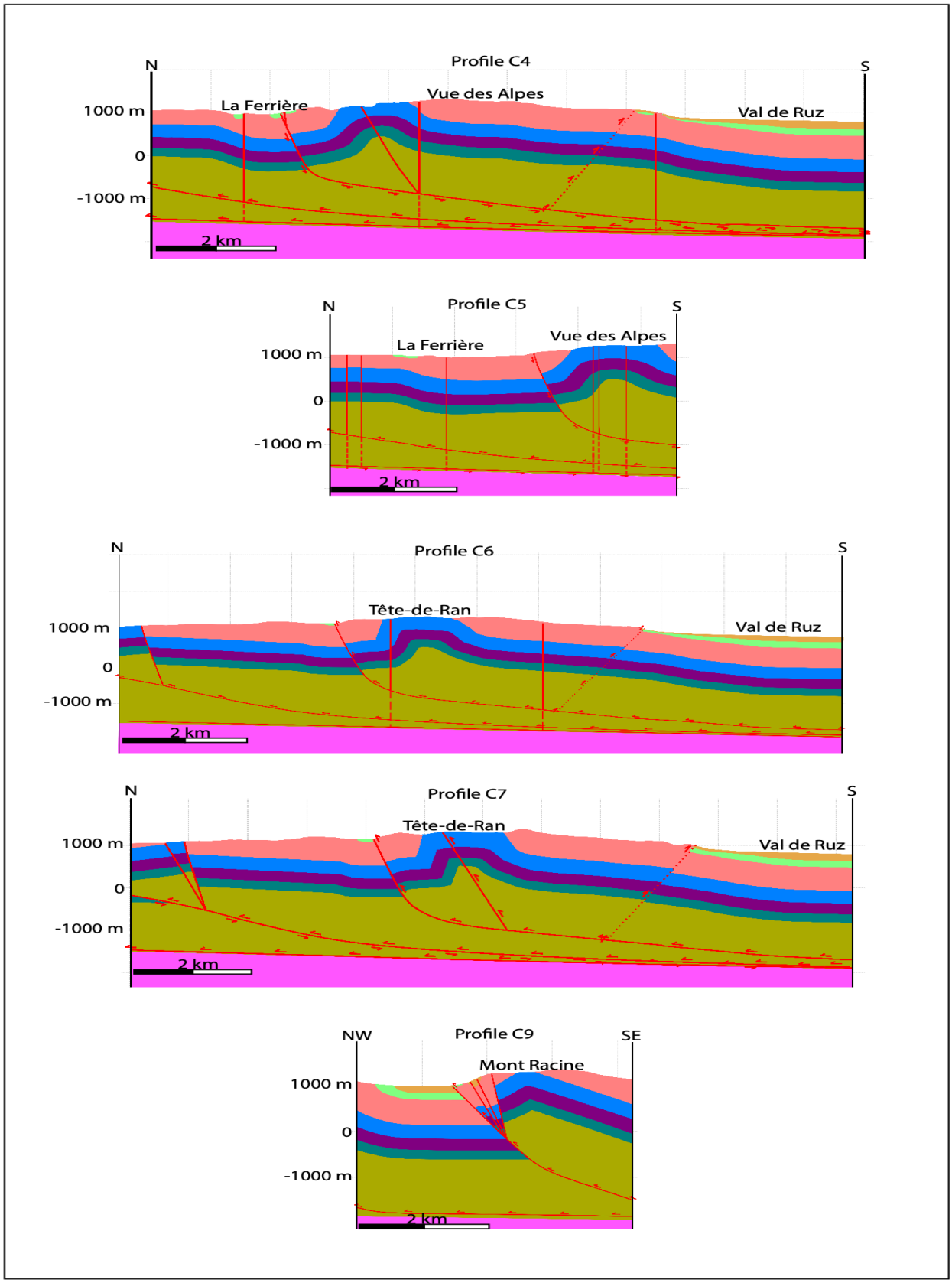

Appendix A.1: Input profiles C4, 5, 6, 7, and 9. See caption of Fig. 4.

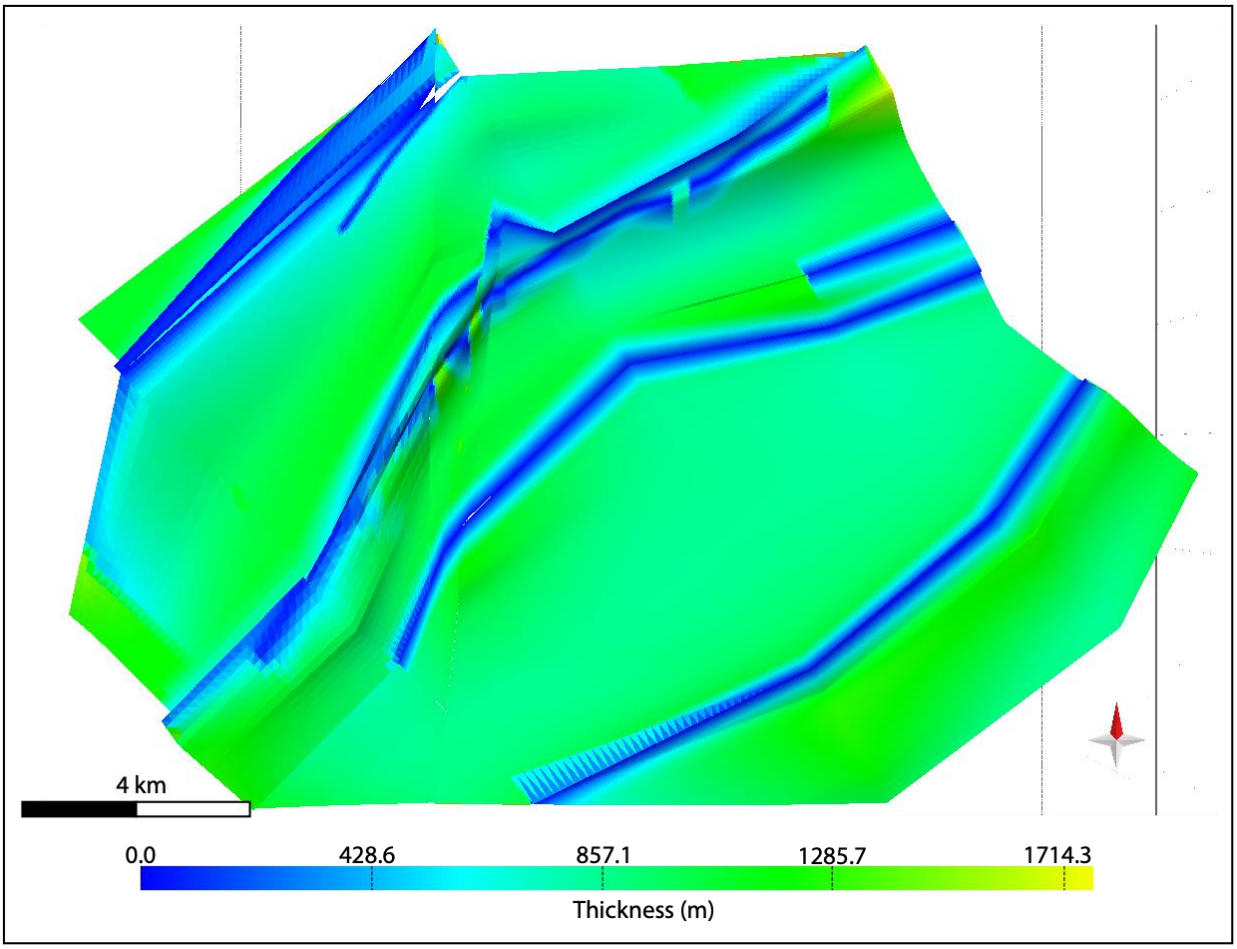

Appendix A.2: Thickness of Muschelkalk, measured in a vertical direction from the top of the unit down to the nearest thrust surface. Slight colour change in the synclinal areas shows northwestward increase in thickness. Low thickness in the anticlines (blue colour) results from the thrusts cutting upward through the unit.

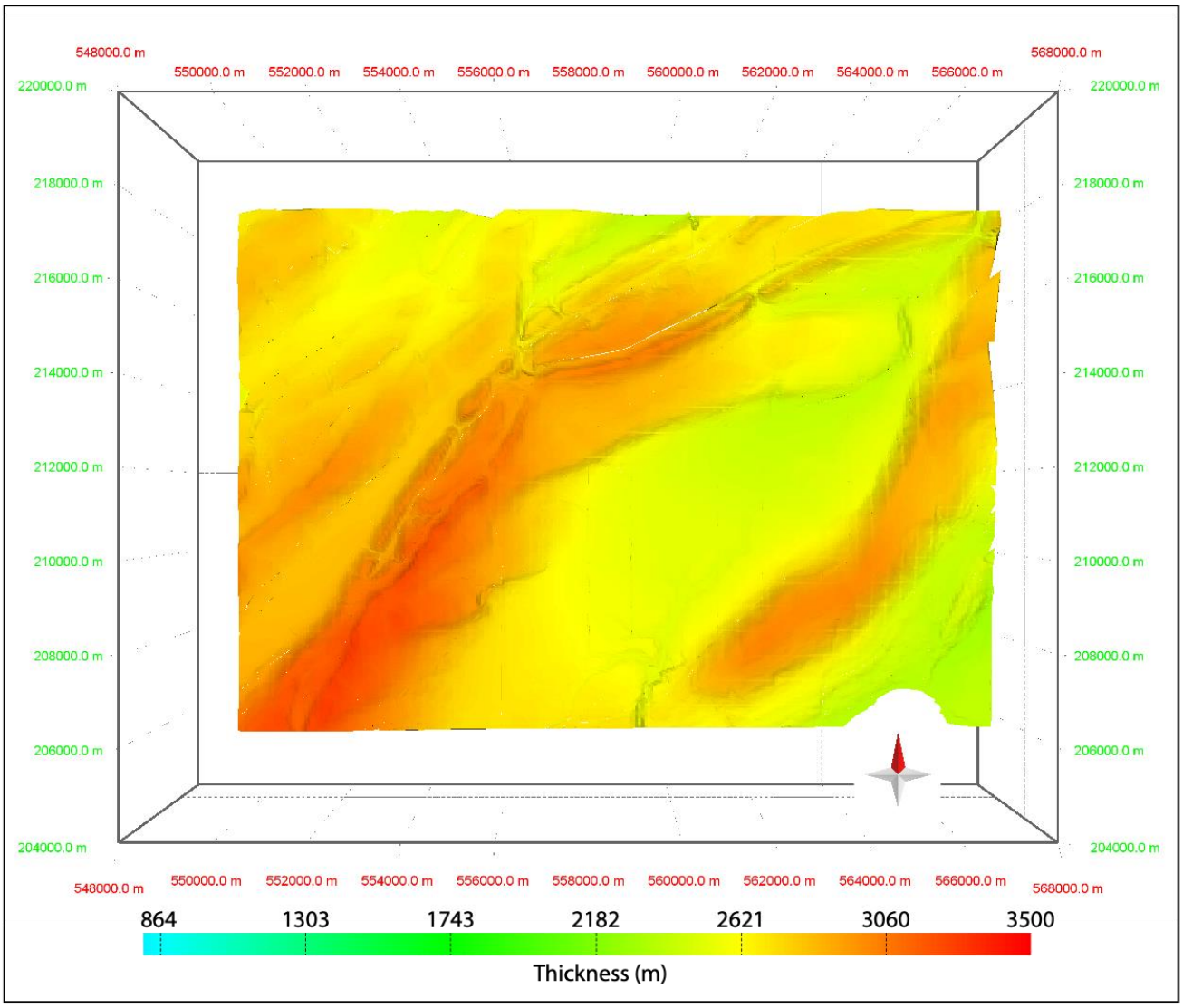

Appendix A.3: Thickness of sediment cover, measured from the Earth's surface down to the top of the basement. The minimum thickness is ca. 2300 m, maximum ca. 3200. Vertical view. Green and red numbers along the box are Swiss coordinates. Red compass needle shows north.

Appendix B: Additional information to chapter 3 and 4.

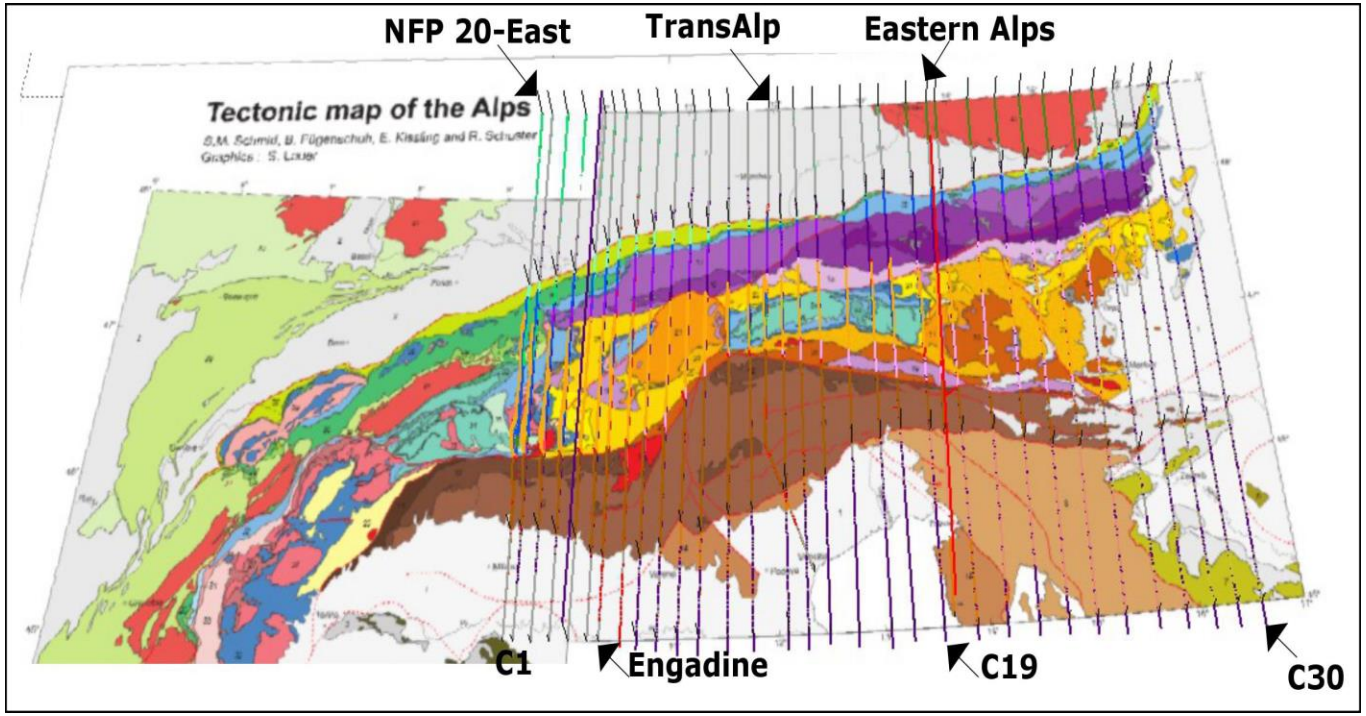

Figure B.1: Locations of the input profiles which used in chapter 3 and 4.

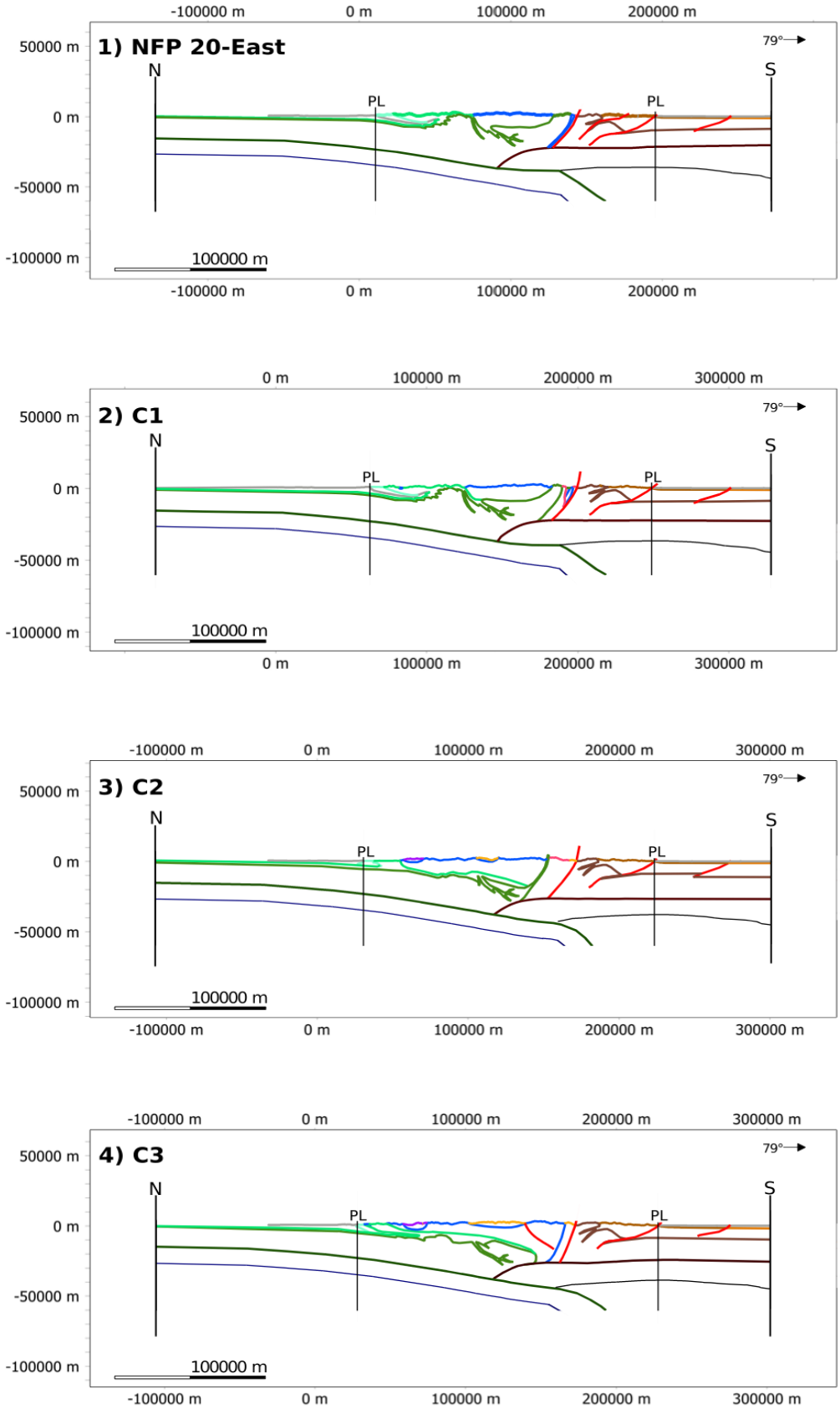

Figure B.2: Input profiles used in Chapter 3 and 4. Location of the profiles: see Fig. B.1. PL: Pin lines for length and volume balancing. Figure captions see Fig 3.6.

Figure B.2: Continued

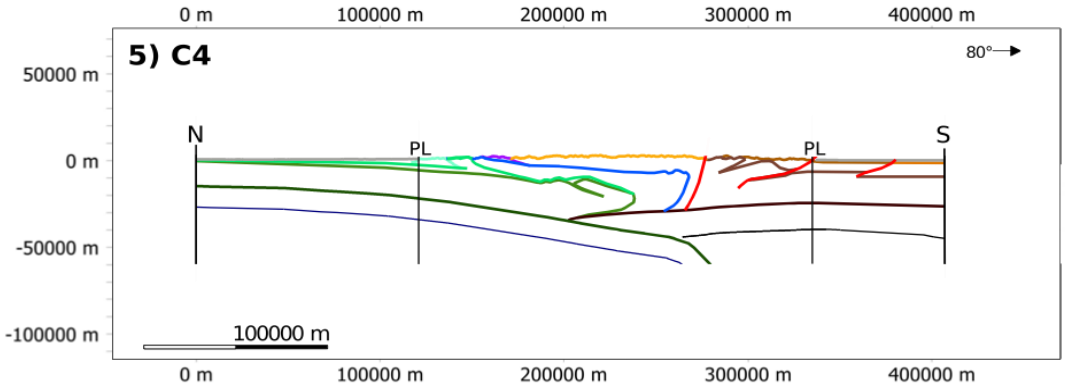

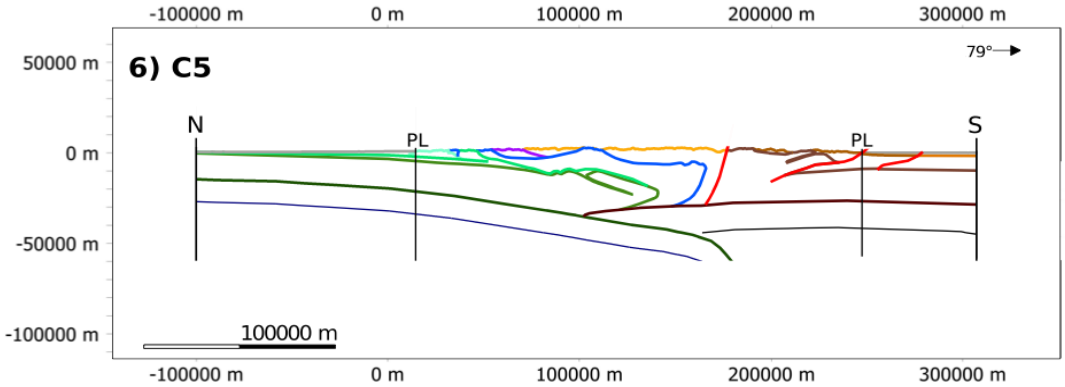

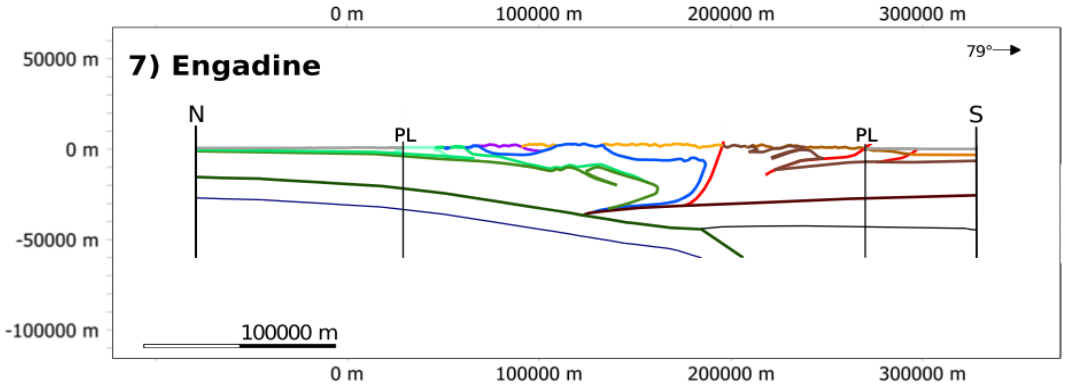

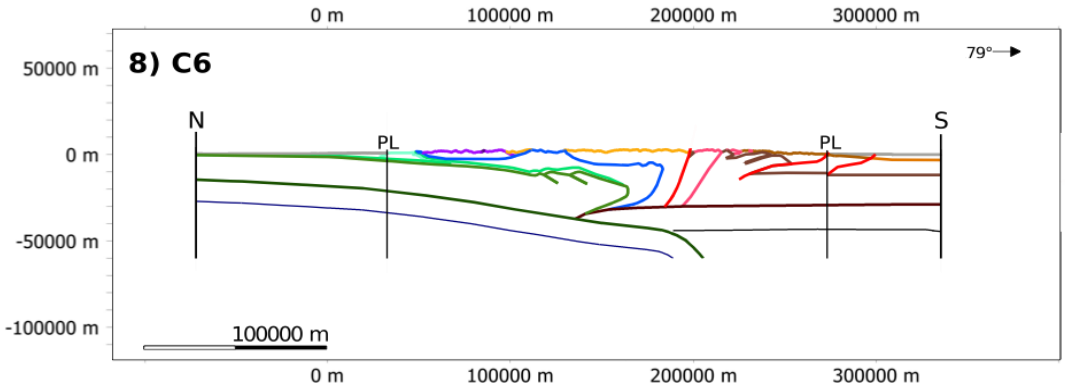

Figure B.2: Continued

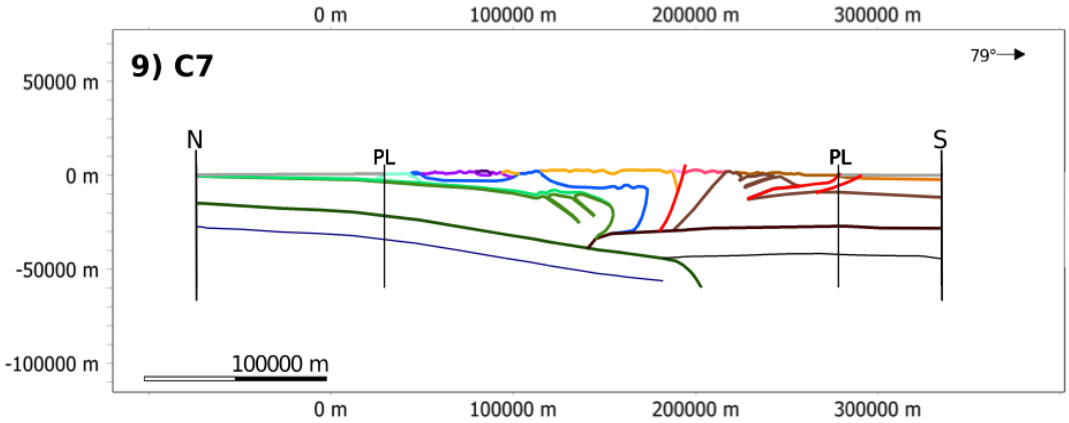

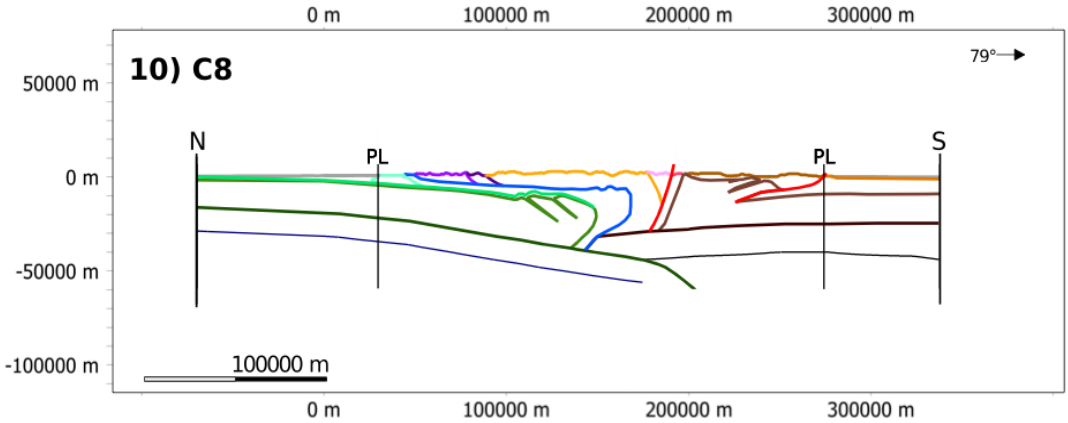

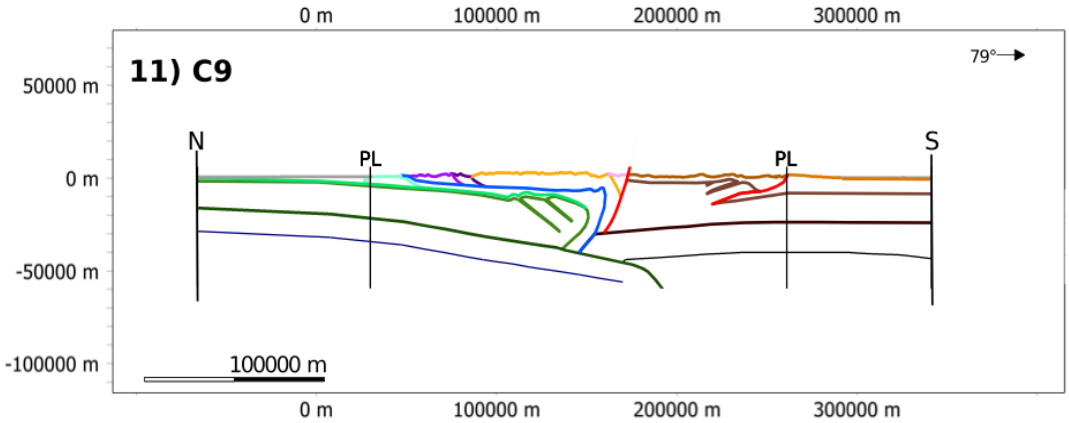

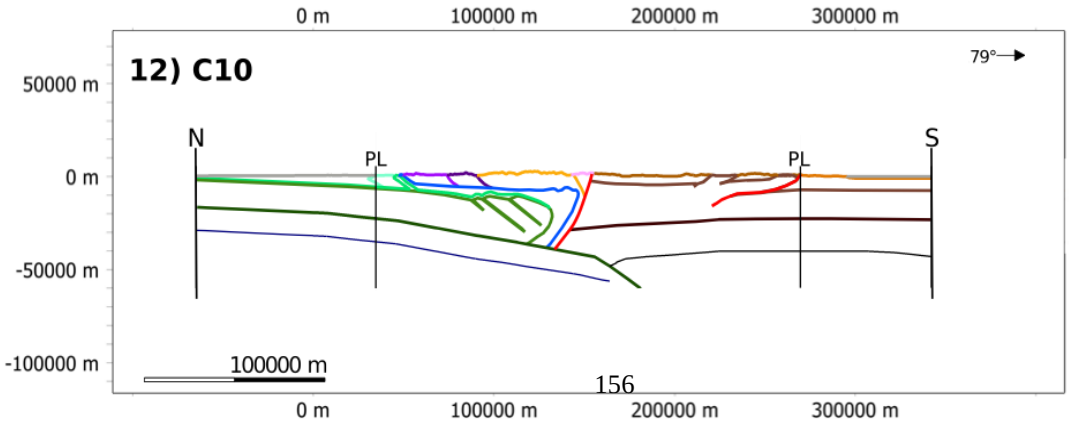

Figure B.2: Continued

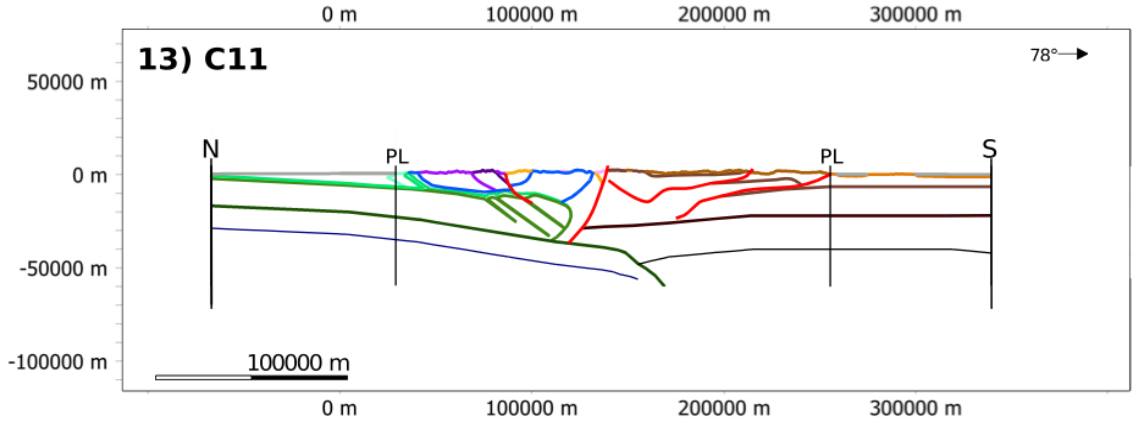

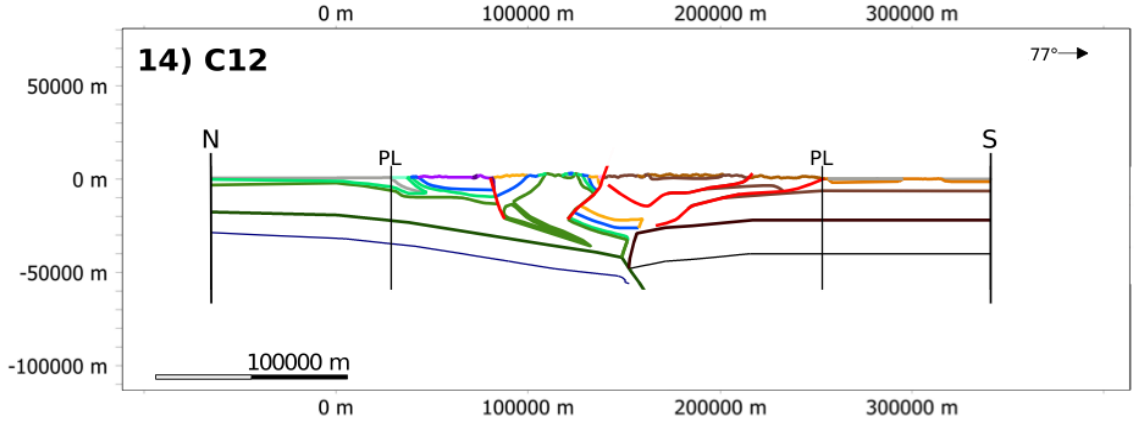

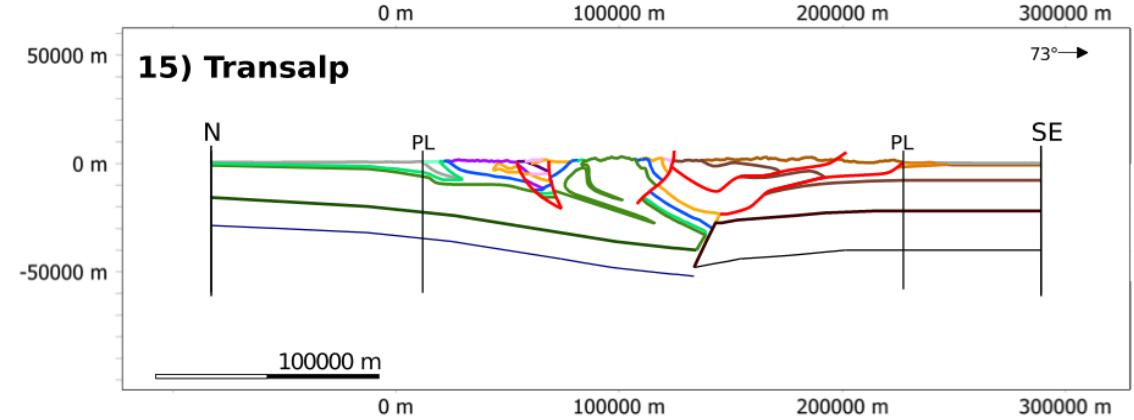

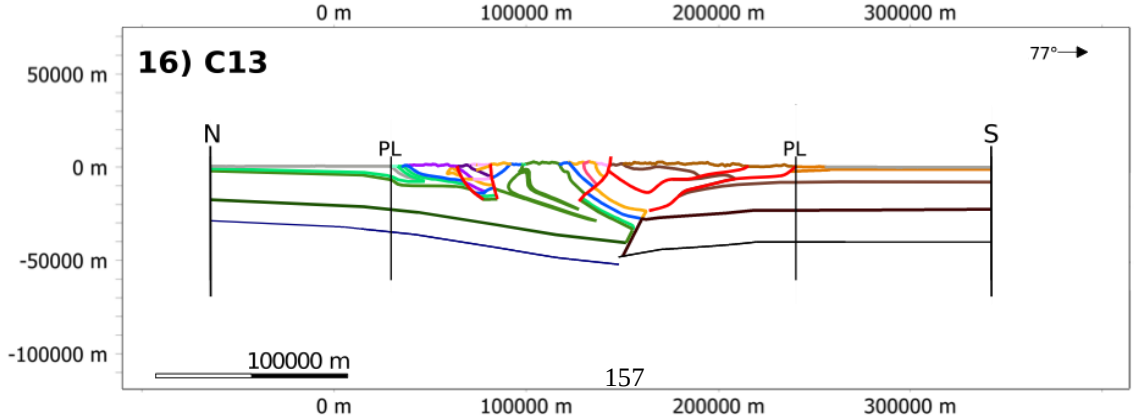

Figure B.2: Continued

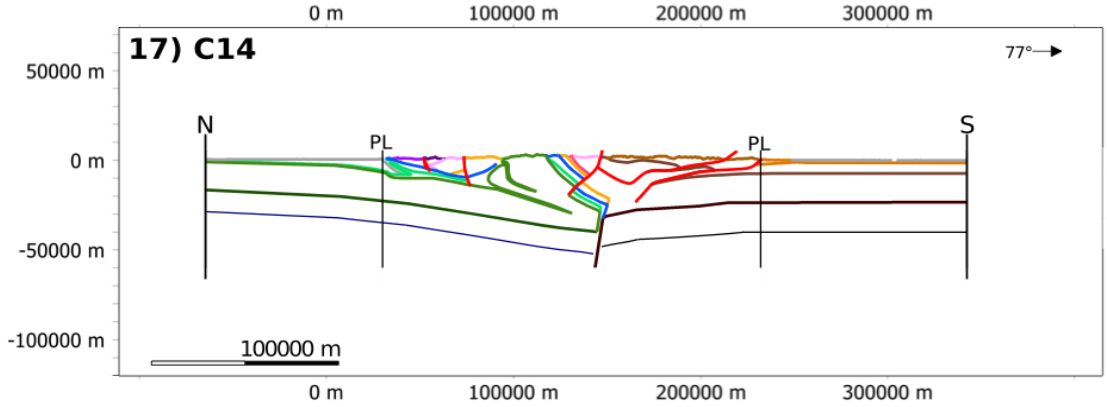

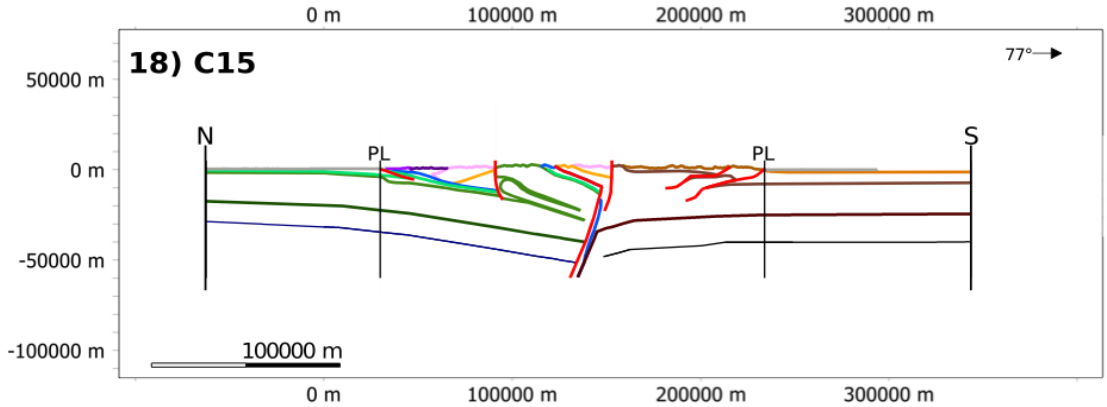

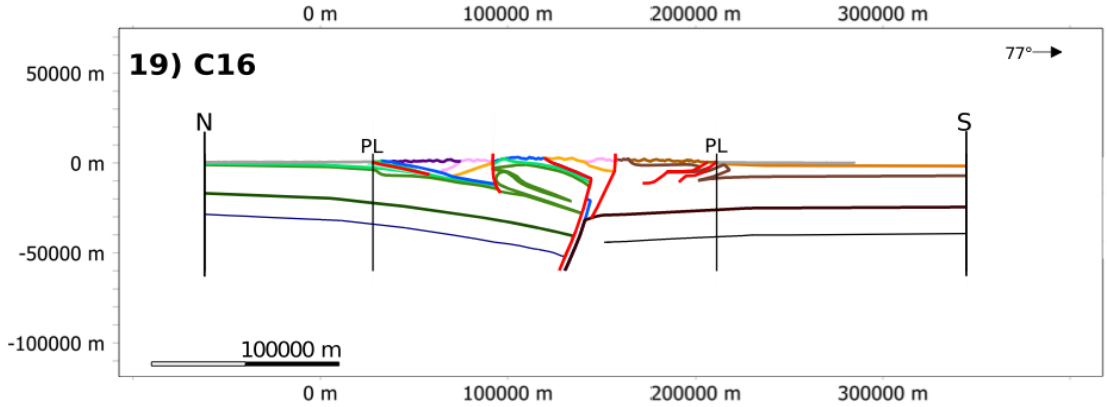

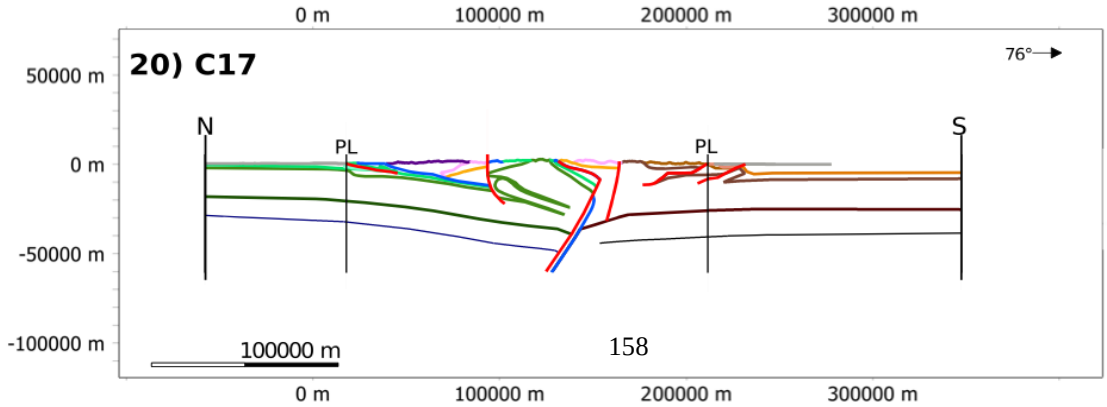

Figure B.2: Continued

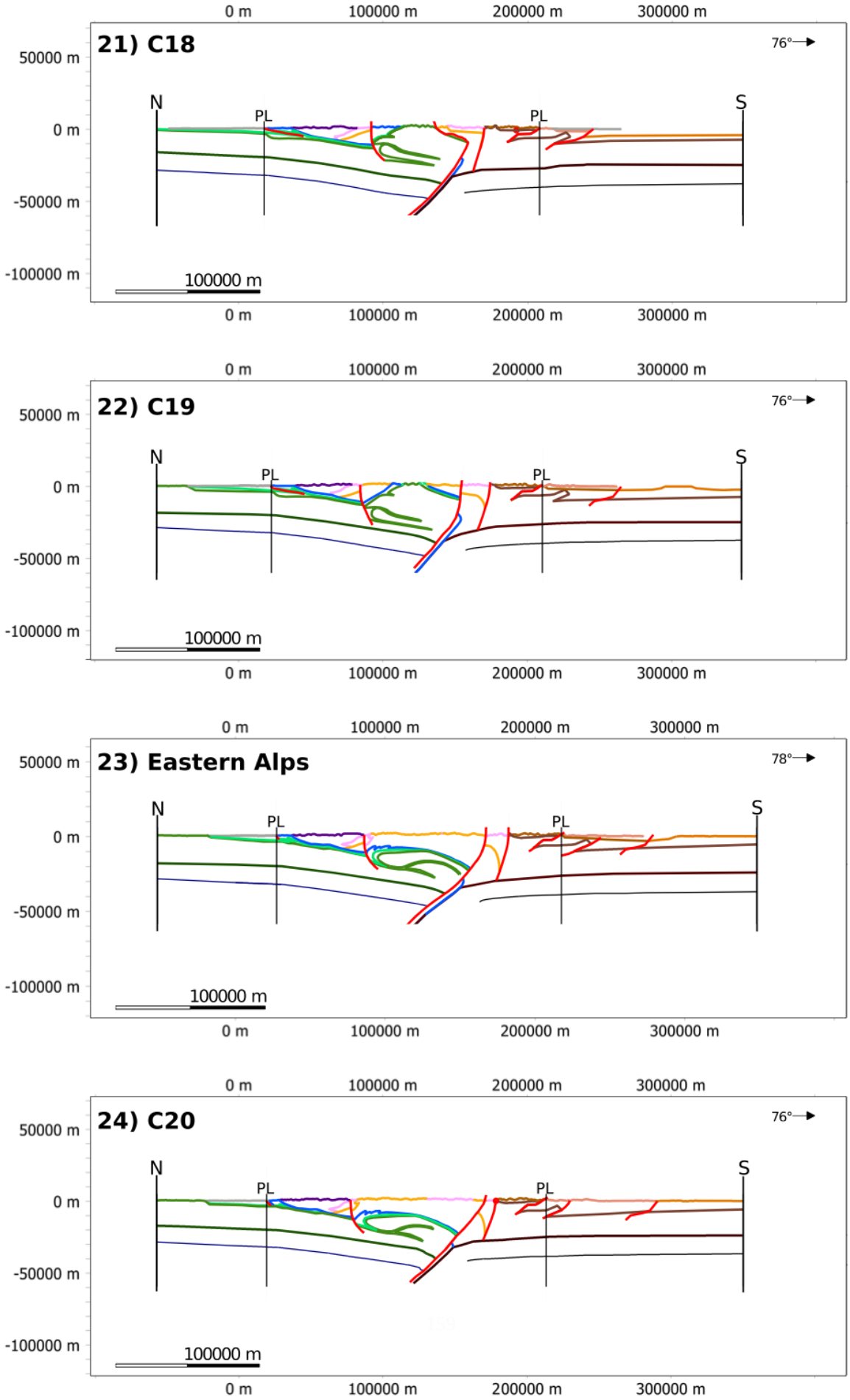

Figure B.2: Continued

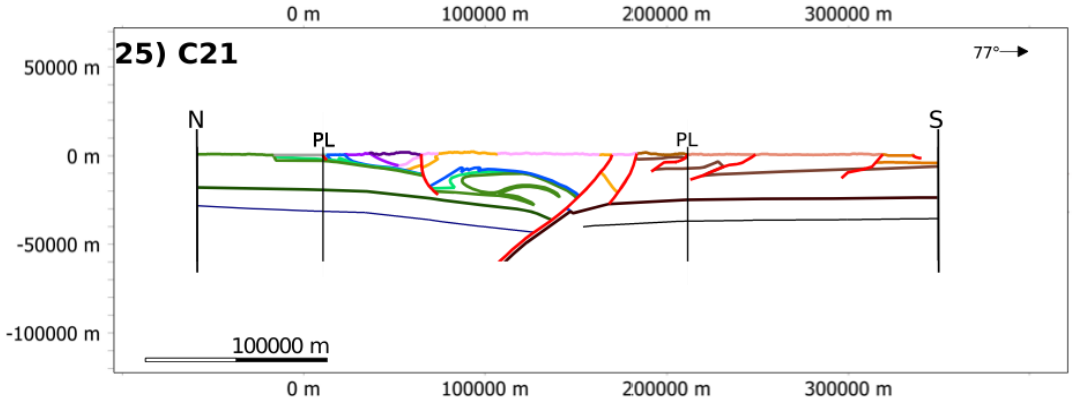

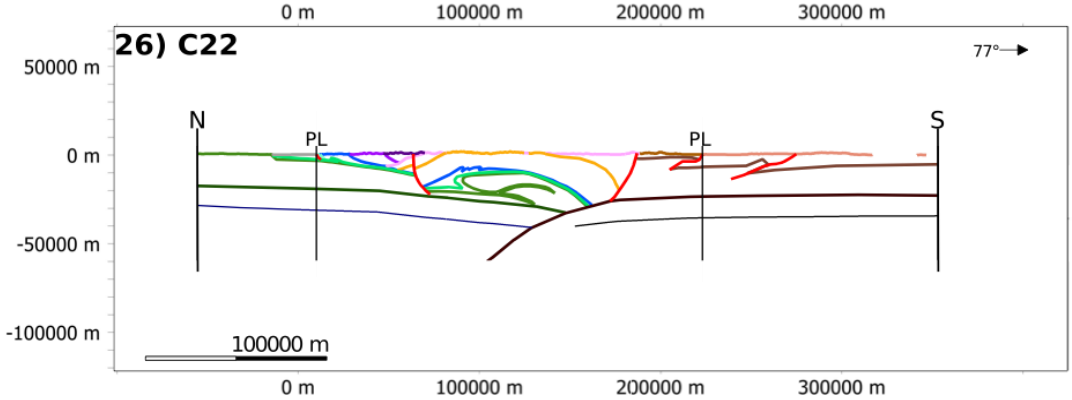

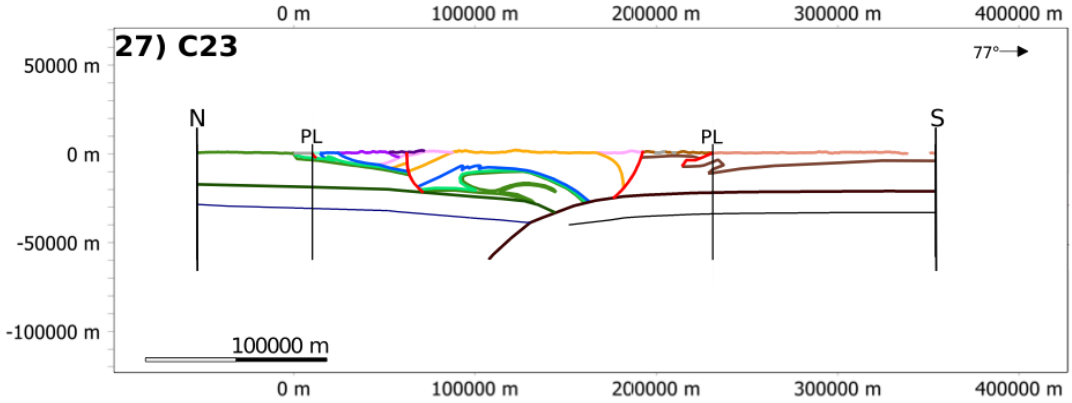

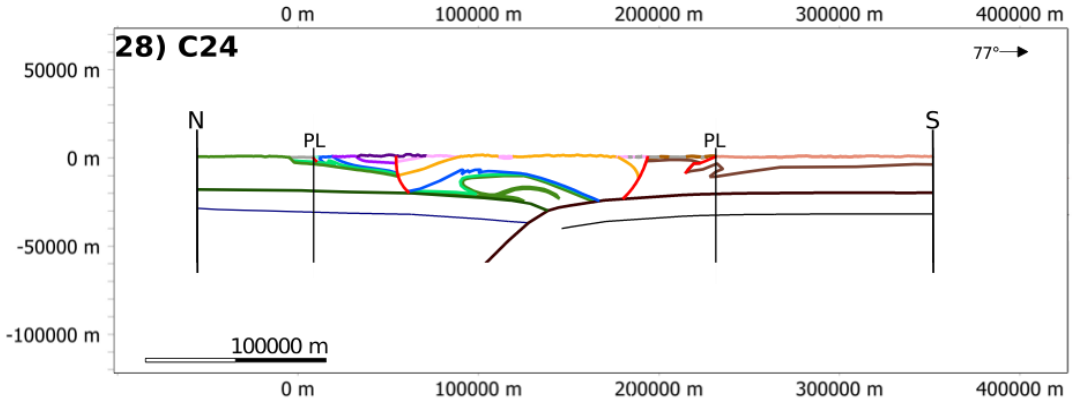

Figure B.2: Continued

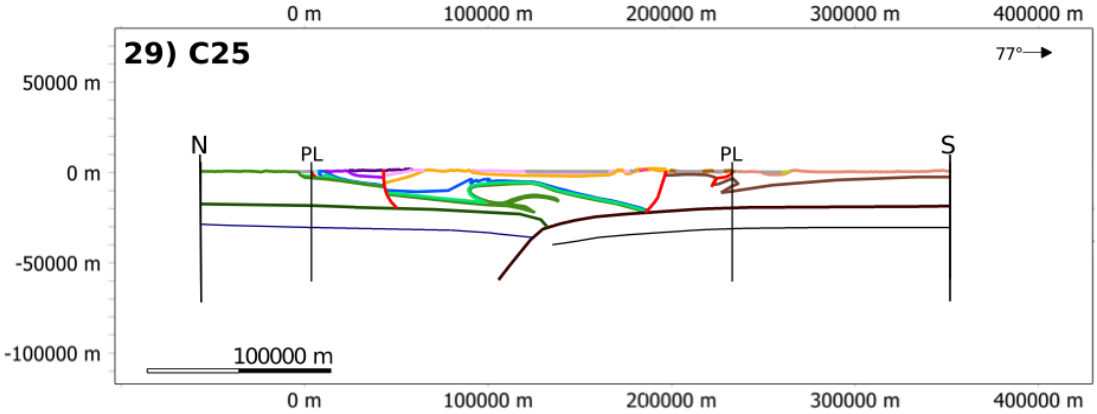

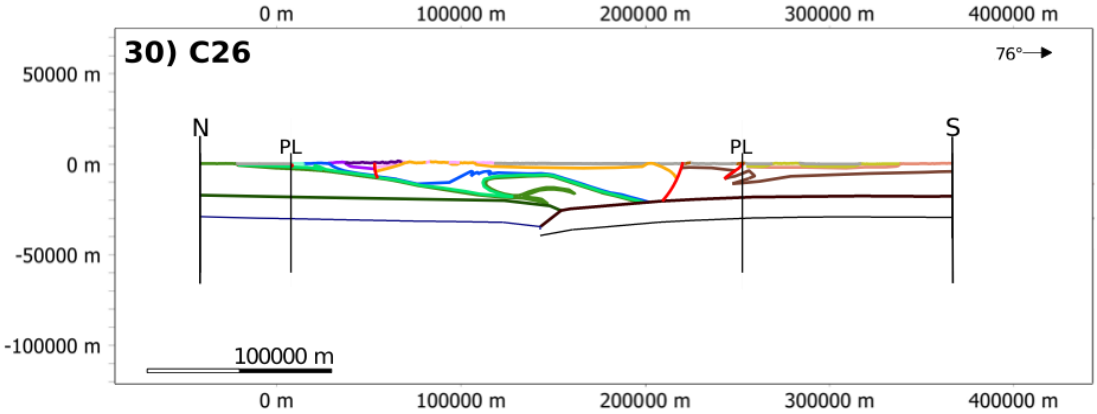

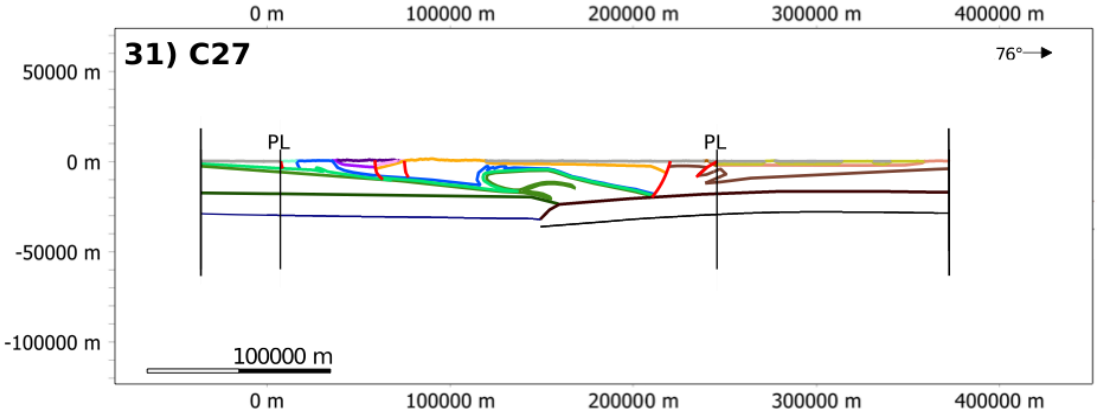

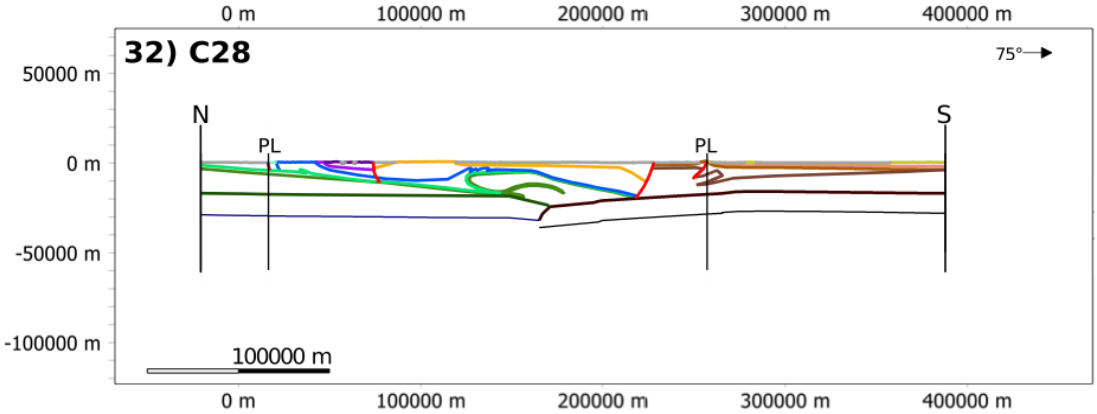

Figure B.2: Continued

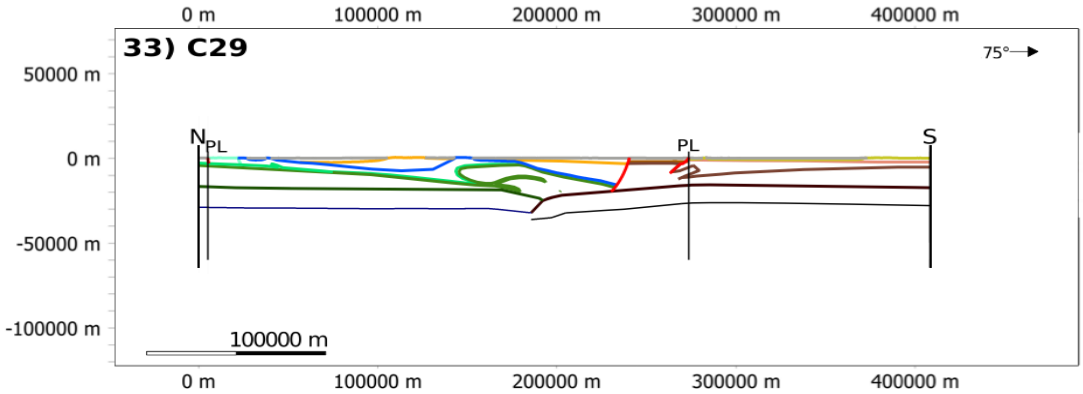

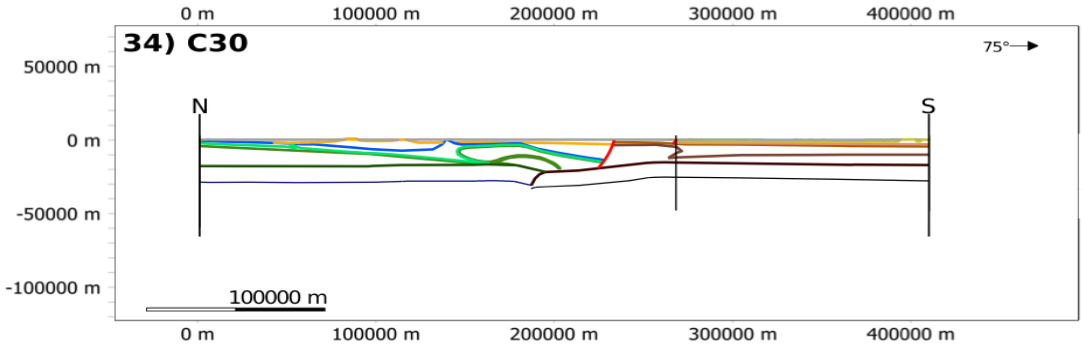

Publications

Journals:

1. M.Yosef Nejad, D., Nagel, T.J., Froitzheim, N. (2017): Three-dimensional modeling of folds, thrusts, and strike-slip faults in the area of Val de Ruz (Jura Mountains, Switzerland) , Swiss Journal of Geosciences. DOI: 10.1007/s00015-017-0261-8.

2. Salimi, F., Yosef Nejad, D., Ayatollahi, S., Vafae, M. (2012): Experimental investigation of ions effect on asphaltene deposition in porous media. 4th national chemical Engineering congress, Sharif University.

3. Mafi, V., Zargar, G., Sheikh Zakaria, J., Yosef Nejad, D. (2011): Miscible gas injection simulation and specification minimum miscibility pressure in one of Iraninan oil reservoirs. Journal of Oil & Gas Energy.

4. Mafi, V., Zargar, G., Sheikh Zakari, J., Yosef Nejad, D. (2011): Immiscible gas injection simulation in one of the Iraninan oil reservoir. Journal of Oil & Energy.

Conference Abstracts:

1. Yosef Nejad, D., Mansfeld, A., Nover, G (2017): Changes of Porosity, Permeability and Carbon capture efficiency during CO2 injection, EGU 2017. DOI: 10.13140/RG.2.2.19688.47364.

2. Yosef Nejad, D., Mansfeld, A., Nover, G (2017): Yosef Nejad, D., Nagel, T.J., Froitzheim, N. (2016): Monitoring CO2 flow (Leakage) in porous media by Electrical Conductivity method, EGU 2017. DOI: 10.13140/RG.2.2.29754.80326

3. Yosef Nejad, D., Nagel, T.J., Froitzheim, N. (2016): Application of Three Dimensional Modelling : a case study through the Val de Ruz area (Jura Mountains) ,TSK 2016, Bonn, Germany

4. Yosef Nejad, D., Nagel, T.J., Froitzheim, N. (2014): Three dimensional modeling of a fold and thrust belt. Student Technical Conference 2014, German SPE Section, Wietze, Germany.